STRUCTURAL GEOLOGY OF ABU SARI AURIFEROUS VEINS IN
NORTHERN SUDAN: AN EXAMPLE FOR SHEAR-HOSTED MESOTHERMAL
GOLD MINERALIZATION IN GREENSTONE BELTS

A THESIS SUBMITTED TO
THE GRADUATE SCHOOL OF NATURAL AND APPLIED SCIENCES
OF
MIDDLE EAST TECHNICAL UNIVERSITY

BY

ERDEM ATALAR

IN PARTIAL FULFILLMENT OF THE REQUIREMENTS
FOR
THE DEGREE OF MASTER OF SCIENCE
IN
GEOLOGICAL ENGINEERING

SEPTEMBER 2019

Approval of the thesis:

STRUCTURAL GEOLOGY OF ABU SARI AURIFEROUS VEINS IN NORTHERN SUDAN: AN EXAMPLE FOR SHEAR-HOSTED MESOTHERMAL GOLD MINERALIZATION IN GREENSTONE BELTS

submitted by **ERDEM ATALAR** in partial fulfillment of the requirements for the degree of **Master of Science in Geological Engineering Department, Middle East Technical University** by,

Prof. Dr. Halil Kalıpçılar
Dean, Graduate School of **Natural and Applied Sciences**   _____

Prof. Dr. Erdin Bozkurt
Head of Department, **Geological Engineering**   _____

Prof. Dr. Erdin Bozkurt
Supervisor, **Geological Engineering, METU**   _____

Examining Committee Members:

Prof. Dr. Gürol Seyitoğlu
Geological Engineering Dept., Ankara University   _____

Prof. Dr. Erdin Bozkurt
Geological Engineering, METU   _____

Assoc. Prof. Dr. Erman Özsayın
Geological Engineering Dept., Hacettepe University   _____

Assist. Prof. Dr. Ulaş Avşar
Geological Engineering Dept., METU   _____

Assist. Prof. Dr. Selman Aydoğan
Geological Engineering Dept., Balıkesir University   _____

Date: 12.09.2019

I hereby declare that all information in this document has been obtained and presented in accordance with academic rules and ethical conduct. I also declare that, as required by these rules and conduct, I have fully cited and referenced all material and results that are not original to this work.

Name, Surname: Erdem Atalar

Signature:

ABSTRACT

STRUCTURAL GEOLOGY OF ABU SARI AURIFEROUS VEINS IN NORTHERN SUDAN: AN EXAMPLE FOR SHEAR-HOSTED MESOTHERMAL GOLD MINERALIZATION IN GREENSTONE BELTS

Atalar, Erdem
Master of Science, Geological Engineering
Supervisor: Prof. Dr. Erdin Bozkurt

September 2019, 121 pages

The gold mineralized quartz vein system has been discovered within the Proterozoic Nubian Shield in the Sudan Northern State Dongola city, Abu Sari Region at North East Africa. Northern Sudan forms part of the Proterozoic Nubian Shield and consists of mainly accreted oceanic terranes that were sutured to Gondwana during the Pan-African orogeny − during approximately 810 to 580 My time interval. Mesothermal gold mineralization formed towards the end of ~550 to 600 my interval, during collisional deformation and large-scale strike-slip faulting along the east African margin.

Gold mineralization occurs across a wide area of quartz veining (at least 7 x 10 km) near the village of Abu Sari, approximately 650 km north of Khartoum. Rocks exposed in the Abu Sari area consist mainly of deformed and metamorphosed greenschist-facies greywackes, and intruding small granodiorite bodies, felsic and mafic dikes.

Mineralized quartz veins are controlled by strike-slip faulting with kinematic indicators occurring along their contacts with the host rock. Understanding the general behaviour of the fault system and the quartz veining will help to understand the

invisible continuation of the mineralized quartz veins, and to determine areas of the bending and turning points of the veins.

To tackle these questions 1:200-scale wall mapping of the quartz veins is done in the 235 meters level of the open pits of the gold mine. The surface level is 250 meters and the drilling data available in the 235 meters level help to understand the relationship between the mineralization and the structures.

The relationships between geological structures in the study area suggest that the region has suffered from five distinct phases of deformation. The first phase is attributed to the emplacement of ophiolites onto the passive margin sediments towards S- to SE, the second phase is represented by N- to NNE-trending open folds and is consistent with ca. E–W shortening, the third phase is associated with continuing strike-slip deformation along the Third Cataract Shear Zone, regional extension because of the thickening of the Saharan Metacraton lithosphere is the fourth phase, and final deformation phase is represented by WSW – ENE-trending strike-slip faulting.

In this model, the early phase of gold mineralization was associated with regional deformation and prograde metamorphism, the second stage of gold mineralization was induced by crustal-scale shear zone deformation causes E – W and NNE – SSW faulting which has formed the pathways for hydrothermal fluids to move upward and enriched the quartz veins trough the junctions of the strike-slip faulting.

ÖZ

KUZEY SUDAN BÖLGESİNDEKİ ALTIN İÇEREN DAMARLARININ YAPISAL JEOLOJİSİ: GREENSTONE KUŞAKLARINDA OLUŞAN VE MAKASLANMA ALANLARI İÇERİSİNDE GELİŞEN MEZOTERMAL TİP ALTIN CEVHERLEŞMESİNE BİR ÖRNEK

Atalar, Erdem
Yüksek Lisans, Jeoloji Mühendisliği
Tez Danışmanı: Prof. Dr. Erdin Bozkurt

Eylül 2019, 121 sayfa

Altın cevherleşmesi içeren kuvars damarı sistemi, Sudan Kuzey Eyaleti Dongola şehrinde bulunan Abu Sari bölgesinde keşfedilmiştir.

Bu altın yatağı Kuzey Afrika'da bulunan Proterozoik yaşlı Nubian Kalkanı içerisinde yer almaktadır. Kuzey Sudan genel olarak birleşen okyanusal kaya katmanlarının yaklaşık 810 – 580 My yaşındaki Pan Afrika orojenezi sırasında Gondwana ile birleşmesiyle Proterozoik yaşlı Nubian Kalkanı'nın parçası olarak oluşmuştur. Altın cevherleşmesi bu periyodun sonlarına doğru ~ 650'den 600My, kıta çarpması deformasyonlarının ve geniş ölçekli doğrusal atımlı fayların Batı Afrika marjında aktif olduğu dönemde meydana gelmiştir.

Altın cevherleşmesi Hartum'un yaklaşık olarak 650 km kuzeyinde bulunan Abu Sari köyünün yakınında kuvars damarları şeklinde geniş bir alanda (en az 7 x 10 km) bulunmaktadır. Abu Sari'de görülen kayaçlar küçük granadiyorit gövdelerinin, felsik ve mafik daykların kestiği deformasyona ve metaformizmaya maruz kalmış yeşil şist fasiyesleri ve gri kumtaşlarıdır.

Cevherli kuvars damarları kinematik göstergeleri ile yan kayaç dokunaklarında olan doğrultu atımlı faylanma ile kontrol edilmektedir. Fay sisteminin ve kuvars damarlarının genel davranışının anlaşılması, mevcut kuvars damarlarının görülemeyen devamlılıklarını, kuvars damarlarının dönüşlerinin ve bükülmelerini anlamaya yardımcı olacaktır.

Bu soruların cevaplarını bulmak üzere altın madeninin açık ocak duvarlarında 235 metre kotunda 1:200 ölçekli duvar haritalaması yapılmıştır. Yüzey seviyesi 250 metre olmakla berabere 235 metre kotuna ait sondaj verileri cevherleşme ve yapı ilişkisinin anlaşılmasında yardımcı olacaktır.

Çalışma alanındaki jeolojik yapılar arasındaki ilişkiler, bölgenin beş farklı deformasyon evresi geçirdiğini göstermektedir. İlk faz, ofiyolitlerin pasif kıta kenarı sedimanlarının üzerine G – GD'ya doğru yerleştirilmelerine atfedilirken, ikinci faz K-den KKD-kadar yönelen ve D – B kısalma ile uyumlu eğilimli açık kıvrımlarla temsil edilir. Üçüncü faz Üçüncü Katarakt Makaslama Alanı boyunca devam eden doğrultu atımlı deformasyon ile bağlantılı olup, dördüncü faz ise Sahara Metakratonu'nun kalınlaşması sonucu oluşan bölgesel genişlemedir. Son deformasyon fazı da BGB – DKD yönlü doğrultu atımlı faylarla temsil edilmektedir.

Bu modelde, altın cevherleşmesinin erken evresi bölgesel deformasyon ve ilerlemiş metamorfizma ile ilişkilendirilmiş olup, altın cevherleşmesinin ikinci aşaması D – B ve KKD – GGB faylanmaya neden olan kıtasal ölçekli makaslanma alanı deformasyonunun açtığı yollardan gelen hidrotermal suların yukarıya doğru hareket etmesi ile oluşmuştur. Bu hareket doğrultu atımlı fayların kesişim yerlerinde kuvars damarları boyunca cevher zenginleşmesine neden olmuştur.

Anahtar Kelimeler: Altın, Kuvars Damarı, Greenstone, Mezotermal Altın Yatakları, Orojenik Altın, Kuzey Doğu Afrika, Nubian Kalkanı, Sudan, Pan Afrika Orojenezi

To my daughter Aren,

ACKNOWLEDGEMENTS

TABLE OF CONTENTS

LIST OF TABLES

TABLES

LIST OF FIGURES

FIGURES

Figure 1.8. Closure of the Mozambique Ocean during the Neoproterozoic resulted in collision of eastern and western Gondwana and formation of so-called Greater Gondwana and East African Orogeny (from Abdelsalam & Stern 1996). Between East and West Gondwana at ~850 Ma Mozambique Ocean started to disappear as they move towards each other with consecutive tectonic activities. The Saharan Metacraton, which was far away from orogenic activity, experienced intraplate an orogenic magmatism between 720 and 700 Ma (Shang et al. 2010b), because of the

CHAPTER 1

INTRODUCTION

1.1 Definition of the Problem: Behaviour of Mineralized Veins

Gold mining in the Sudan region goes back at least to the time of the Middle Kingdom Egyptian. According to the studies of Barbour (1961), ancient workings for gold and precious stones date back to the period between 2000 and 1600 BC.

The Republic of the Sudan has hundreds of gold mines and prospects, and many of them are still of economic importance. Gold mineralization is a part of the Pan-African Orogeny and occurs in three major styles (Elsamani *et al.* 2001).

The first type of gold mineralization is known as volcanogenic massive sulfide (VMS) deposits, syngenetic with acidic calc-alkaline island-arc volcanism, where gold deposition occurred at about 715 Ma ago. The second type is attributed to remobilization and precipitation of gold in silica-barite and barite formations during collisional orogeny at around 650 Ma ago. The third type, which is the case for this thesis study, is related with the post-collisional movement and retrograde metamorphism at approximately 550 Ma. Remobilization of gold from VMS deposits along structurally more favourable places in the form of auriferous quartz veins occur along first and second order shear zones (Elsamani *et al.* 2001).

Such quartz veins with many mesothermal gold deposits occur in Sudan Northern State Dongola city, Abu Sari region. The exact source of gold and origin of fluids at Abu Sari (the main concern of this thesis) are however still unclear, and the evidence suggests possibility of different stages of gold mineralization. There are different hypothesis proposed to shed light on the existing controversies over the origin and evolution of mineralization in Abu Sari region; they are summarized below: (1) One model claim that gold-bearing quartz veins have formed along reverse fault planes and

associated extensional structures, which occurred during deformation and metamorphism of the Proterozoic country rocks. The lack of strong alteration selvedge in host rock quartzites around quartz veins suggests that the fluids were in approximate equilibrium with the Nubian Shied rocks, thus supporting a metamorphic fluid origin (Richards, 2010). (2) In contrast, the close spatial association between the breccia veins and rhyodacitic dikes suggests a possible link to syn-deformational felsic magmatism (Richards, 2010). Magmatic fluid origin for a secondary younger vein system controlled by strike-slip faulting seems likely because there are 2−5 meters alteration zones with intense pyrite mineralization, as expressed by the limonite and hematite occurrences.

Understanding which type of quartz veins host the gold mineralization and the structural control and mechanism(s) that affects behaviours of quartz veins are very crucial issues in finding and locating new gold mineralized quartz vein systems in Abu Sari area of Sudan.

Mining is done only at economic quartz vein systems in Abu Sari area and the largest three of them are selected for further study in order to address these questions as outlined in the preceding paragraph. These systems are named as southern vein, northern vein, and the eastern vein (further information is available in Section 2.2.3) (Figure 1.1). Each system is composed of hundreds of quartz veins with different length, thickness, mineralization, texture, and structural pattern.

There are three major types of mineralization in the subject area of this study. First type is associated with vein sets (0.5 to 13 meters thick) that cut foliation of the greenstone. This type of vein sets forms the main ore of the *southern vein* and some parts of the *eastern vein*.

Mineralized vein sets are parallel to the main foliation in the host rock greenstones and quartzites. These veins are boudinaged and occur as lens-shaped bodies, reflecting parts of large-scale pinch-and-swell structures. '*Pinch-and-swell*' term is used here for a 'structural feature common in quartz veins and pegmatites in metamorphosed

2

rocks, in which the vein is pinched and thinned at frequent intervals, leaving expanded parts between' (verbatim from Neuendorf *et al.* 2011; Glossary of Geology - Ramberg, 1955). As can be understood from the description, these types of vein sets have variable thickness reaching up to 4 meters. *Eastern veins* can be encountered in this group. Mineralized boudinaged veins are observable only at *Eastern veins* which are parallel to the general foliation trend.

Mineralization also appears to be associated with shearing of the previously existing quartz vein system(s) due to faulting that caused change in the general trend of the quartz veins. The shearing has also resulted in re-mineralization and deposition of gold through new porous spaces. There are only minor massive, continuous quartz veins of this type of mineralization system. Whereas frequently repeating quartz veinlets and quartz fragments in the drilling cores suggest shearing of a massive vein. *Northern veins* are examples of such mineralization (Figure 1.1).

According to the site observations, boudinaged vein sets are the oldest and least mineralized among all three mineralization stages. This type of mineralized quartz vein supports a metamorphic fluid origin as there are no alteration selvedge (Figure 1.2).

Foliation-cutting vein sets are the second type of mineralization. These veins are steeply dipping, massive, continuous quartz veins and appear to be controlled by strike-slip faulting; there are alteration selvedge up to 6 meters in width. Intense pyrite mineralization and iron oxidation are also common in this type of mineralization (Figure 1.3).
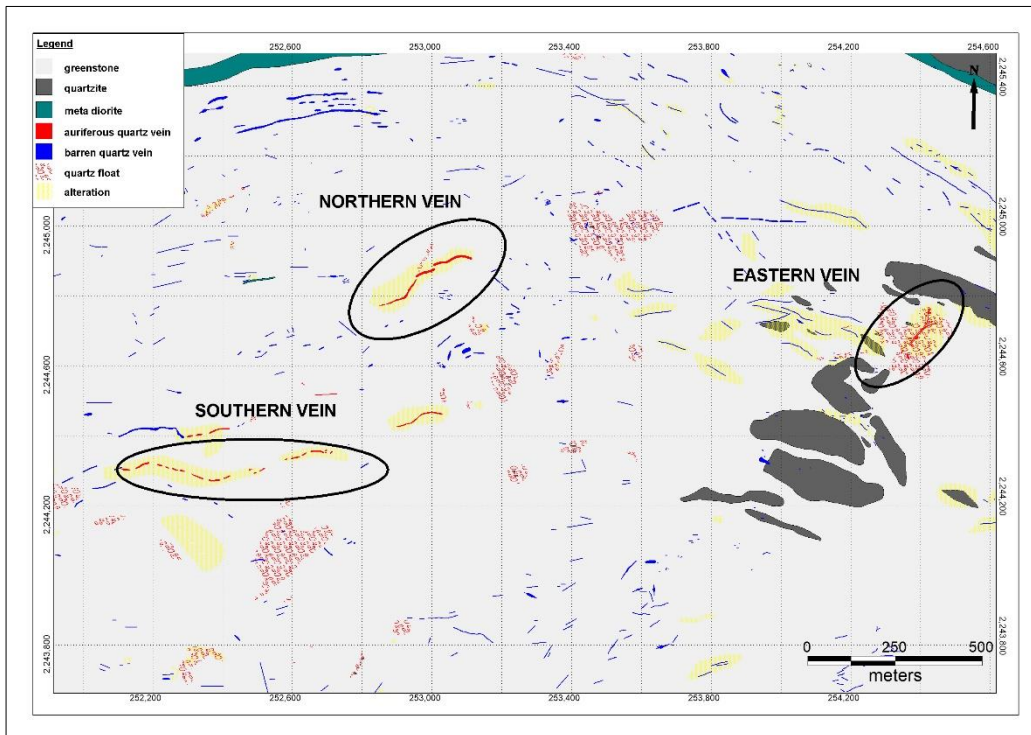
Figure 1.1. Simplifed map showing the distribution of quartz veins in the Sudan Northern State Dongola city, Abu Sari region.

Figure 1.2. Narrow folded and boudinaged quartz veins lacking alteration selvedge in quartzite.

Finally, Finally, third type of mineralization is sheared and displaced E–W- to SW–NE- trending quartz vein system. It gives the highest thickness of mineralization and the highest gold grades (Figure 1.4).

As is seen from the above-given brief, the origin of gold mineralization and structural mechanisms that control the auriferous quartz veins are not clear. The answers to above questions have far more implications and would be useful for the better understanding of gold mineralization not only in the Abu Sari area but whole North-eastern Sudan. This research aim of this thesis is therefore to study the gold-bearing quartz veins of the Nubian Shield in the Delgo-Abu Sari area. The structural control and possibility of a shear zone that may control the gold mineralization and quartz veining will be explored.
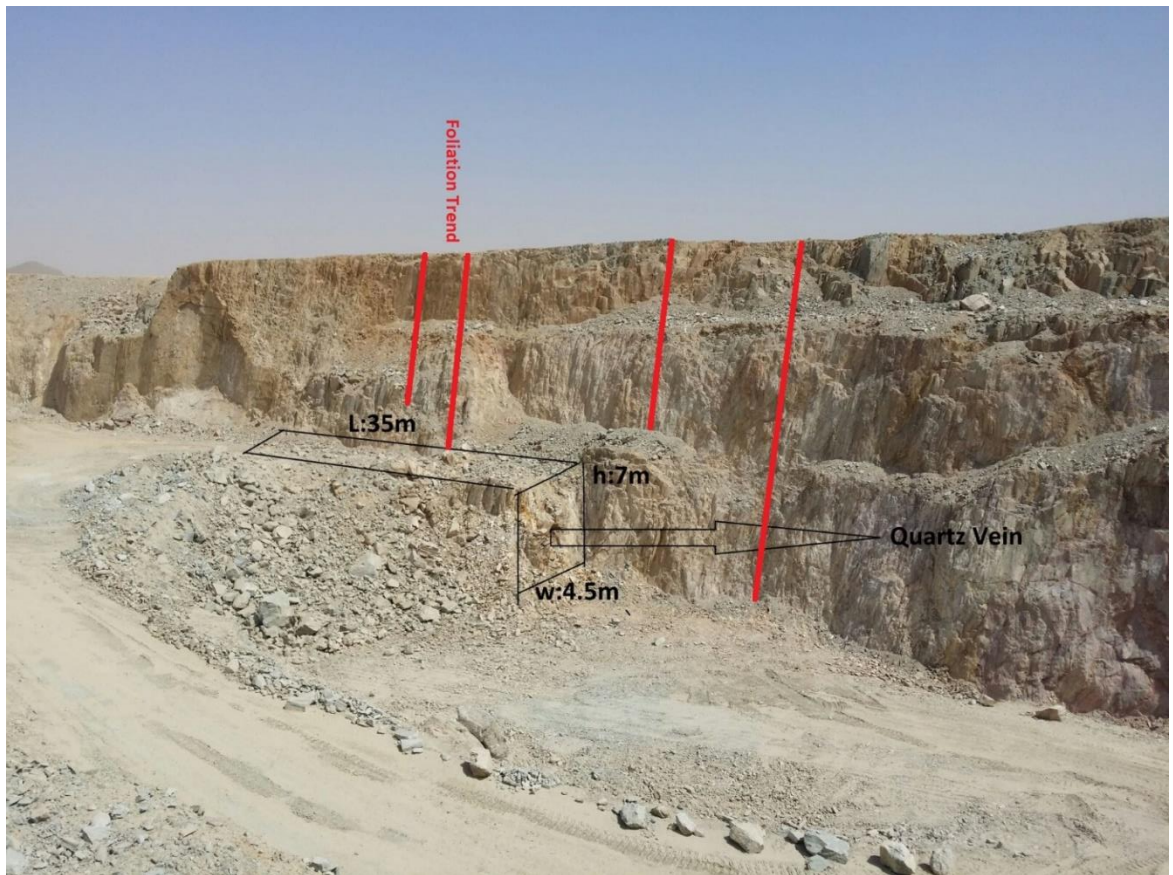
Figure 1.3. Field view of E–W-trending massive quartz vein of the southern ore. Note that vein(s) cutting across foliation in intensely altered greenstone.

Figure 1.4. Field view of mineralized shear zone within the northern ore.

The main objectives of this study are therefore to investigate: (i) the reason why some of the quartz veins are mineralized and the others not, (ii) why the mineralized quartz veins suddenly change direction or suddenly terminate, and (iii) why some parts of mineralized quartz veins have higher gold grades than other parts. In conclusion, the structural control of veining and gold mineralization will also be discussed.

1.2 Location of the Study Area

The subject Abu Sari area is located on the edge of a suture zone of Pan-African Orogeny, related to the closure of Mozambique Ocean, which separated Saharan Metacraton and Arabian-Nubian Shield (ANS) (Figure 1.5).

The term 'Pan-African' was coined by W.Q. Kennedy (1964) on the basis of an assessment of available Rb-Sr and K-Ar ages in Africa. The Pan-African was interpreted as a tectono-thermal event, some 500 Ma ago, during which a number of mobile belts formed, surrounding older cratons.

Pan-African term is now commonly used to describe an orogenic cycle during the period of ~870 to ~550 Ma reflecting opening and closing of oceans, collision of crusts causing regional tectonic, magmatic, and metamorphic activity (Kröner & Stern 2004).
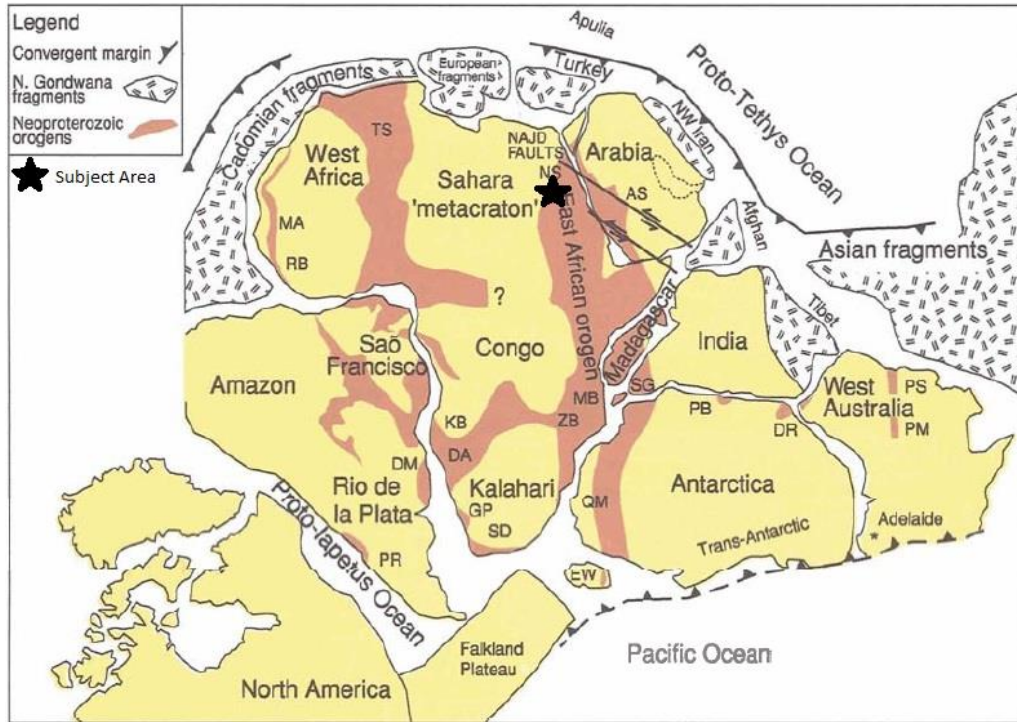
Figure 1.5. Map of Gondwana at the end of Neoproterozoic time (~540 Ma), showing the general arrangement of Pan-African belts. AS− Arabian Shield, BR− Brasiliano, DA− Damara, DM− Dom Feliciano, DR− Denman Darling, EW− Ellsworth-Whitemore Mountains, GP− Gariep, KB− Kaoko, MA− Mauretanides, MB− Mozambique Belt, NS− Nubian Shield, PM− Peterman Ranges, PB− Pryolz Bay, PR− Pampean Ranges, PS− Paterson, QM− Queen Maud Land, RB− Rokelides, SD− Saldania, SG− Southern Granulite Terrane, TS− Trans-Sahara Belt, WB− West Congo, ZB− Zambezi (from Kröner & Stern 2004).

Cratons are old and stable parts of the lithosphere and are defined as 'part of the crust which have attained stability and has not been deformed for a long time'; thus, they are Precambrian in age (Bates and Jackson 1980). The term '*metacraton*' is used to describe a craton that has been remobilized during an orogenic event, but original characteristics are still identifiable (Abdelsalam 2002).

The *Saharan Metacraton* is a term used to refer to 'the pre-Neoproterozoic, but sometimes highly remobilized during Neoproterozoic time – continental crust which occupies the north-central part of Africa and extends in the Saharan Desert in Egypt, Libya, Sudan, Chad and Niger and the Savannah belt in Sudan, Kenya, Uganda, Congo, Central African Republic and Cameroon' (Abdelsalam *et al.* 2002) (Figure 1.5).

The Arabian-Nubian Shield (ANS) is an exposure of Precambrian crystalline rocks on the flanks of the Red Sea. It extends from Jordan and southern Israel in the north to Eritrea in the south and Egypt in the east to Saudi Arabia and Oman in the east (Blasband *et al.* 2000) (Figure 1.6). The ANS is the northern half of a great collision zone called the East African Orogeny (Figure 1.5). This collision zone formed near the end of Neoproterozoic time when east and west Gondwana collided to form the supercontinent Gondwana at the end of a Wilson Cycle and defined the Pan-African Orogeny (e.g., Stern 1994; Abdelsalam 1996).

According to these models, gold mineralization in the subject area of this thesis should occur in the Nubian Shield but not to the Saharan Metacraton (see following paragraphs for more information); this is animportant information because one can narrow the exploration area to locate new gold mineralization. Moreover, this information would also be very useful to understand the different types of gold mineralization and their controlling mechanisms.
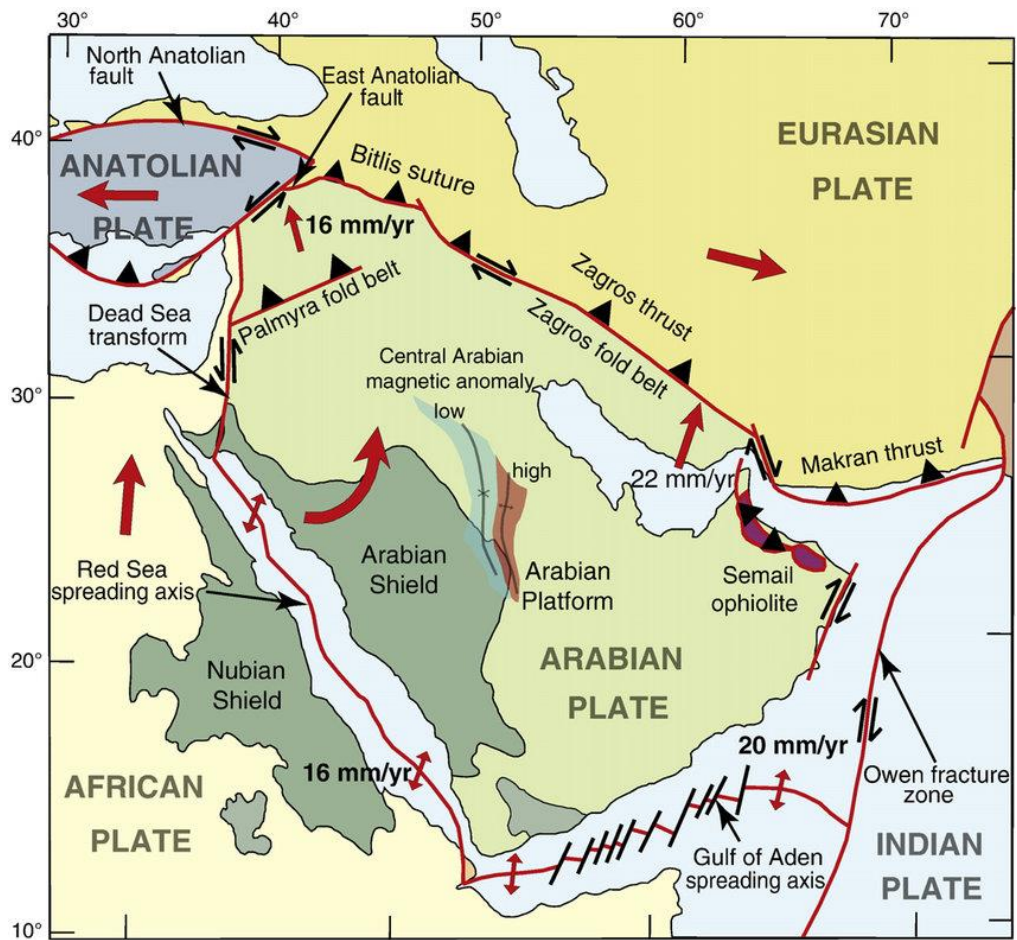
Figure 1.6. Map showing the distribution of the Arabian-Nubian Shield (from Stern & Johnson 2010). Star shows the location of the thesis study.

The work site (Block 17 licence) is located near a village called Abu Sari and lies between two major settlements − Wadi Halfa in the north and Dongola in the south (Figure 1.7). Abu Sari is connected to Delgo, which is a settlement in Northern Province of Sudan. The mineral deposit site lies 640 km (7 hours) north of Khartoum. The area is accessible by the two-lane tarmac highway that runs from Khartoum to the south, through Dongola and the study area, and onwards to Wadi Halfa.

Most of the Northern Sudan is dominated by an arid desert climate. Temperatures are generally high throughout the year with the highest daily mean temperature of about 43° C during May and June. The field studies were conducted in April 2015 and at

9

that time the weather was mild, even cold at night time. Sandy winds were dominant through days and nights.

Figure 1.7. Location map of the study area.

There is no vegetation in the Northern Sudan and in the study area. Sand dunes cover the area in some parts whereas in and near the study area they are not dominant. The absence of vegetation and sand dunes has made it easy to observe major structures from both Landsat images and even Google Earth.

The area has no established electrical power network in North Sudan. There are small size generators in the surrounding villages, which are primarily used for pumping water from the Nile. In the site, there is a modern camp built by the mining company, which has comfort and technology that is needed. 4X4 vehicles make it easy to access even in sandy roads.

1.3 Methods of the Study

This research lasted for about two-and-half-years and involved both (i) field studies and (ii) laboratory studies. The study mapping along the walls of open pits at 1:200 scale, during which structural features, such as faults, tension cracks, quartz veins and veinlets, faults are all noted.

The field studies include: (i) mapping of rock units and structural features, such as folds, foliation and lineation at a scale of 1/5000, and open pit-wall mapping at available areas at a scale of 1/200, (ii) sampling for petrographic determination, (iii) measurement of attitude for foliation and lineation, (iv) detailed kinematic analysis to determine the sense of motion during deformation. Different rock units are, based on their physical appearance and mineral content, distinguished and mapped. To analyse and determine characteristic quartz vein behaviours 2880 rock samples and 10000 meters of diamond drilling borehole data are analysed and interpreted. All observations, detailed descriptions and coordinates are recorded in the field notebook during the excursion.

Laboratory studies are performed at the Middle East Technical University Geological Engineering Department. Laboratory studies include (i) petrographic analyses, (ii) integration of new observations with existing data of Abu Sari area, and (iii) finally comparison and interpretation of available to data to understand the origin and structural evolution of the mineralized quartz veins.

1.4 Geological Overview of Northern Sudan

Collision between West and East Gondwana ended up with a more than 5000-km-long orogenic belt, and that was an important era in the formation of Greater Gondwanaland (Abdelsalam 1995). This event is called as East African Orogeny (EAO) by Stern (1994); he inferred that most of Neoproterozoic time was occupied by its evolution as an example of a complete Wilson Cycle (Figure 1.8).
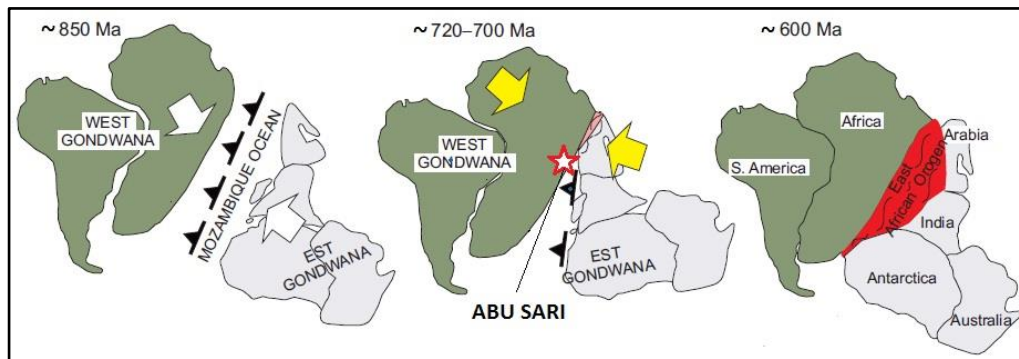
Figure 1.8. Closure of the Mozambique Ocean during the Neoproterozoic resulted in collision of eastern and western Gondwana and formation of so-called Greater Gondwana and East African Orogeny (from Abdelsalam & Stern 1996). Between East and West Gondwana at ~850 Ma Mozambique Ocean started to disappear as they move towards each other with consecutive tectonic activities. The Saharan Metacraton, which was far away from orogenic activity, experienced intraplate an orogenic magmatism between 720 and 700 Ma (Shang et al. 2010b), because of the first collisional contact between East and West Gondwana. 750–720 Ma Egyptian desert gneiss terrane characterizes this event and after the collision, thickening of the asthenospheric mantle end up with sodic-alkaline magmatism. End of East and West Gondwana collision in the South was approximately 600 Ma ago. This process started at the north and continued to the south resulting in the formation of the Mozambique belt. The 5000-km-long suture of the East African Orogeny including the Arabian-Nubian Shield and the Mozambique belt highlights the East and West Gondwana collision belt (from Kongnyuy 2010).

The Precambrian basement of the Sudan and adjacent areas in North-eastern Africa can be divided into two major geodynamic systems, namely gneisses with interfolded supracrustal meta-sediments and a dominantly low-grade juveline ophiolitic island arc assemblage (Vail 1983). The two types of basement comprise distinct tectonic domains: an older (Archean/Early–Middle Proterozoic) sialic continental plate (east Saharan Craton according to Schandelmeier *et al.* 1987) and the Late Proterozoic Pan-African Arabian-Nubian Shield (Gass 1981; Vail 1983), respectively. The high-grade older unit makes up most of the basement exposures west of the River Nile, while rocks belonging to the Arabian-Nubian Shield dominate the region east of the River

Nile.

Study area is situated within the Nubian Desert. The Nubian Desert constitutes part of the Saharan Metacraton and also include a total of 108 gold occurrences (lode and placer types) underlain by Middle to Late Proterozoic rocks (Ahmed 1998). These units called '*the Basement Complex*' consist of older gneisses, metamorphic volcano-

sedimentary sequences, granitoid intrusions, ultrabasic-serpentinitic rocks, volcanic rocks, and alkaline syenite-granite complexes. These rocks are unconformably overlain by Lower Paleozoic and Upper Cretaceous Nubian Sandstones, recent superficial deposits, and sand dunes.

The area consists mainly of a sequence of pervasively schistosed rocks with evidence of regional greenschist facies metamorphism. They form low relief outcrops of dominantly mafic metavolcanics, amphibolites, and chlorite schists. These rock types are generally repeated throughout the sequence (Elsamani *et al.* 2001).

Northern Sudan forms part of the Proterozoic Nubian Shield, and consists mainly of accreted oceanic terrains that were sutured to Gondwana during the Pan-African Orogeny, from approximately 810 to 580 Ma (Stern and Kröner 1993; Goldfarb *et al.* 2001). Gold mineralization has occurred towards the end of this period from ~ 650 to 600 Ma, during a time of collisional deformation and large-scale strike-slip faulting on the east African margin (Stoeser & Camp 1985; Goldfarb *et al.* 2001).

Plutonism occurred throughout this orogenic period, transitioning from sync-orogenic calc-alkaline compositions (El-Nadi 1989), to more alkaline post-orogenic granitoids (Vail 1987). Younger mafic volcanic and intrusive rocks are related to extensional tectonics.

Subject area is located on the NE of the Republic of Sudan which is a part of the Neoproterozoic crust of Nubian Shield (Figure 1.9). Approximately 900−550 Ma arc volcanism and calc-alkaline batholitic granitoids involved terranes are brought into contact along NE-trending arc-arc sutures marked by ophiolite occurrences (Abdelsalam 1998). Evaluation of this boundary is still uncertain because of lack of enough evidence as they are buried under the sands of Nubian Desert. N−S trending, sub-vertical shear zone named as Keraf Zone (Almond and Ahmed 1987) forms the boundary between the Neoproterozoic and Mesoproterozoic rocks (Figure 1.10). Thesis study area is located approximately 250 km west of the Keraf Suture. According to Abdelsalam (2003), a zone of N-trending sinistral strike-slip faults and

N- to NE-trending folds marks the collision zone between the Saharan Metacraton in the west and Arabian-Nubian Shield in the east. This contact is represented by the Third Cataract Shear Zone within which the gold mineralized quartz veins has occurred (Figure 1.11). Approximately 200-km-long and 40-km-wide shear zone (Stern and Abdelsalam, 1996) is well exposed near the Third Cataract Nile. Dominant structures are early N- to NE-trending folds and subsequent N-trending sinistral strike-slip faults (Figure 1.11).
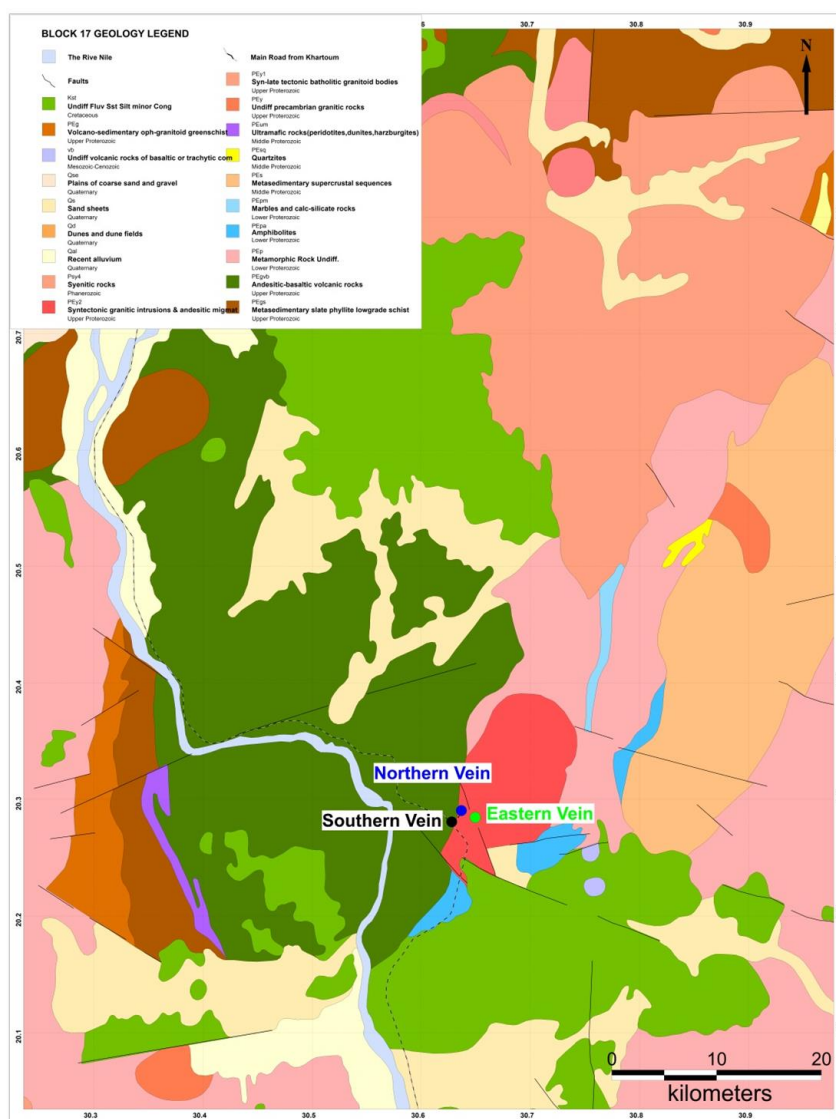
Figure 1.9. Geological map of the study area (Digitized from Geological Research Authority of Sudan, 2004)

14
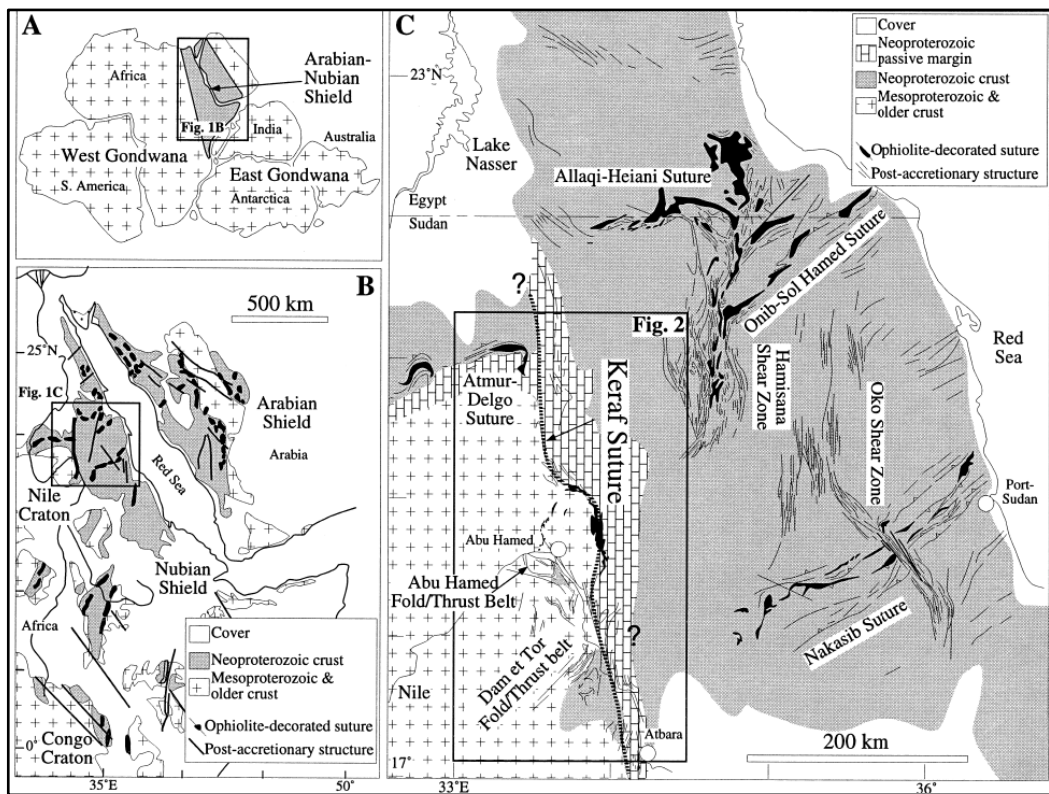
Figure 1.10. Structural and geological features of northern Sudan (from Abdelsalam 1998).
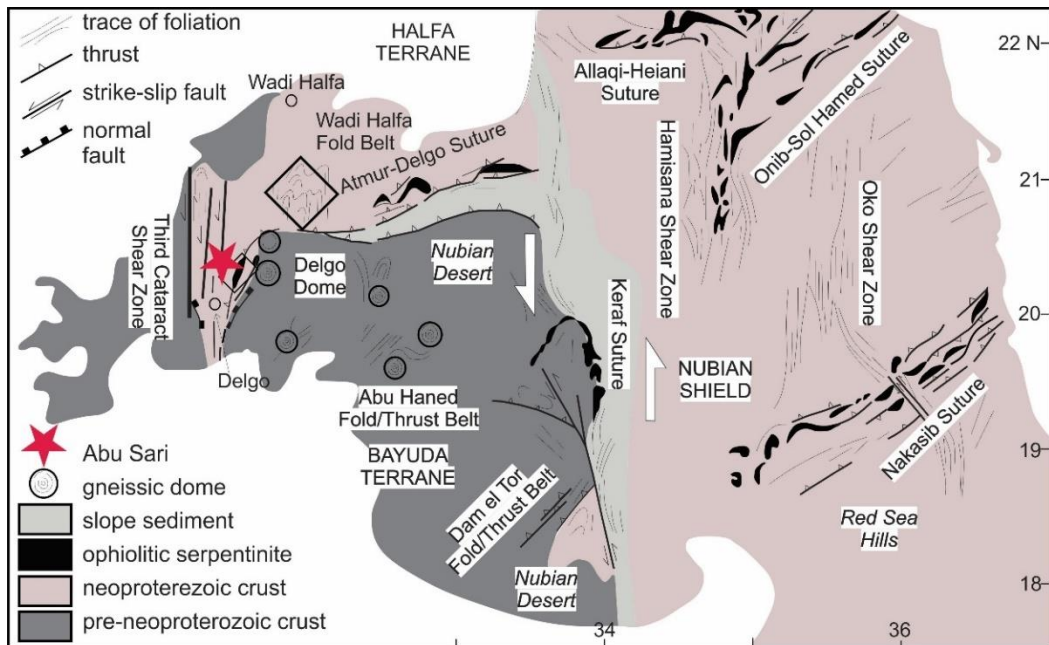
Figure 1.11. N-trending strike-slip faulting at Third Cataract Shear Zone, ~50 km north of Delgo (from Abdelsalam 2003).

15

1.5 Literature

This study is the first to explore the structural control on gold mineralization in Abu Sari area, north-eastern Sudan. There are only few articles written about Abu Sari and Delgo region of north-eastern Sudan as compared to any other parts of the region because of both the remoteness of the area and probably ongoing political issues in Sudan as well. A summary of relevant articles will briefly be presented in this section.

Pan-African Orogeny is focus of interest since the term coined by W.Q. Kennedy in 1964. The subject area is located at the most northern part of that chain of geological events (Figure 1.8).

Kröner and Stern (2004) worked on Pan-African Orogeny and North African Phanerozoic Rift Valley. Their work also covers Saharan Metacraton and Arabian Nubian Shield in which the Abu Sari area is located. Pan-African orogenic cycle formed the main subject of this work and it was attributed to the result of ocean closure, arc and microcontinent accretion and final suturing of continental fragments to form the supercontinent Gondwana. The paper concluded that although arc accretion and continent formation in the Arabian-Nubian shield are reasonably well understood, this process is still very speculative in the Mozambique Belt.

Kröner and Stern (1993) studied Late Precambrian crustal evolution in NE Sudan with isotopic and geochronologic constraints. This study claimed that timing of suturing between East and West Gondwanaland is 600–700 Ma.

J.R. Vail have studied geology of north-eastern Sudan. His research focused especially on geological reconnaissance of northern Sudan (1971), basement complex of northeast Africa (1976), and Pan-African tectonism (1983, 1985, 1988). Although none of his studies is specifically about the subject of the present thesis study, the geological features in Abu Sari area are part of a regional system that Vail studied mostly. He worked on age and structure of the African shield, and mainly concluded that around 1000 Ma Pan-African Mozambique Belt truncates older structures in the eastern Uganda and southern Sudan, which are covered by greenschist volcanic

assemblages. Ca. 550 ± 150 Ma granites and regional metamorphism also occur in the area. In addition, extensive late Proterozoic volcano-sedimentary sequences with associated ophiolite complexes make up the Arabian-Nubian Shield. Granitic to diorite batholithic rocks and younger syn-orogenic to late orogenic calc-alkaline igneous complexes disrupt the layered sequences.

Collision of Arabian-Nubian Shield with West Gondwana and the fragments, which are preserved as the Saharan Metacraton along Keraf Suture about 600 Ma ago, have always been very attractive for many scientists (Vail 1983, 1985, 1988; Almond & Ahmed 1987; Abdelsalam & Dawoud, 1991; Abdelsalam *et al.* 1995, 1998, 2000; Abdelsalam & Stern 1996) and mine exploration companies for several decades.

Stern and Dawoud (1991) concluded that an episode of deep-seated igneous activity occurred in northeast Africa with the association of granite, charnockite, and enderbite dated at ~740 Ma.

Upper Cretaceous−Tertiary basalts from the Nubian Desert have been studied in terms of their K-Ar ages, Sr-isotopic compositions and chemistry (Satir *et al*. 1991). The REE patterns of basalts are consistent with partial melting of mantle peridotites. Magma production peaked close to the Cretaceous−Tertiary border at about 70 Ma in the northern region (Kerma) and 60 Ma in the southern region (Bayuda Desert). Sr isotope initial ratios indicate a depleted upper mantle source, with typical values around 0.7031 (Kerma region) and 0.7030 (Merowe/Bayuda Desert region).

Late Cretaceous to early Tertiary igneous rocks are also studied Franz *et al*. (1993) where age, geochemistry, structural features of different rock types are described. This work mainly concludes that volcanic activities are present in whole NE African craton, as mainly represented by basaltic magmatism during Late Cretaceous to Tertiary time interval, with minor activities during the Jurassic and Triassic.

Abdel-Rahman *et al*. (1993) studied Keraf back-arc basin and Nubian Shield margin of Abdel in northern Sudan. In the discussion part of the article, he summarized that the Gabgaba suture (a highly strained N−S-trending lineament) is the boundary

between Nubian Shield and the craton in the west of Nile. This major boundary is a broad swinging zone rather than a simple N−S-trending structure, since at least two divisions, the Nakasib and Delgo sutures, are present.

Denkler *et al.* (1994) also examined tectono-metamorphic evolution of the Neoproterozoic Delgo suture zone, Northern Sudan. They worked along narrow NNE-trending Neoproterozoic belt of low-grade volcano-sedimentary rocks with high grade migmatite basement rocks.

Schandelmeier *et al*. (1994) identified a previously unrecognized belt of ophiolitic nappe remnants in north-eastern Sudan. The ophiolite belt is interpreted as a suture, namely the Atmur-Delgo suture zone, and is composed of serpentinites and carbonitized rocks that are very close to the study area (Figure 1.12). The NE-trend of this zone shows similarity between shear zone(s) that controls the gold mineralization in the area.

Geochemical and radiogenic isotope constraints about the Neoproterozoic Delgo suture zone, the evolution of the suture zone and understanding of crustal growth in Northern Sudan have formed the subject of a research by Harms *et al*. (1994). This study concluded that formation of ocean floor has taken place in or similar to a supra-subduction environment at 750 Ma.

Intrusion of syn-tectonic subduction-induced batholiths into the continental margin and the neighbouring island arc has occurred during 760−650 Ma. The continental shelf sediments and HGB-West were metamorphosed at about 700 Ma during the closure of the oceanic basin and the ophiolite was probably obducted at this time. A third final event at about 550 Ma affected the whole area and gave rise to large-scale late tectonic granite intrusions.
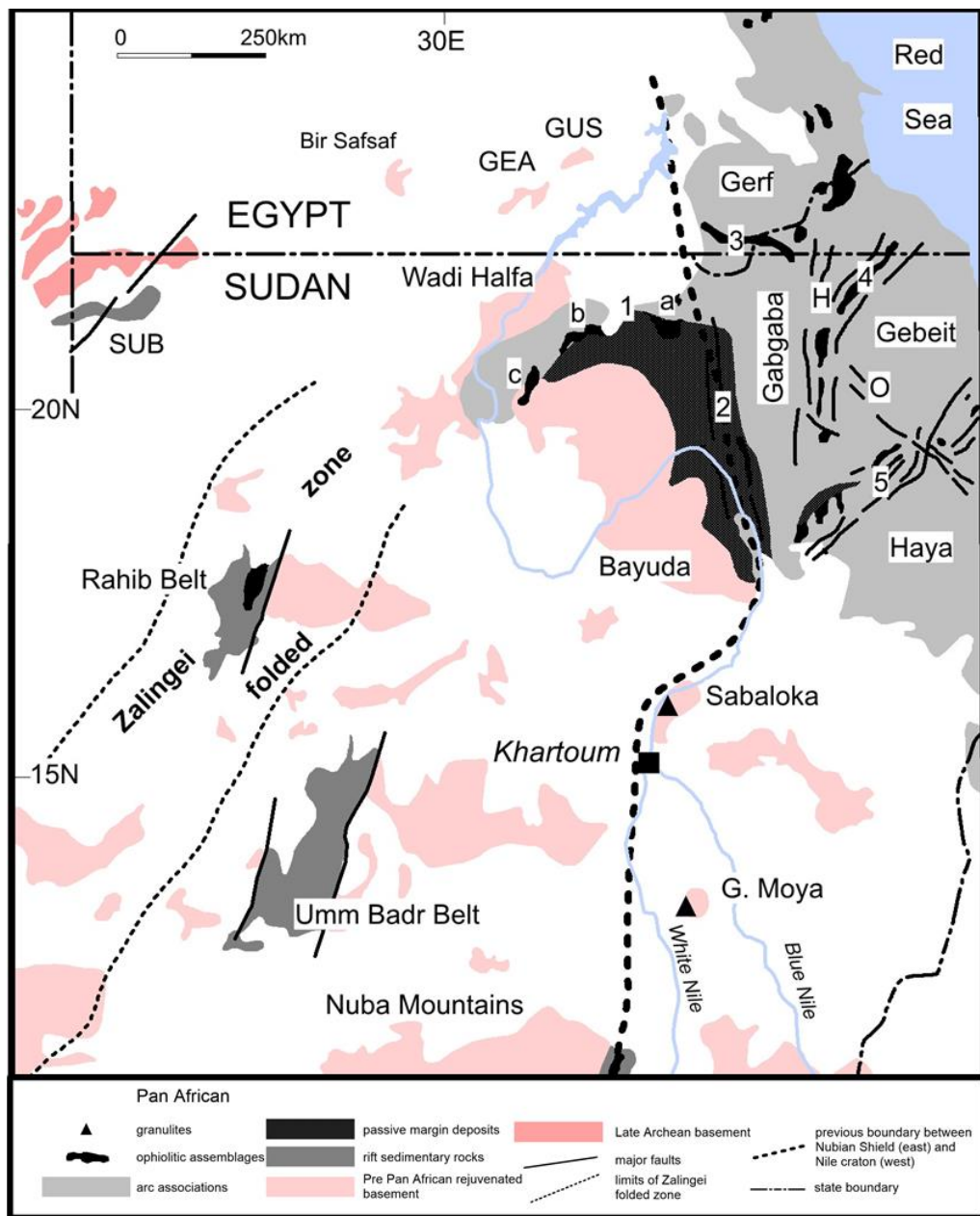
Figure 1.12. Geological map of northern Sudan showing distribution of major rock types and geological structures (from Schandelmeier et al. 1994). 1– Atmur-Delgo suture with (a) Siniat ophiolite, (b) Atmur ophiolite, (c) Delgo ophiolite, 2– Keraf zone, 3– Allaql-Heiani suture, 4– Onib-Sol Hamed suture, 5– Nakasib suture, O– Oko shear zone, H– Hamisana shear zone, SUB– Southern Uweinat belt, GEA– Gebel El Asr, GUS– Gebel Umm Shaghir.

Höhndorf *et al*. (1994) performed Rb-Sr isotopic analyses on 14 selected anorogenic alkaline igneous complexes. They concluded that that the igneous activity in the Sudan appears to be essentially continuous from Neoproterozoic to the Cenozoic.

19

Stern *et al.* (1994) studied evolution of the east Saharan Craton. This paper provides new geochemical and isotopic data on the evolution of the western foreland to the Nubian Shield of north-east Africa.

Mohamed G. Abdelsalam is one of the scientists who have worked in north-eastern Sudan. His studies with Robert J. Stern shed light on Precambrian structures of north-eastern Sudan (Abdelsalam and Stern 1996), Neoproterozoic deformation in the north-eastern part of Saharan Metacraton (Abdelsalam *et al.* 2003), and deformational history of the Keraf Zone (Abdelsalam *et al.* 1995, 1998). For Keraf zone they suggested that oblique collision between arc terranes of the Arabian-Nubian Shield and the Nile craton along the Keraf zone has occurred at ~750−650 Ma.

Abdelsalam and Stern published two papers in 1993. One of them concluded that Nakasib suture (Red Sea Hills, northern Sudan) has evolved through a complete Wilson cycle orogeny from rifting, through passive margin formation, to closure of the basin and suturing. The second paper was about the Nakasib suture, examination of other sutures of the Arabian-Nubian Shield.

One of his leading paper is about Saharan Metacraton and is co-authored with Jean-Paul Liégeois and Robert J. Stern (Abdelsalam *et al.* 2002). Arabian-Nubian Shield forms the basement in north-eastern Africa and represents a juvenile continental crust (Abdelsalam & Stern 1996); the study area is located at its most western part (Figure 1.13).
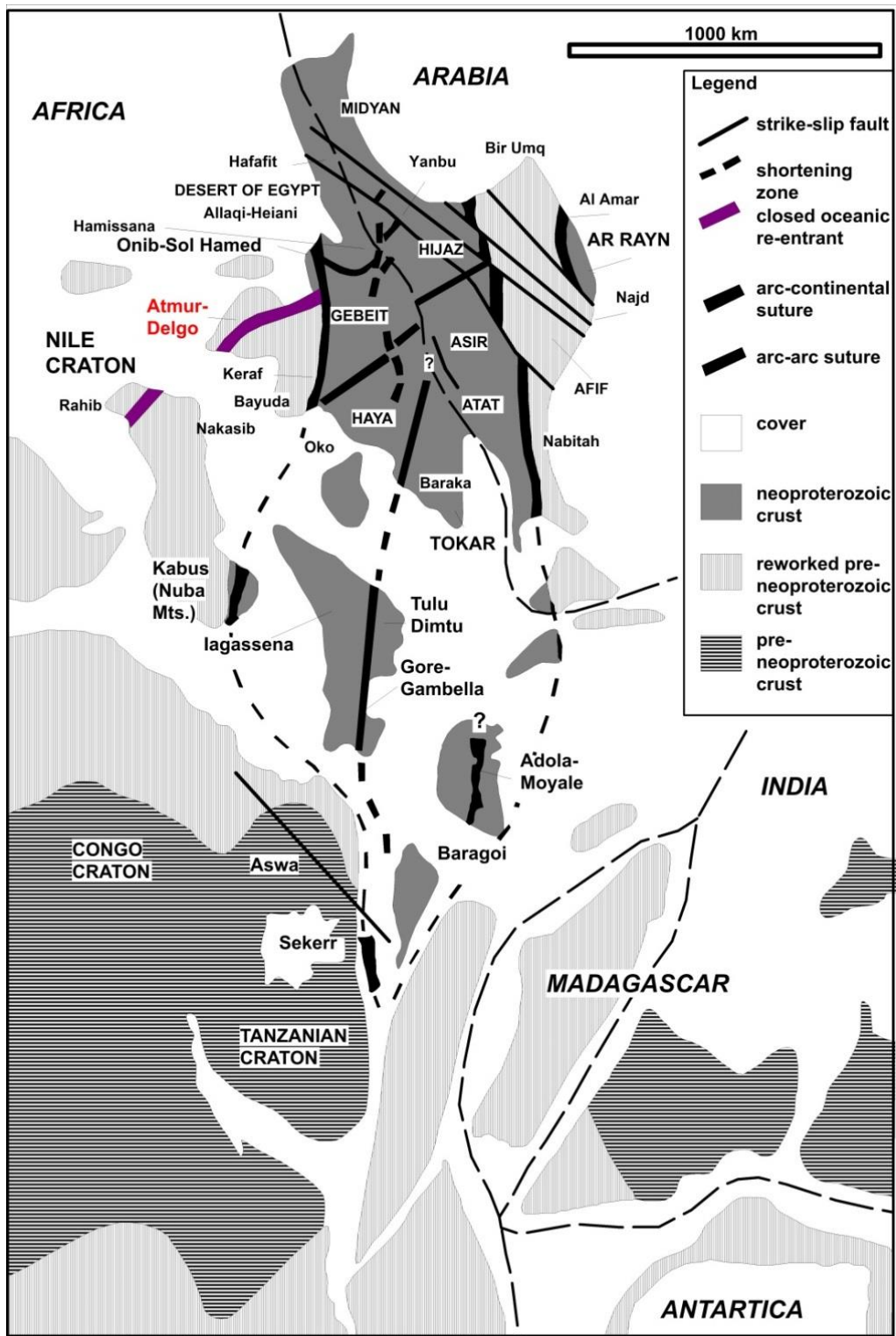
Figure 1.13. Sketch tectonic map of the Arabian-Nubian Shield (from Abdelsalam & Stern 1996).

A structural and petrological study (Blasband *et. al.* 2000) was about an extensional metamorphic core complex in the northern Arabian-Nubian shield with the presence of the Late Proterozoic rocks in the Wadi Kid area, Sinai, Egypt.

Pan-African gold mineralizations in the Red Sea Hills of Sudan has been studied by Elsamani *et al.* (2001). Gold mineralizations are classified. They concluded that gold mineralization in the Pan-African domains occurs near sulfide mineralization zones, and that mineralization commonly occur in zones of collapse of the extensional basins and/or collisional sutures, and along shear zones that formed during the 650 Ma and 550 Ma orogeny.

The Precambrian basement of the Arabian-Nubian Shield is very attractive for modern gold exploration companies as it hosts around 250 gold production sites; many were mined during different periods of ancient Egyptian history (Klemm *et al.* 2001). One of these sites is examined in detail during this work (Figure 1.14).
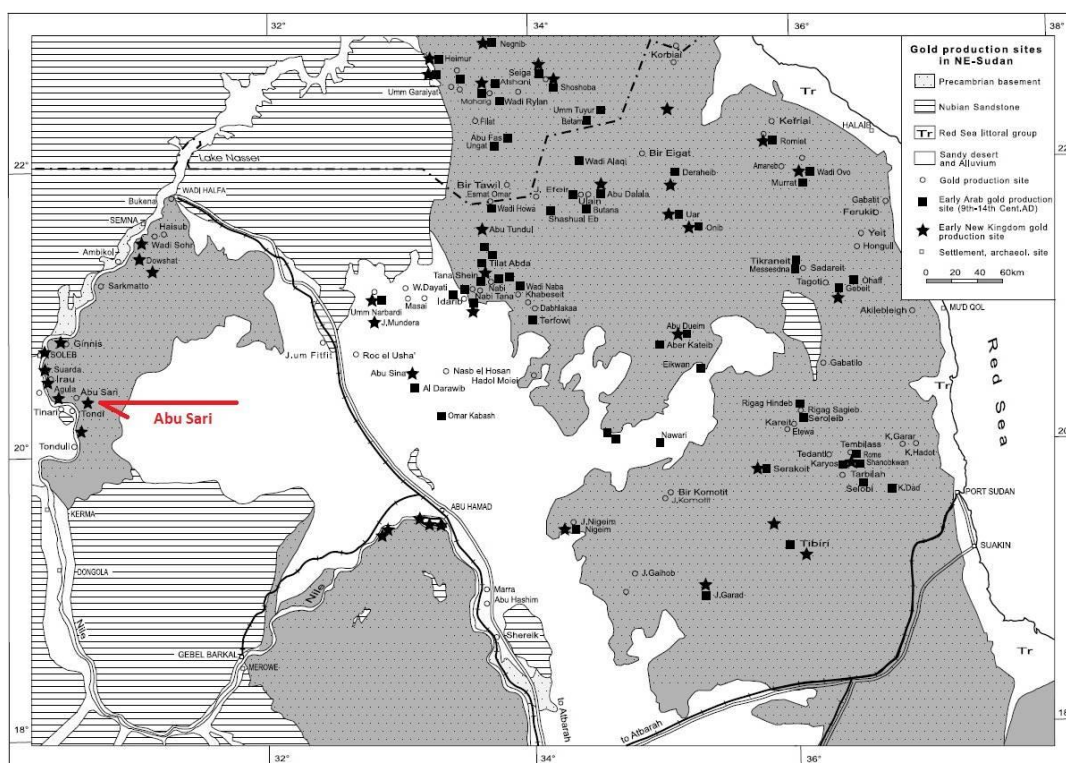
Figure 1.14. Distribution of the gold production sites in north-eastern Sudan (from Klemm et al. 2001).

22

The book entitled '*Gold and Gold Mining in Ancient Egypt and Nubia: Geoarchaeology of the Ancient Gold Mining Sites in the Egyptian and Sudanese Eastern Deserts*' by Rosemarie Klemm and Dietrich Klemm has two editions: published by Springer Berlin Heidelberg Media in 2012 and by Springer Science & Business in 2013. The book covers historical evolution of gold mining activities in the Egyptian and Nubian Desert (Sudan). This book is a milestone for gold explorers in the region.

The geochronological data from the area of interest is scarce; there are few zircon U-Pb ages from the granitic intrusion exposed in central North Sudan near Abu Sari − a neighbouring region to the study area.

Küster et al. (2008), looked for an evidence of a Bayudian event (920–900 Ma) preceding the Pan-African orogenic cycle (860–590 Ma) at the eastern boundary of the Saharan Metacraton with the help of zircon geochronology and Sr, Nd, Pb isotope geochemistry of granitoids from Bayuda Desert and Sabaloka (Sudan).

According to the zircon U-Pb age analyses of Kongnyuy *et al.* (2012) from the selected six rock samples, there are four different age groups: 3025 Ma, 728 to 702 Ma, 630 to 600 Ma, and 554 Ma (Figure 1.15).

Shang *et al.* (2010) published two papers on zircon and titanite ages from the central north Sudan basement and ring complex granitoids of Sudan. For the central north Sudan west of the Keraf suture, crystalline basement of the Saharan Metacraton encompasses migmatite gneisses and granites; whole rock geochemistry indicates an I-type potassic calc-alkaline meta- to peraluminous composition. Granite zircon U–Pb and Pb–Pb evaporation analyses yield an identical age range (597±25 – 602±3.5 Ma). Similar ages (597±8.6 – 603.8±2 Ma) are obtained for the migmatite gneisses as well. On the other hand, in the second paper the authors concluded that 707–718 Ma A-type magmatism in Sudan was caused by the collisional contact between East and West Gondwana. The 600 Ma titanite recrystallization ages are referred to tectono-thermal

effects of the culminating phase of the Pan-African Orogeny during collision of East and West Gondwana, forming the Mozambique belt.
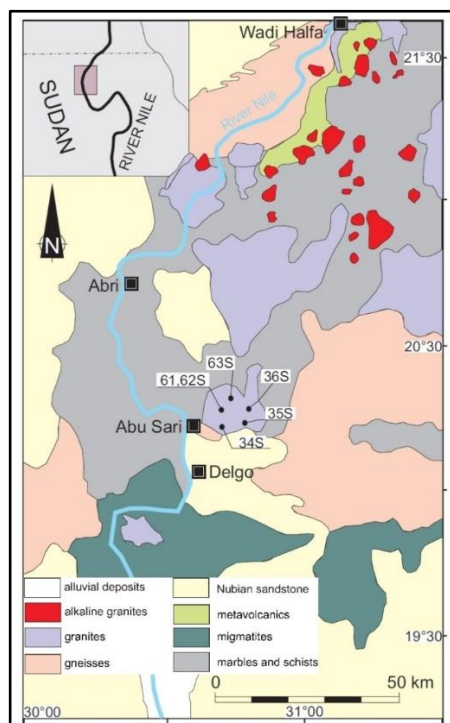
Figure 1.15. Sample location map of Kongnyuy et al. (2010)

Mokhles K. Azer (2014) studied the petrology of the Neoproterozoic serpentinized ultramafics in the Nubian Shield. Spinel compositions suggest that the mantle peridotites of the Gabal El-Degheimi area are similar to fore-arc peridodites of suprasubduction zone environments.

Babiker *et al.* (2015) conducted geological mapping and gold prospecting studies, based on remote sensing, at 80 km north of Abu Sari. GIS applications are used in mapping and gold prospecting with ground check and sampling.

As a mineralogical study on magmatic arc rocks that hosts porphyry Cu-Au mineralization in the Gebeit area of the NE Sudan is also conducted (Bierlein *et al.* 2016). The study mentioned about the similarities between Neoproterozoic magmatic-hydrothermal system and Tertiary–Cenozoic porphyries in circum-Pacific metallogenic belts.

Ibrahim *et al*. (2016) studied structural and litho-tectonic controls on Neoproterozoic base metal sulfide and gold mineralization in North Hamisana shear zone. Although the Gebeit area and Hamissana area are approximately 500 km far away from this thesis study area, this work is considered among important studies to understand different types of mineralization in NE Sudan region.

Late Neoproterozoic adakitic lavas in the Arabian-Nubian shield, Sinai Peninsula, Egypt formed the subject of article by Abdelfadil *et al*. (2018). They studied, at the northernmost segment of the Arabian-Nubian Shield, the Sahiya and Khashabi volcano-sedimentary successions exposed near the southern tip of the Sinai Peninsula. The authors described two distinct eruptive phases in the series of intermediate to acidic lavas and associated pyroclastic deposits of Neoproterozoic successions. The first eruptive phase, well exposed at Wadi Sahiya, includes basaltic andesite, andesite and dacite with minor rhyolite. The second eruptive phase, well exposed at Wadi Khashabi, includes only dacite and rhyolite.

El-Bialy and Shata (2018) studied granitoides of Yahmid-Um Adawi area, located in the southeastern part of Sinai Peninsula; two coeval suites are described: post-collisional alkaline (608–580 Ma) and calc-alkaline (635–590 Ma) granitoides. The calc-alkaline granitoids are magnesian and peraluminous to metaluminous, whereas the alkaline ones are magnesian to ferro-alkaline to slightly metaluminous. Both granitoid suites exhibit many of the typical geochemical features of A-type granites.

Cox *et al.* (2018) studied Late Neoproterozoic adakitic magmatism of the eastern Arabian Nubian Shield and dated at 633.2±9.0 Ma. They intrude the forearc Ad Dawadimi Basin, which is composed of metapelitic schists and greywacke along with ophiolitic mélanges of boninitic affinity; they have undergone inversion and deformation by ~ 620 Ma. This adakitic magmatism, while intruding parts of the Ad Dawadimi Basin, pre-dates this deformation, but is possibly coincident with basin closure.

CHAPTER 2

DESCRIPTION OF ROCK UNITS

2.1. Introduction

Abu Sari region rock units are represented mainly by greenschist facies metamorphic rocks and granitic intrusions that record regional tectonism and metamorphism during Pan-African Orogeny (at approximately 700 Ma ago) in northeast Africa. These rocks are overlain unconformably by Cretaceous Nubian sandstones; cover of wind-blown sands and unconsolidated debris is extensive (Vail, 1976). The auriferous and barren quartz veins occur in both greenschist facies rocks and granite(s). General trend of quartz veins is E−W; there are also N−S-trending quartz veins as well (Figure 1.1). Quartz floats cover large area(s) as patches; they show a clear trend at some parts and are interpreted as cover above buried quartz veins.

As is summarized in Chapter 1, basement complex of Arabian-Nubian Shield has previously been studied by many scientists (e.g., Vail 1971, 1976, 1983, 1985, 1988; Abdelsalam *et al.* 1995, 1998, 2002). Previous studies have mainly focused on the age of different rock units and tectonic cycle of Pan-African Orogeny. In the present study, we aimed at mapping different lithologic units, which are host rocks to quartz veins; a special emphasis is given to study/explore for gold mineralization controlling structures (Figure 2.1 and 2.2). 1:200-scaled open pit wall maps from the available parts of the mine site formed the fundamental part of this study in order to understand structural control on gold mineralization. Of course, general geological mapping of the area (modification of previous geological map) was also carried out. The available geochemical data is integrated and interpreted as well. Petrography of host rocks to quartz veins is also performed. During mapping, foliation and mineral lineation are also measured.

27
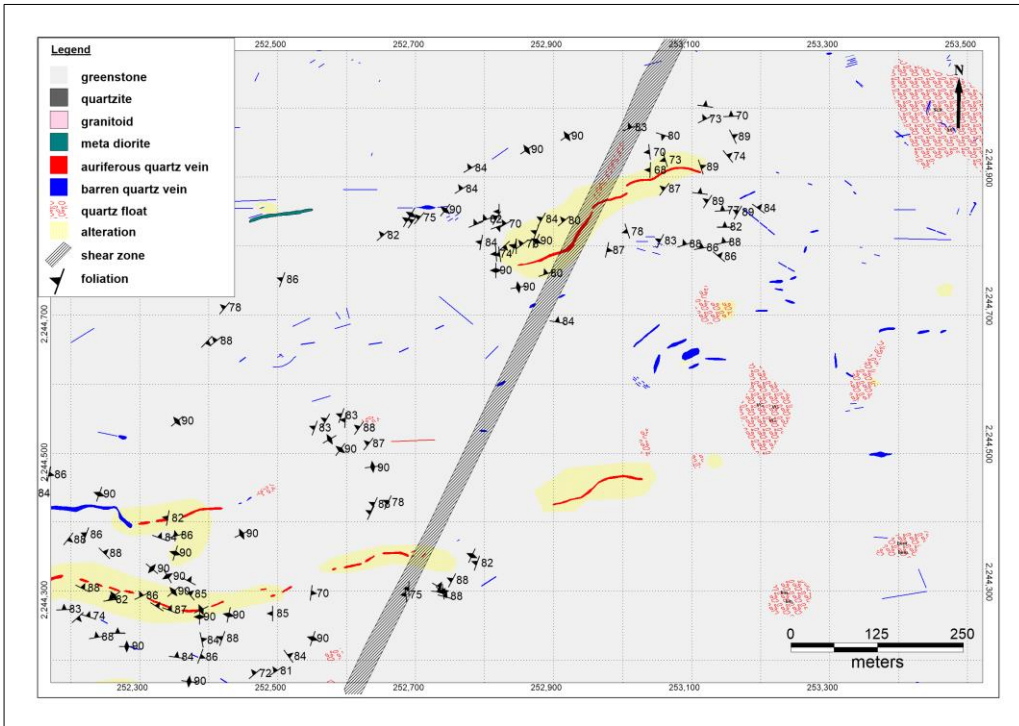
Figure 2.1. Geological map of the Southern and Northern veins at 1:5000 scale.
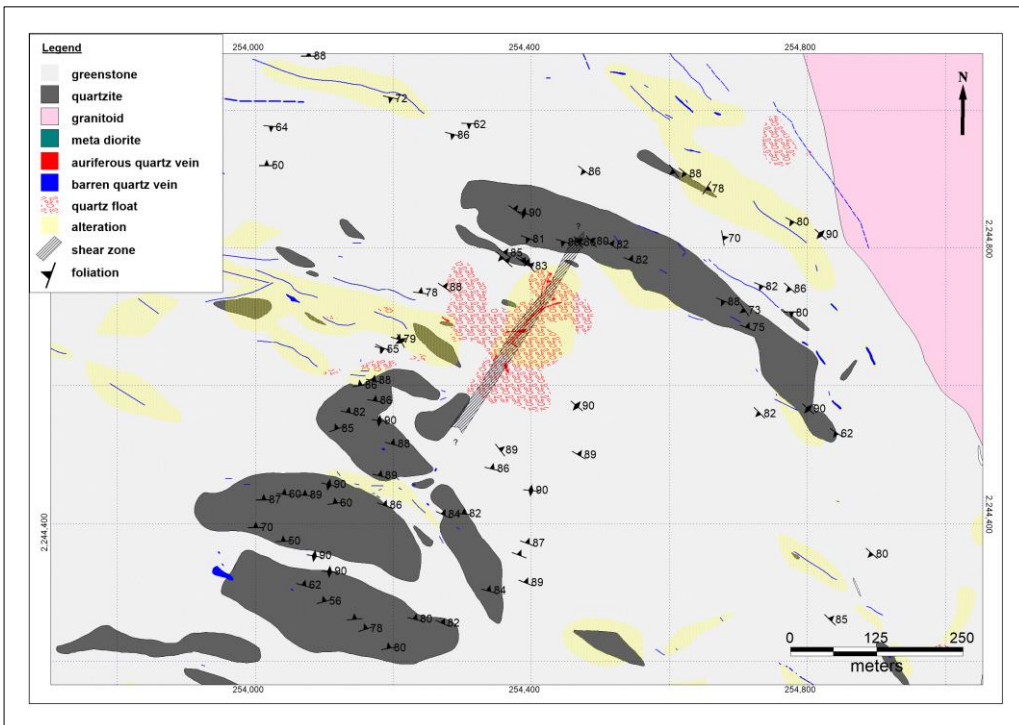
Figure 2.2. Geological map of the eastern vein at 1:5000 scale.

28

2.2. Rock Units

Three different rock units are mapped in the study area: (1) greenstones, (2) quartzites, and (3) granitic intrusions. In addition to these, quartz veins are the most important elements.

2.2.1. Greenschist Facies Greenstones and Quartzites

Metamorphic rocks are classified in subdivisions according to their reveal temperature and pressure conditions in the earth. One of the major divisions is greenschist facies which the rocks formed typically under temperatures around 400°C and pressures of 1 to 4 kilobars. These low temperature and pressure conditions are generally associated with regional metamorphism. Cause of the rocks to be greenish and schistose is colour of many common minerals, such as orthoclase, muscovite, chlorite, serpentine, talc, and epidote.

Greenstone is a dark basaltic rock that once was solid deep-sea lava metamorphosed at greenschist facies conditions during regional metamorphism (Figure 2.3). They are composed of epidote, chlorite, actinolite and/or green amphiboles. They form the most abundant rock type in the study area; they are exposed in a large area that extends from Nile to the Red Sea. The protolith rocks are interpreted as basalts, rhyolites, intermediate volcanic rocks and sediments of the Nubian Shield. Granitic intrusions invaded these greenschist facies rocks (cf. Vail 1976).
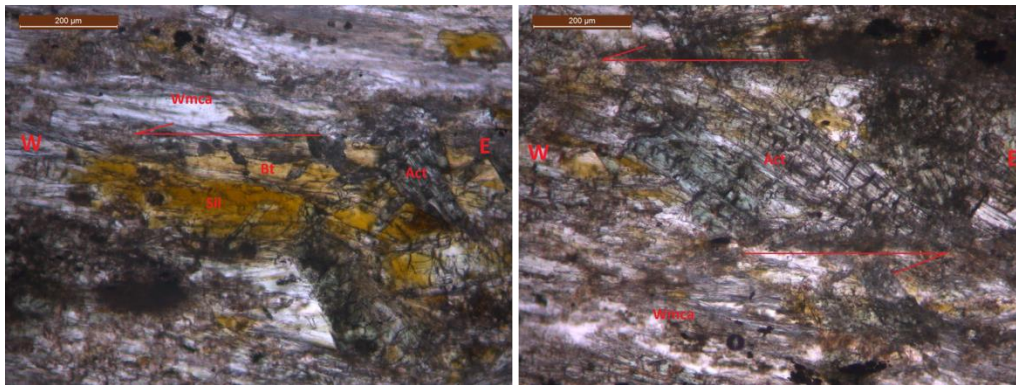
Figure 2.3. Greenstone oriented sample thin section view showing top to the left (west) motion according to the shaped of the minerals. Wmca = White Mica. Bt = Biotite. Sil = Sillimanite. Act = Actinolite.

The rock has a typical dark colour known as black desert varnish; the fresh exposures, however, display a typical green colour. In fact, black desert varnish is common to all rocks and many occasions fresh exposures are need for distinction and description of variable rock types (Figure 2.4).

Figure 2.4. Field view of greenstone with quartz veinlet (qv). Pen is 10 cm long.

Greenstone is pervasively altered at the edges of especially southern vein of the Abu Sari area. The altered rocks are marked by white colour along margins of the quartz veins. As gets far from the vein, the colour becomes light yellow to dark yellow; as

soon as it is fresh, the rock is green again. Main alteration is argillic with mostly sericite and illite minerals. Carbonitization is also observable at some parts, especially at northern vein system (Figure 2.5).

Figure 2.5. ~5-meters-long wall with pervasively altered greenstone at the edge of mined out quartz vein. Note white to yellow colour of altered zones.

Pyrite mineralization and iron oxide formation as a result of weathering of pyrite is common especially in areas where gold mineralization exists. Pyrite cubicals are also visible along slickensides of the strike-slip faults (Figure 2.6).

Figure 2.6. Oxidized pyrite cubes along NW−SE-striking strike-slip fault plane.

The foliation is penetrative and mineral lineation is visible. The generally trend of foliation is NNE–SSW (015–020°) (Figure 2.7a) while the foliation trends in ~N–S direction (000–010°) in the southern vein pit (Figure 2.7b).
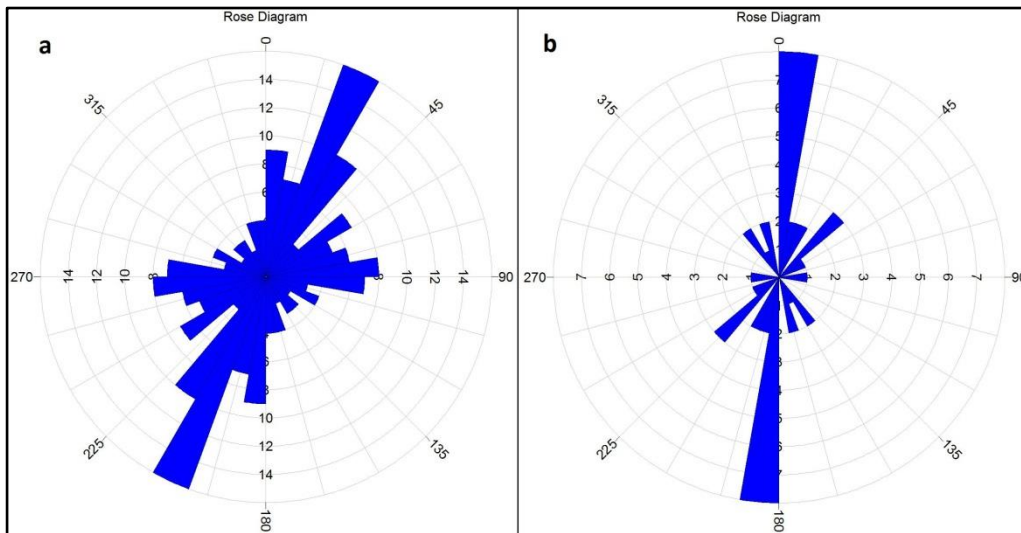
Figure 2.7. Rose diagrams of foliation trend of the greenstones (a) in general (207 measurements) and (b) in the southern vein pit (110 measurements).

Greenstones in the Abu Sari area are metamorphosed pyroclastic rocks intercalated with schists, slates and marbles; metaconglomerates are common in the east and west of the study area. They are composed mainly of quartz pebbles within a sandy matrix (Agula Unit; Denkler *et al.* 1994).

According to Babiker *et al.* (2015), gold mineralization in Wadi Umm Beckol-Wadi Akasha area, which is located nearly 80 km north of Abu Sari area, is related with quartz veins in the silicified carbonate graphitic schist, the finely-crystalline quartzite, and the areas of shearing, silicification in the metavolcanics with carbonatization.

Quartzite in the Abu Sari region is a type of metamorphic rock which is originally sandstone. They form relatively large exposures especially in eastern vein area. Because of its resistance to weathering, quartzites stand out and form black and sharp ridges; their physical appearance is therefore used as criteria for their recognition from a distance (Figure 2.8).

Figure 2.8. Field view of quartzites from eastern vein area. Note typical desert varnish colour.

Similarly, gold mineralization in Abu Sari is related with (1) altered greenstone including sericitic and illitic minerals, (2) sheared, carbonatized, and silicified shearing zones, and (3) finely-crystalline quartzite in association with a syn-tectonic granitic pluton.

2.2.2. Granitic Intrusions

Syn-tectonic granitic intrusions of Abu Sari region are mapped as Upper Proterozoic rocks in the geological map of Sudan, prepared by Geological Research Authority of the Sudan (GRAS 1988) (Figure 2.9).

Figure 2.9. Digitized geological map of Northern Sudan, Abu Sari area (from Geological Research Authority of the Sudan).

As the geology map of GRAS is in 1:1000000 scale, some details would be overlooked. The exact boundary of this granitic intrusion is just very close to eastern vein (Figure 2.10).
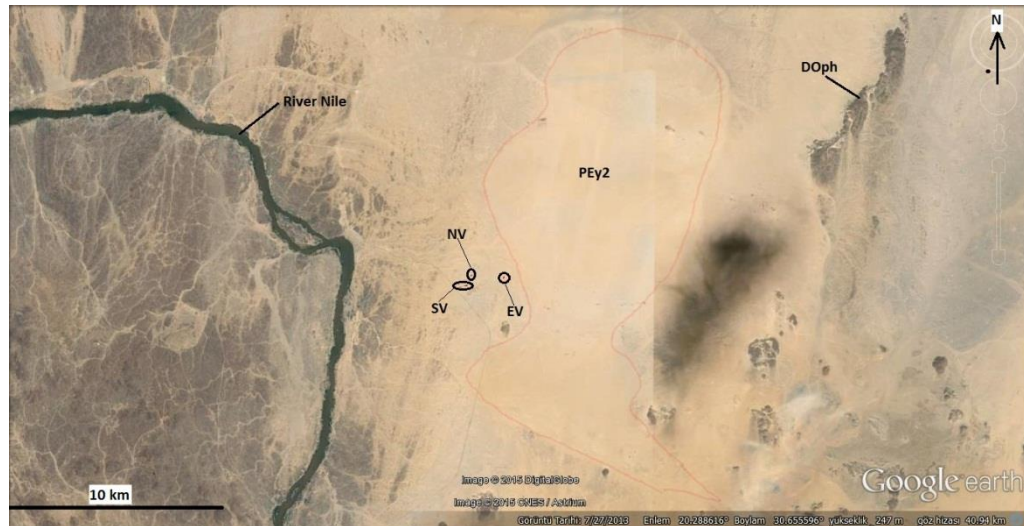
Figure 2.10. Google Earth Image from the study area, showing approximate boundary of the syntectonic granitic intrusion and locations of the open pits. DOph− Delgo Ophiolite, PEy2− Syntectonic granitic intrusion, NV− Northern Vein, SV− Southern Vein, EV− Eastern Vein.

Kongnyuy *et al.* (2010) studied the age, petrography, and geochemistry of the syntectonic granitic intrusion of Abu Sari. Age comments of this study mentioned shortly before in literature survey part (see section 1.5). According to this study, there are three different textures at different parts of the granite: (i) non-foliated rock with centimeter size feldspar phenocrysts, (ii) slightly foliated rock with less feldspars, and (iii) strongly foliated dark grey rock. These rocks with different textures are characterized with similar mineral content; plagioclase, potassium feldspar, hornblende, quartz, and biotite from essential minerals. Varying ranges of SiO_2 content of 65−75 wt.% imply felsic composition.

Granite in the study area is pinkish, slightly foliated and is composed of 1−2 cm feldspar-hornblende phenocrysts, few biotite and quartz. Argillic alteration, which is probably supergene, is observed along margins of quartz veins (Figure 2.11). Quartz

35

veins in the granite are barren with only minor gold mineralization along localized parts/zones.
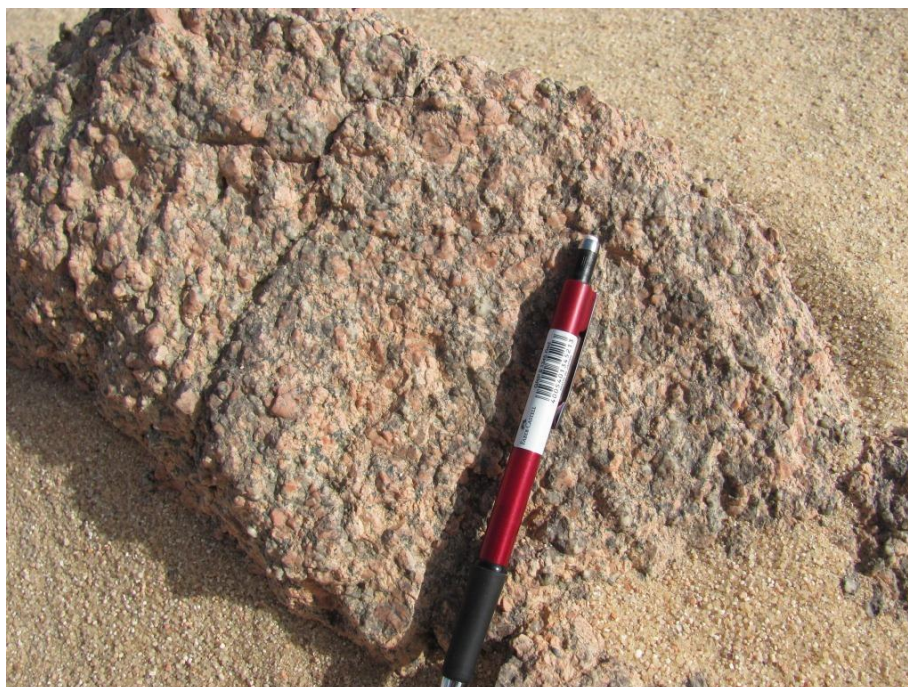
Figure 2.11. Close-up view of the syn-tectonic granitic intrusion, ~500 m east of Eastern Vein. Note large pinkish feldspar crystals. The dark coloured minerals are hornblende. Pen is about 10 cm long.

2.2.3. Quartz Veins

Quartz veins are very dense and distributed all over the Abu Sari greenschist units and granitic intrusion. They are oriented mainly in E–W; occasional NW–SW and NE–SW-trending veins are also present (Figures 2.1, 2.2 and 2.11). They show variable textures, thickness, mineralization, and lengths. Vein widths range from a few centimetres to more than 10 m; their length may reach up to one km.

Some veins, especially the ones located ~350 m north of the northern vein, are folded along with the metasedimentary rocks of the greenschist facies. On the other hand, quartz veins that cut the granitic intrusion are straight, planar and not folded (Figure 2.12).
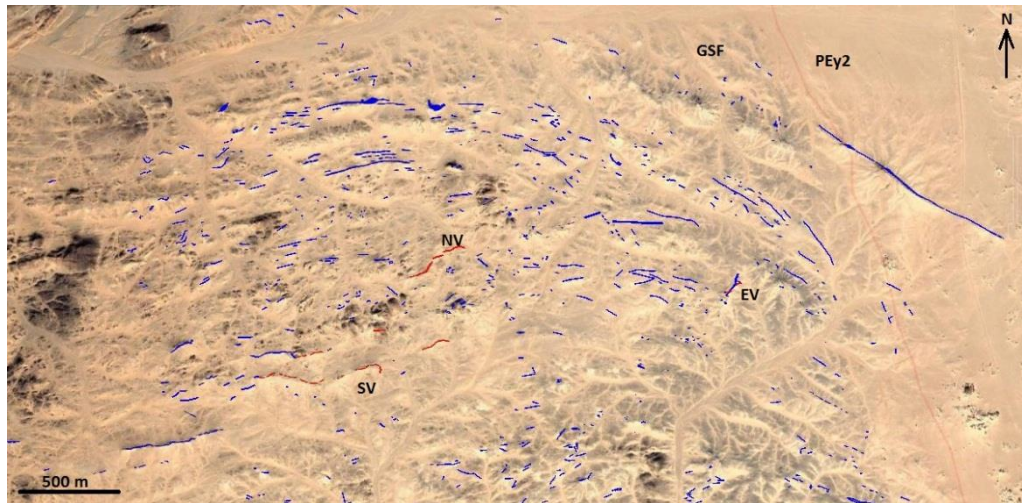
Figure 2.12. Google Earth image of Abu Sari quartz vein zone. Blue indicates barren and red, mineralized quartz veins. PEy2– syntectonic granitic intrusion, GSF– Greenschist Facies, NV– Northern Vein, SV– Southern Vein, EV– Eastern Vein.

There are 3 major trends of quartz veins: (1) E–W-trending veins are mostly folded because of regional tectonism or undulated because of strike-slip faulting (southern vein system); (2) NW–SE-trending veins are concordant with foliation in the folded metasedimentary rocks and mostly have no gold mineralization, and (3) NE–SW-trending undulated veins with strike-slip content (some part of northern vein and eastern vein systems). In addition to these, there are a few N–S-trending quartz veins in the region. A great majority of the quartz veins are steeply dipping between 75° and 90°.

Four principal types of quartz veins are observed in the Abu Sari area: (1) milky white coloured massive bull quartz veins with no gold mineralization; (2) white and grey coloured, oxidized, fractured massive quartz veins within altered greenstone-pyrite and gold mineralization are common; (3) tension cracks adjacent to massive quartz veins filled with quartz; and (4) boudinaged mineralized quartz veins lacking alteration selvedge.

Milky white colored bull quartz veins are very hard, resistant, non-fractured and are associated with breccia and stockwork textures in some places (Figure 2.13).

Figure 2.13. Close-up views from barren milky bull (in the left) and brecciated quartz veins (in the right).

The most important type of quartz vein in the field is massive veins as they carry gold. These veins cut general foliation trend in the greenstones. They are not present in granitic intrusions. Fractured texture of massive grey quartz veins let gold-bearing fluids to penetrate and deposit. The contact between host rock and the massive quartz vein is not straight but curved because of deformation associated with strike-slip faulting; such relationships are well exposed on the walls of the open pits. The veins are mainly composed of quartz with gold, pyrite, iron oxides (hematite, limonite), tourmaline and rare malachite.

An alteration halo, leading to various amounts of silicification, sericitisation, sulfidation, and argillic alteration (illite) of the host rock, over a couple of metres distance, is associated with the sites of hydrothermal circulation and gold-bearing vein deposits (Figures 2.14 and 2.15). The massive and internally deformed nature of these bull quartz veins suggests that they have formed progressively during faulting. In addition, the variety of quartz vein types changing from bull veins, folded veins, boudinaged veins, fault-related veins, breccia veins, and different trends of the vein systems suggests more than one phase of veining. These stages are most probably both syn-deformational and post-deformational with respect to Pan-African Orogeny.
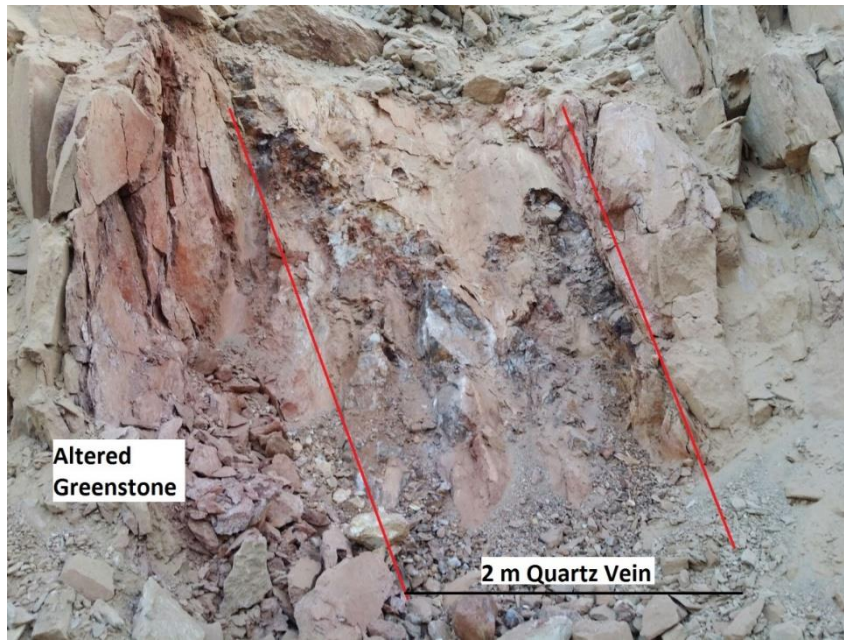
Figure 2.14. Oxidized gold ore of E–W-trending southern vein dipping to the north. Alteration zones in greenstone wallrocks are common. Distance between two red lines is about 2 meters.

Figure 2.15. Hand specimen of fractured massive grey quartz vein from southern vein (a) and closer photo of hand specimen showing iron oxide minerals and gold filling fractures in the quartz vein (right). (Pen is 10-cm long).

Tension cracks adjacent to the auriferous quartz veins are very common especially at southern vein open pit walls. These types of quartz veins, with some exceptions, have

no gold mineralization (Figure 2.16). Most are gash fractures, suggesting a possible semi-brittle shear zone deformation. Although tension fracture filling quartz veins don't have any gold mineralization, vein orientations are used to determine the kinematics where high pore fluid pressure predominate (many hydrothermal environments).
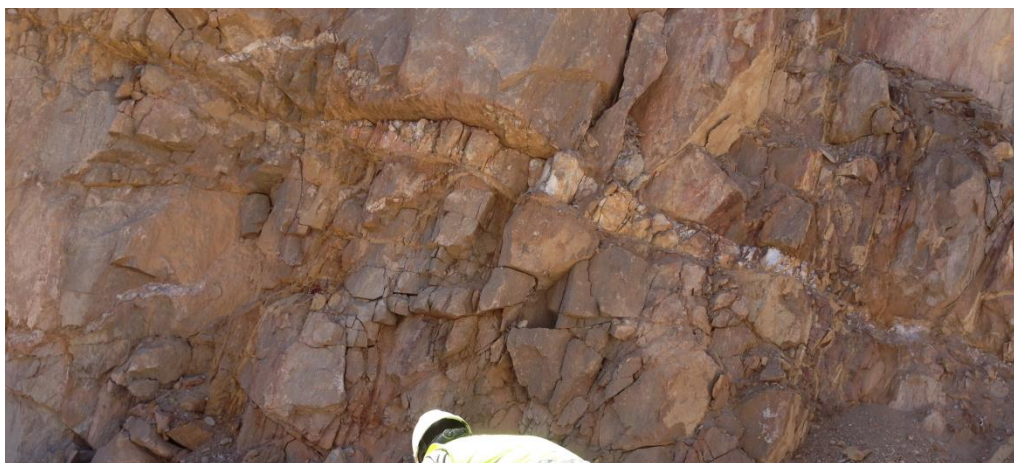
Figure 2.16. Tension crack (arrowed) filled with intensely jointed quartz vein at the wallrock of the southern vein.

Mineralized boudinaged quartz veins are only observed near eastern veins at Abu Sari region. They have no alteration selvedge and develop parallel to general foliation in the host rocks. These veins also show pinch-and-swell structures. They are almost perpendicular with changing thickness from 5 centimetres to 1 meter (Figure 2.17).

At the eastern vein area of Abu Sari, boudinaged quartz veins are cut and displaced by massive eastern vein. The jointed texture and gold-bearing geochemistry of these boudinaged veins may be attributed to their close relationships with mineralization of eastern vein.
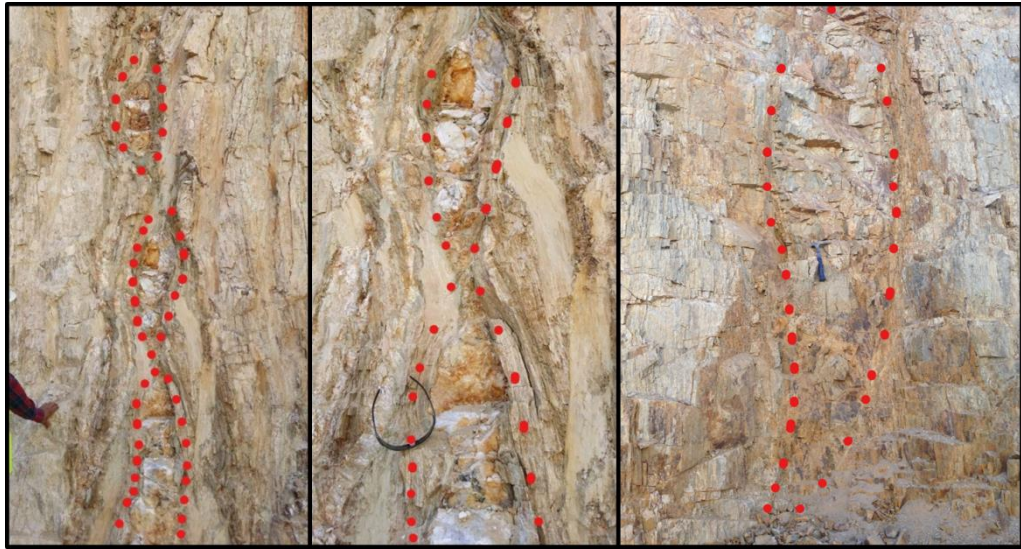
Figure 2.17. Field views from the boudinaged quartz veins cut by massive eastern vein. Sunglasses in the middle photo 25cm long, hammer in the third photo 35cm long.

CHAPTER 3

OPEN-PIT WALL MAPPING

3.1. Introduction

Open-pit wall mapping was conducted in three vein sets of the study area: The Southern vein, the Northern vein, and the Eastern vein sites. The aim of the mapping campaign is: (i) to identify all structural elements across pit walls, (ii) to map them at a scale of 1:200, (iii) to explore for possible relationship(s) between the structures and auriferous quartz veins and finally (iv) to discuss the role of structural elements in localizing gold mineralization. Initially, it was planned to map pit walls from one end to other but because of ongoing mining activities and blasting operations it was not possible to map some parts of the open pit walls. Facing walls of the open pits are mapped, then compared and correlated. During mapping, for simplicity, open pit walls are divided into zones of about 20-m-long zones and each zone is mapped separately. Zones along the northern walls are labelled with odd numbers, while southern walls, even numbers. Below, the results of mapping campaign will be documented.

3.2. Southern Vein Mapping

Southern Vein pit is located at the southwest of the Abu Sari mine area (Figure 1.1). The vein is an approximately E–W-trending structure and displays, in map pattern, an undulated/corrugated geometry (Figures 1.1 and 3.1). It consists of three parallel mineralized quartz veins with variable thickness, length, and grade of mineralization. The most economical of all is the most southern quartz vein, which is 0.5 to 13-meters thick and 650-meters long (Figure 1.1). Southern vein comprises two major pits, as western and eastern pits, where a total of 24 zones are defined. The eastern pit comprises 16 zones, while the western pit, 7 zones (Figure 3.1).
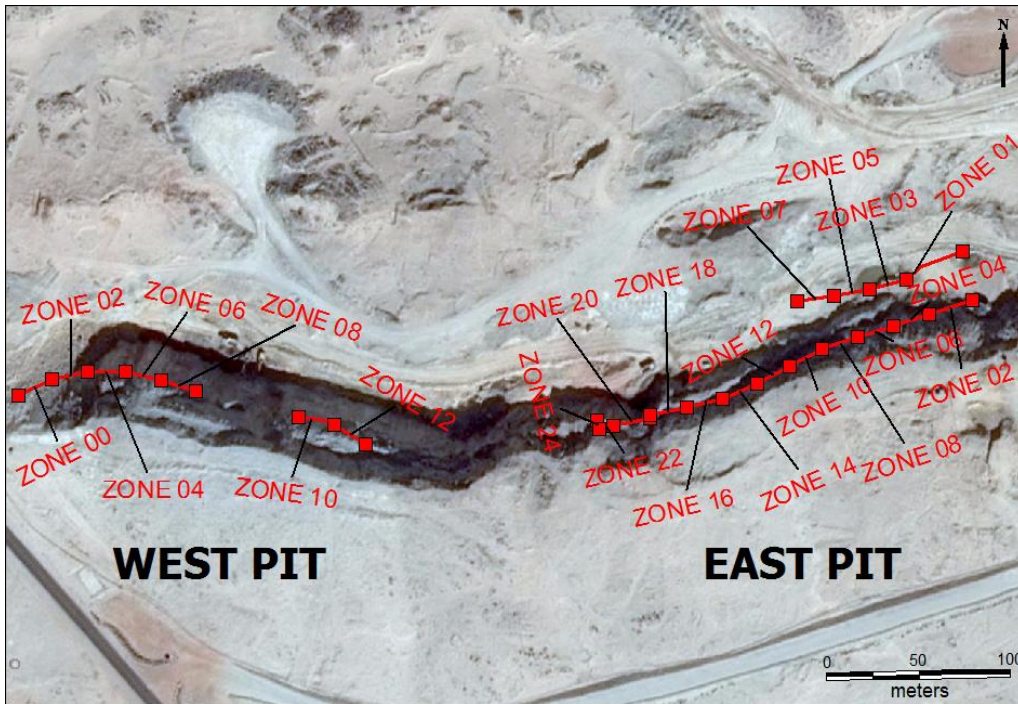
Figure 3.1. Map showing defined zones of western pit and eastern pit of the Southern vein. See Figure 1.1 for location.

3.2.1. Southern Vein: Eastern Pit Mapping

Eastern pit of the Southern vein is mapped at seven different zones (Figure 3.1). The information about each zone will briefly be given below.

Zone 01 is the starting area of the Southern vein open pit excavation works (Figure 3.2). As Zone 01 is the entrance of the Southern Vein open pit area, the wall is too far away from the main quartz vein system and mineralization. There are only a few quartz veinlets cutting the N−S foliation of unaltered greenschists. Conjugate fractures and strike-slip fault planes are also mapped (Figure 3.2).

Figure 3.2. View from Zone 01 illustrating major structural elements. Note that there are 3 strike-slip faults with well-developed slickenside surfaces. They all occur at the expense of quartz veins, indicating genetic relationship between faulting and veining. QV– quartz vein.

Zone 02 is the opposite side of Zone 01, which is the first zone of the southern wall of the Southern Vein open pit (Figure 3.3). Different from the northern wall, southern wall is on the edge of the main quartz vein system. As a result of that, different levels and types of alteration, tension cracks filled with quartz, intensely deformed planes occur as common structural features. Zone 02 is very important, because this part is the place where there is a sudden change (a bend) in the general trend of the main quartz vein. As it is observable on Figure 3.3, greenschists at the eastern part of the bend along the vein is fresh; controversially the western part is intensely altered and deformed.
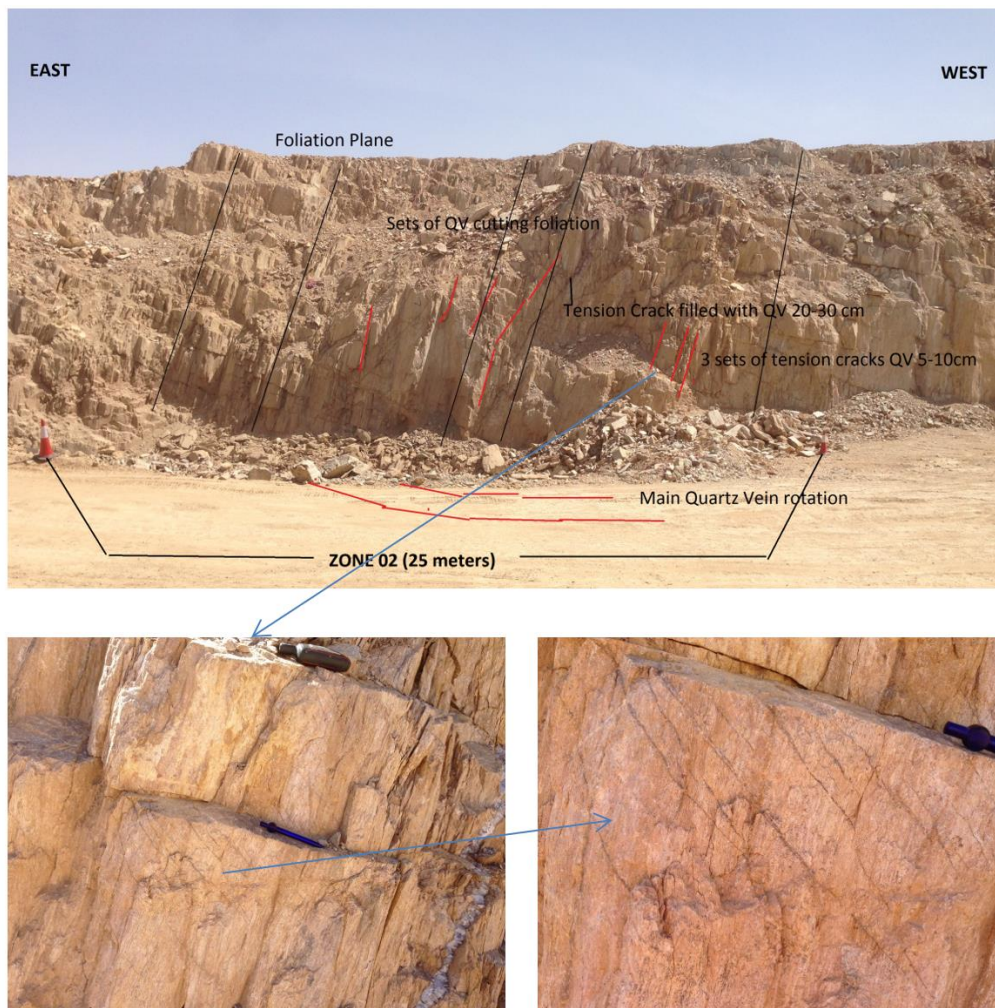
Figure 3.3. General view of Zone 02 illustrating major structural elements on the eastern wall of the Southern Vein. Left bottom: 3 sets of quartz veins cut by 2 sets of thrust faults with an attitude of 045°/22°N with GPS on, and 132°/19°W with pencil on. Right bottom: close-up views of tension cracks below the thrust fault.

Zone 03 of the northern wall of the Southern Vein open pit is dominated by strike-slip faults. Almost unaltered greenschists (foliation trends in N−S direction) have white clay occurrences along fault surfaces. There are different sets of strike-slip and normal faults (Figure 3.4). There is no mineralization or quartz veining in Zone 03 as the wall is too far from the main Southern Vein system.
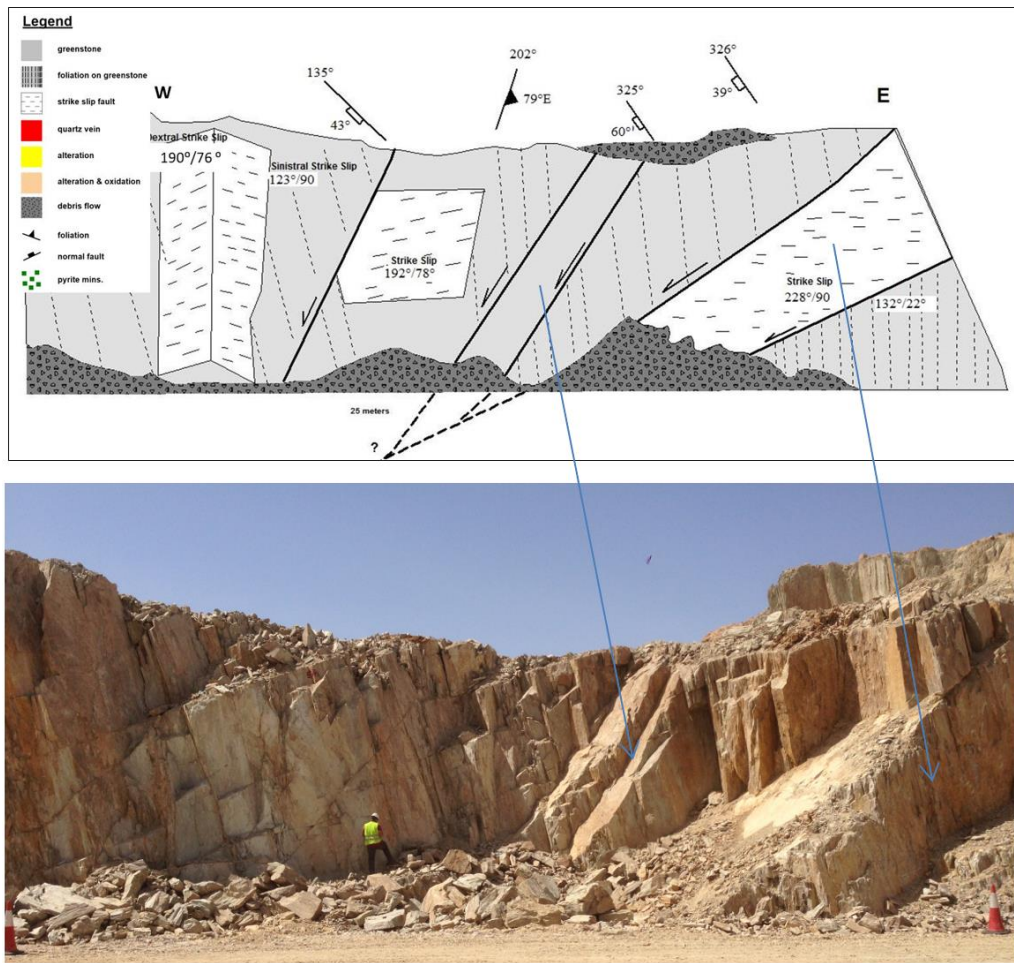
Figure 3.4. General view and wall map of Zone 03. Four sets of normal faults with ~N325^{0} azimuth cut by dextral and sinistral strike slip faults.

Similar to Zone 03, Zone 05 and Zone 07 have no gold mineralization or show evidence for hydrothermal alteration (Figure 3.5).
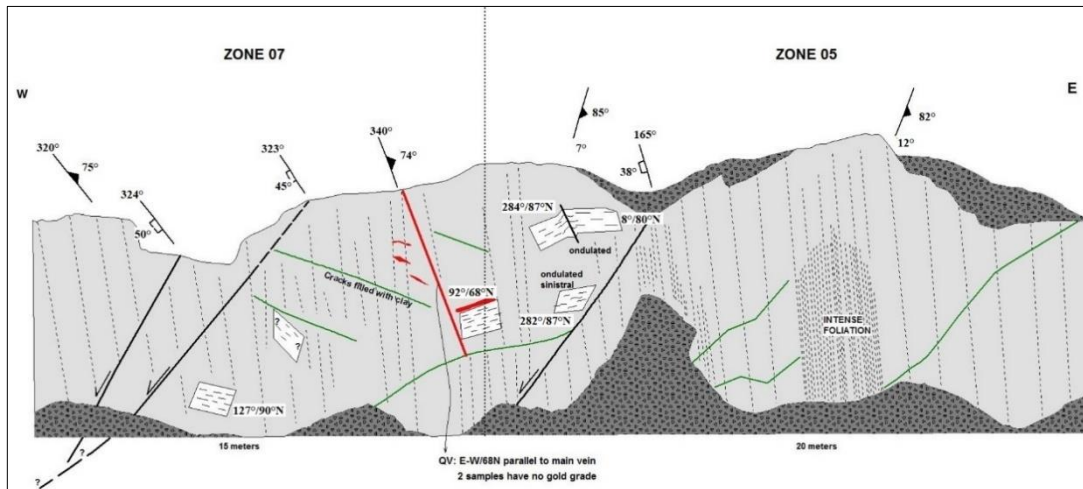
Figure 3.5. Wall map of Zone 05 and Zone 07. Note abundance of slickensides. (Please refer to Figure 3.4 for map legend).

There are only minor cracks filled with clay at both Zone 05 and Zone 07, and additionally one quartz vein occurs parallel to the main vein with no gold grade. There is around 25−35 meters gap between the main mineralized quartz vein system and the northern wall. There is 2−5 meters of alteration zone at the edges of the mineralized main quartz vein. Alteration system gets disappearing away from the main quartz vein. Unfortunately, wall mapping studies have only been done up to the end of Zone 07 along the northern wall of Southern Vein because of intense blasting and excavation activities during mapping.

Tension cracks filled with quartz are dominant in Zone 04. Intense pyrite mineralization with visible cubical crystals is also common but pyrites suddenly disappear along a strike-slip fault with a clay halo; no pyrite is observed to the west of this fault (Figure 3.6). There are 2 different directions of motion suggested by lazy-Z shaped en échelon tension gashes in Zone 4. The tension cracks in location (a) suggest a top-to-the-left (east) motion whereas at location (b) of the same zone just 10 meters west are consistent with top-to-the-right (west) motion (Figure 3.7).
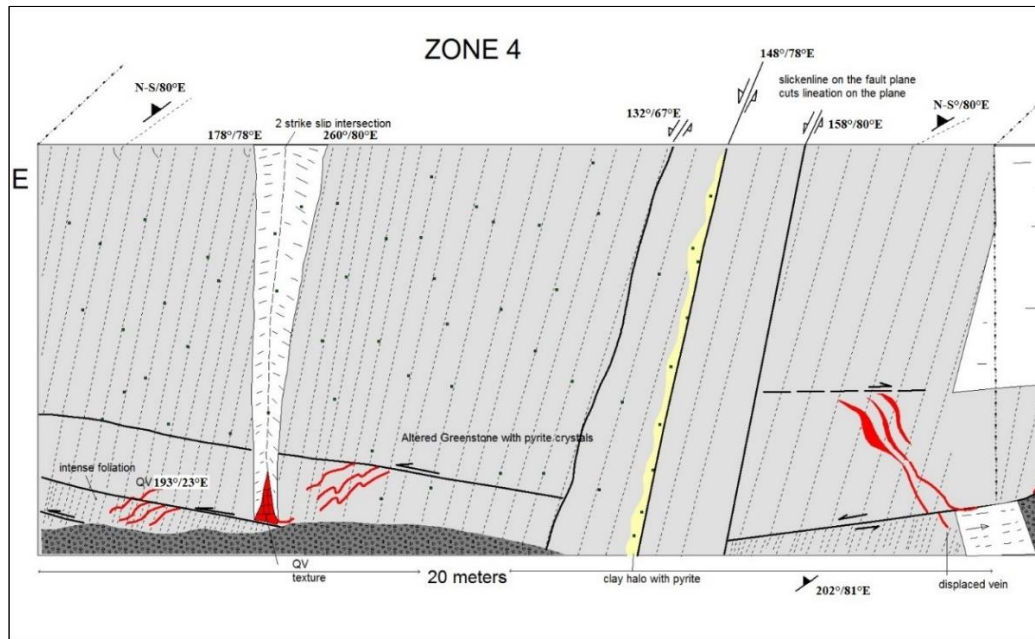
Figure 3.6. Wall map of Zone 04. (a) and (b) indicate location of Figure 3.7. (Please refer to Figure 3.4 for map legend).

Figure 3.7. Views from lazy-Z shaped en échelon tension gashes, suggesting top-to-the-left motion, Pencil is 10cm long. (a) and one top-to-the-right motion (b) in 10 meters distance. See Figure 3.6 for location.

49

Zone 06 is marked with a large-scale undulated/corrugated polished surface. As it is too high to climb; the fault plane data is not obtained but the orientation of the sliplines indicate a dominant strike-slip motion along this surface. A curved fracture with dip decreasing and finally becoming almost horizontal at its lower levels is also characteristic feature of this zone. It appears to displace en échelon tension gashes of Zone 04 (location b) and suggests a possible reverse motion. The footwall of this probable listric reverse fault is marked by intense quartz veining (Figure 3.8).
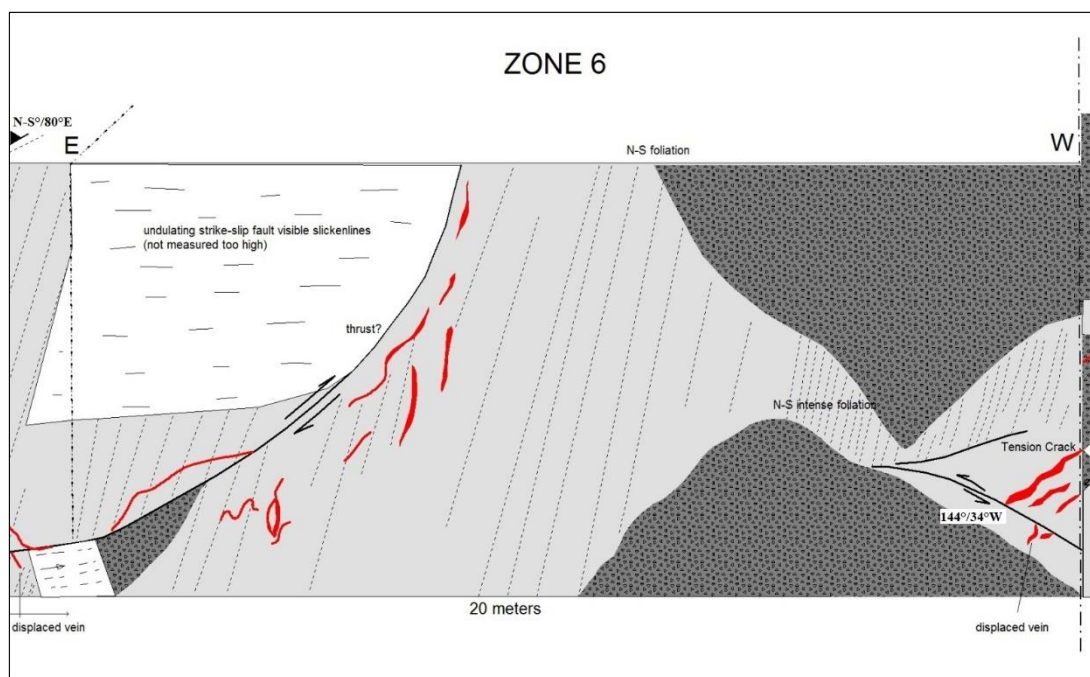
Figure 3.8. Wall map of Zone 06. (Please refer to Figure 3.4 for map legend).

Debris, which was fell down because of the blasting operations, covers almost half of the Zone 06 (Figure 3.8). Between the upper and lower debris on the most western part of the zone, lazy-Z shaped en échelon tension gashes, which are almost in the same trend with those in the Zone 04 (location a) suggests top-to-the-left (east) motion. 144°/24°W-trending reverse fault cuts and displaces the bottom parts of these en échelon tension gashes. This suggests that tension cracks are relatively the oldest and cut by relatively younger reverse faulting. Finally strike-slip faulting cuts both the tension cracks and the reverse faulting as relatively the youngest structure in this map.

Zone 08 and Zone 10 are marked by occurrence of relatively large-scale reverse faults. In the first 10 meters of the Zone 08 from the east, there are tension gashes with similar trend as in the Zone 04 (location a). Intense pyrite mineralization along the strike-slip faults is also common. Strike-slip faults appear to cut the reverse faults (Figure 3.9).

Remnants of the main mineralized quartz vein are visible on the most eastern part of the Zone 08. Intensity of mineralization and quartz veining increases as getting closer to the main quartz vein system. Trends of the lazy-Z shaped tension gashes supports the movement of the greenstone from west to the east with reverse faulting in the area. These cracks seem to be generated during top-to-the-left (east) motion of reverse faults.

As the northern wall is approximately 25 meters far away from the mineralization, the characteristics of northern and southern walls are very different from each other. Northern wall is composed of unaltered greenstone and is characterized by normal faulting, conjugate faults and strike-slip faults. There are only few barren quartz veinlets. Different from northern wall, southern wall is pervasively altered as suggested by pyrite mineralization in some parts; there are lots of tension cracks filled with quartz. Some reverse faults are observed but no normal faults. The fault planes are extensive and polished surface of strike-slip faults are visible up to 20 meters along strike at some parts of the southern wall. The strike-slip faults cut the foliation of the greenstones, reverse faults and the tension gashes; the strike-slip faults are therefore the youngest structures. Rake angles are mostly 00° and all show undulated/corrugated surfaces with high, almost vertical dip angles.

Zone 12 and Zone 14 form important sections in the area as almost 20-meters-long strike (040°/30°N, R= 00°) left-lateral strike-slip fault cuts and displaces tension cracks (Figure 3.10). There are also secondary (small-scale) strike-slip faults with an attitude of 182°/85° N and almost horizontal sliplines (R= 00°). The general attitude of regional foliation in this area is N−S/80°E and they are cut by almost all other

structures cut the foliation. Weak alteration and/or lack of alteration suggest that the mineralized main vein is located far away from this part.
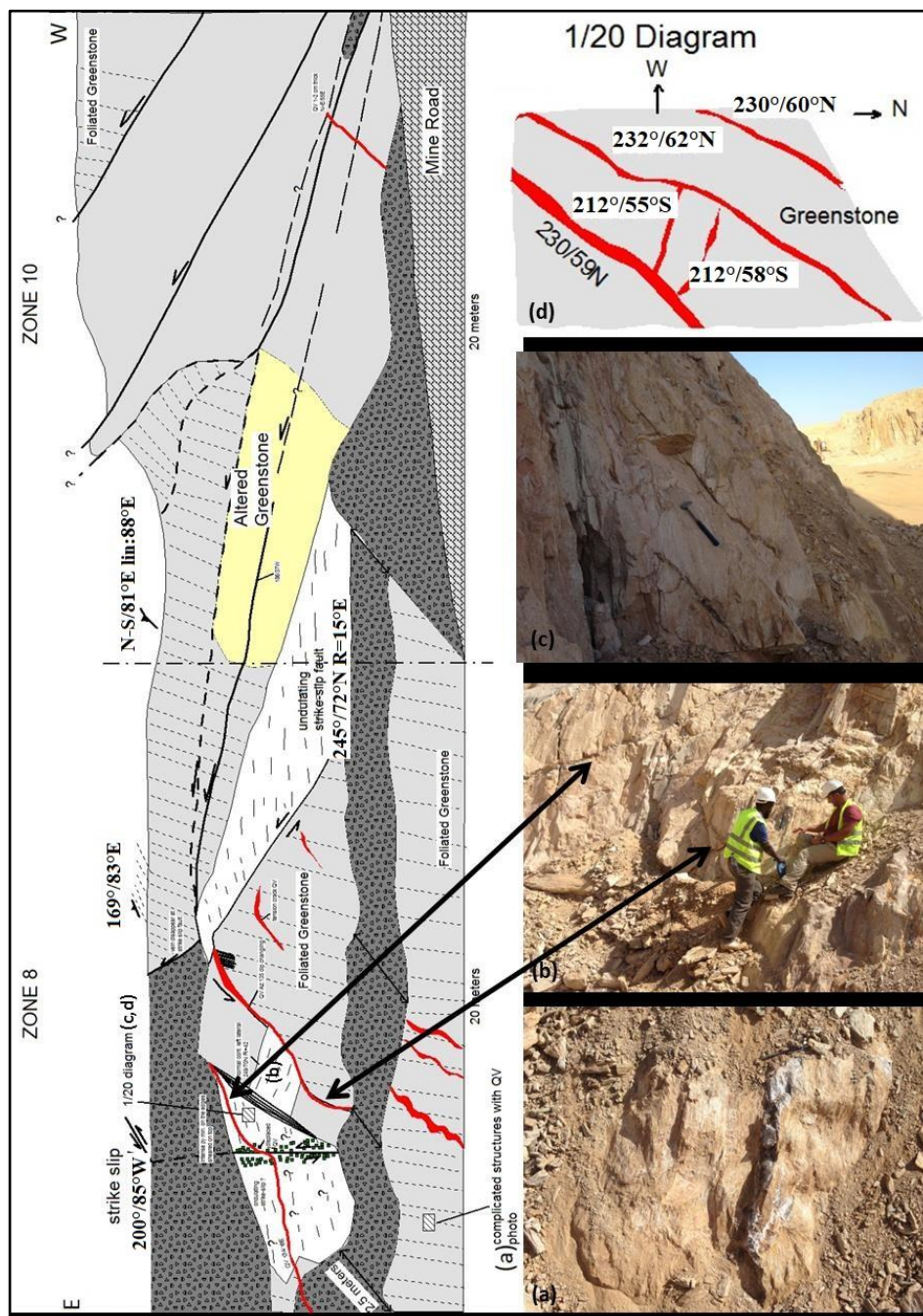
Figure 3.9. Wall map of Zone 08 and Zone 10. Views from (a) remnants of the main quartz vein system, (b) parallel to subparallel sets of quartz veins, and (c) undulating strike-slip fault surface with quartz stockwork. (d) Sketch of stockwork at a scale of 1/20. (Please refer to Figure 3.4 for map legend).
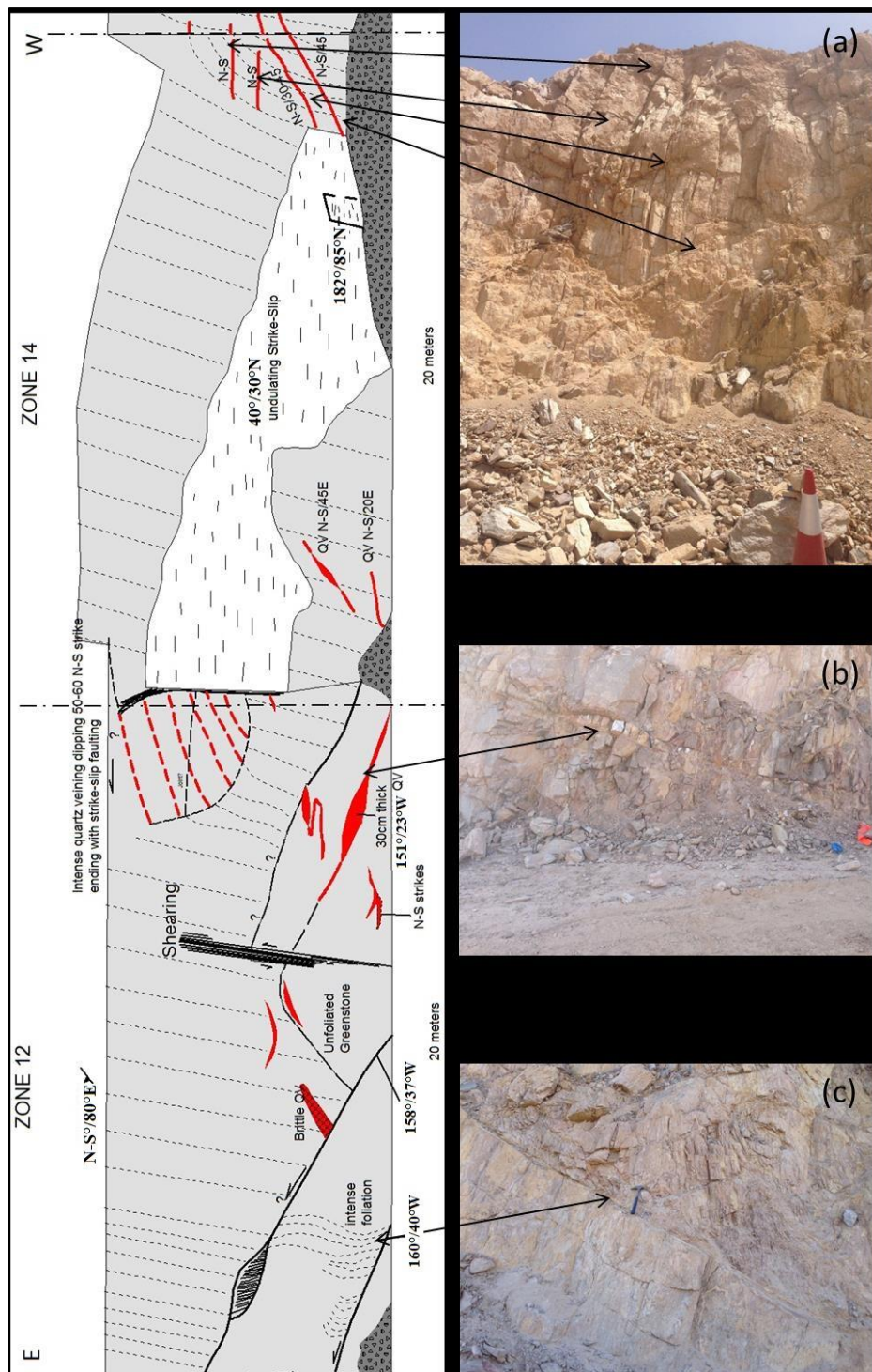
Figure 3.10. Wall map of Zone 12 and Zone 14. View of (a) several parallel N−S-trending and 30–45° dipping cracks filled with quartz (tension gashes?), (b) about 30-cm-thick tension crack filled with quartz and (c) disturbed N−S foliation dute to reverse faulting (160°/40°W). QV−quartz vein. (Please refer to Figure 3.4 for map legend).

Tension gashes form common structural elements in Zone 16 on the southern wall of the Southern Vein (Figure 3.11). General trend of these tension gashes is similar to those of Zone 04 (location a), and suggest a top-to-the-left (east) motion. Displaced quartz veins support top-to-the-left (east) thrust faulting in this region. Dip of foliation in the hanging wall and footwall of thrust fault is also different.
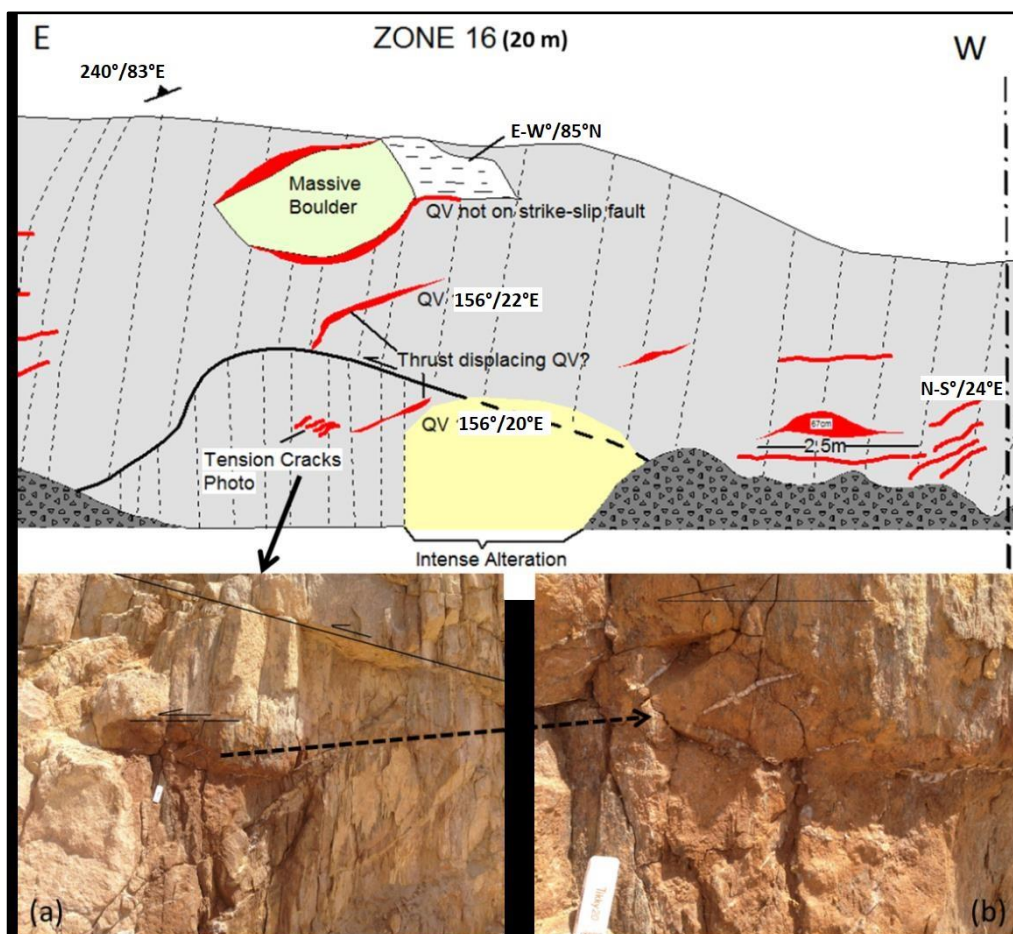
Figure 3.11. Wall map of Zone 16. Close-up views from the thrust fault (a) displacing the quartz vein and causes change in the dipping of foliation of the greenstone and minor tension gashes (b). The tension gashes are consistent with top-to-the-left (east) shearing. QV– quartz vein. (Please refer to Figure 3.4 for map legend).

Zone 18 is marked by relative scarcity of tension gashes. There are quartz veinlets cut and displaced by a strike-slip fault and a shear zone (Figure 3.12).
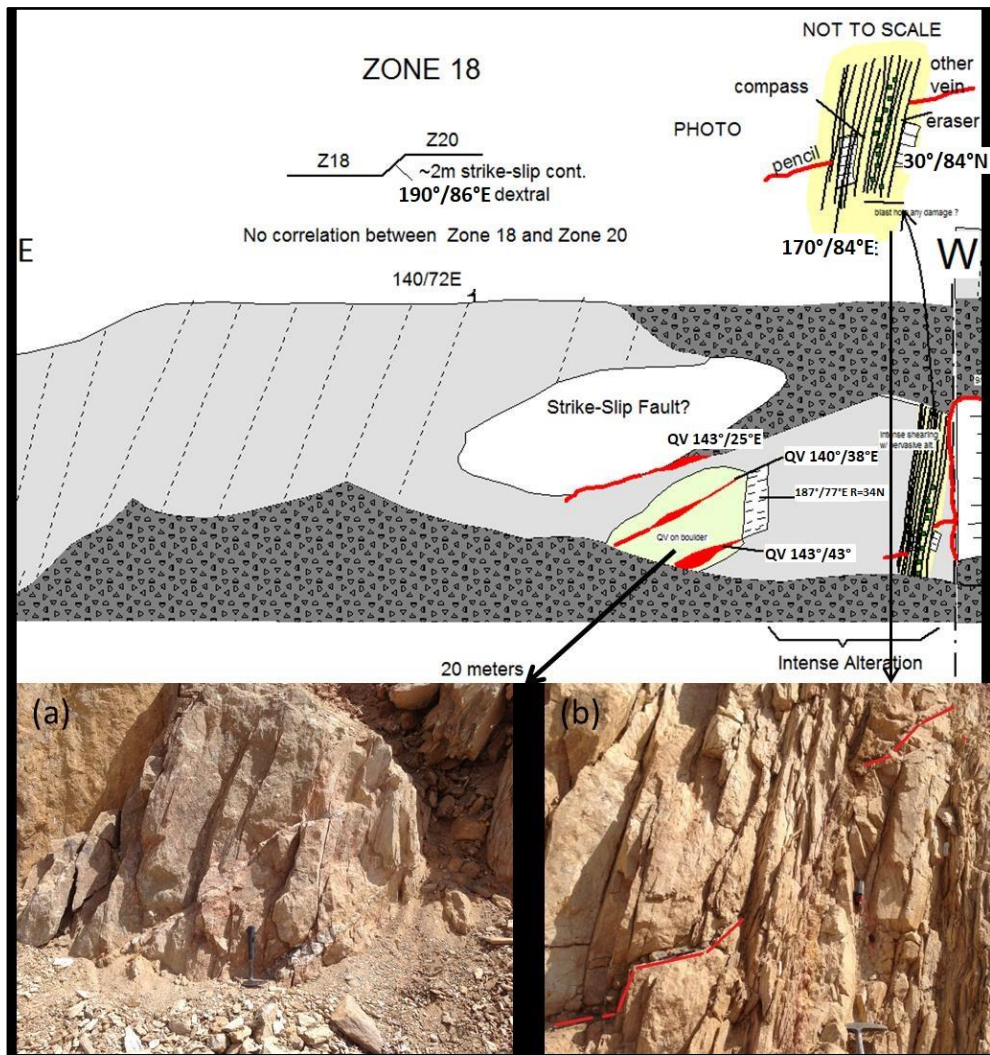
Figure 3.12. Wall map of Zone 18. Close-up views from tension gashes cut by strike-slip faults (a) and quartz vein cut and displaced by a shear zone (b). (Please refer to Figure 3.4 for map legend).

Zone 20 starts from approximately 2 meters after Zone 18, as illustrated in Figure 3.12, because of the shape of the open pit area. The boundary between Zone 18 and Zone 20 is a strike-slip fault. West of the strike-slip fault is characterized by a zone of intense alteration and quartz veining (Figure 3.13). Shapes and trends of the tension gashes are similar to general trend as in other parts of the wall. Tension gashes are however disturbed by a relatively younger movement that also results in intense alteration.

55
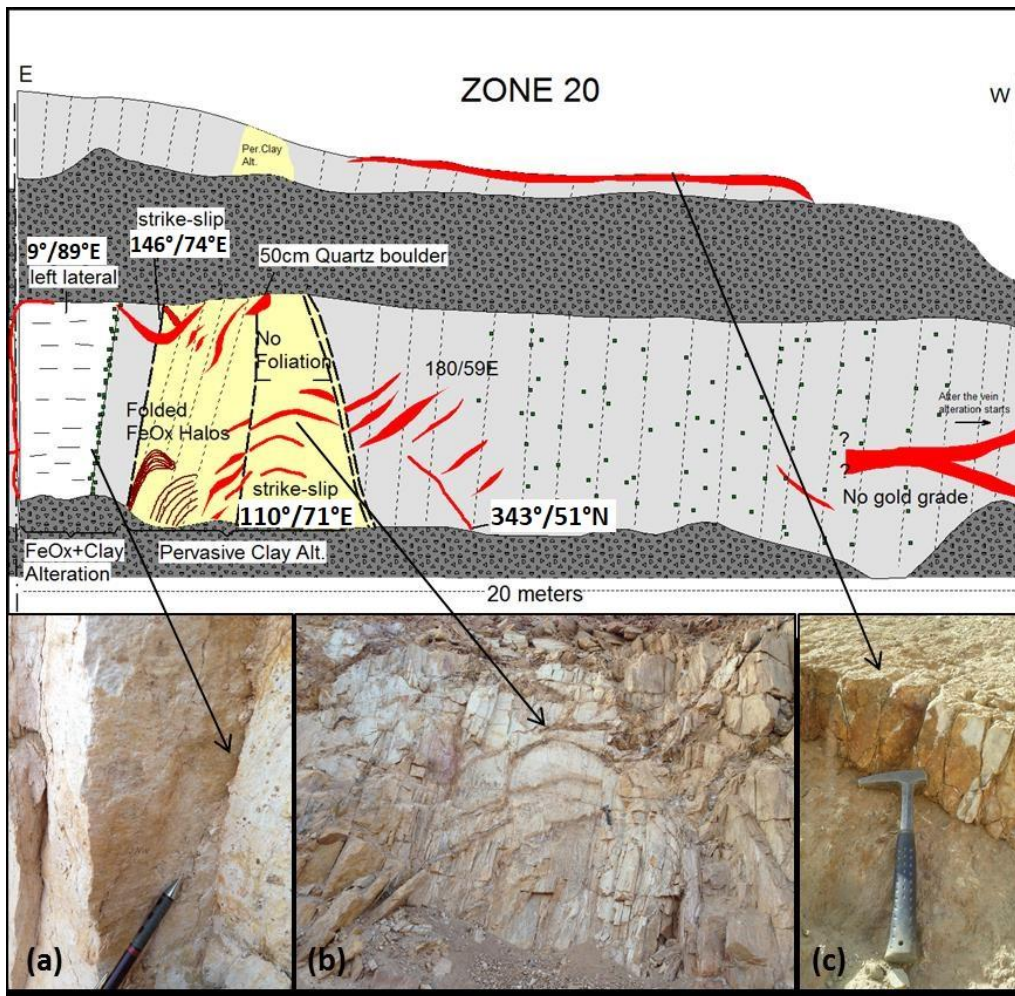
Figure 3.13. Wall map of Zone 20. Close-up views from sinistral strike-slip faults marked by intense along strike pyrite mineralization (a), quartz veining cut and displaced by faulting and marked by pervasive clay alteration (hammer in the middle) (b), and quartz vein (c). (Please refer to Figure 3.4 for map legend).

Zone 22 and Zone 24 are oriented perpendicular to each other are the last zones in the Southern Vein East Pit. These zones form core of main gold mineralization and are marked by intense alteration patterns.

Main mineralized quartz vein of the gold system is observed in Zone 24. Increase in the intensity of pyrite mineralization closer to the main gold mineralized vein is interpreted as the evidence for hydrothermal fluid circulation and for origin of gold. Although some part of the vein has been mined out from the northern part, 1−2 meters of the vein still remains (Figure 3.14).
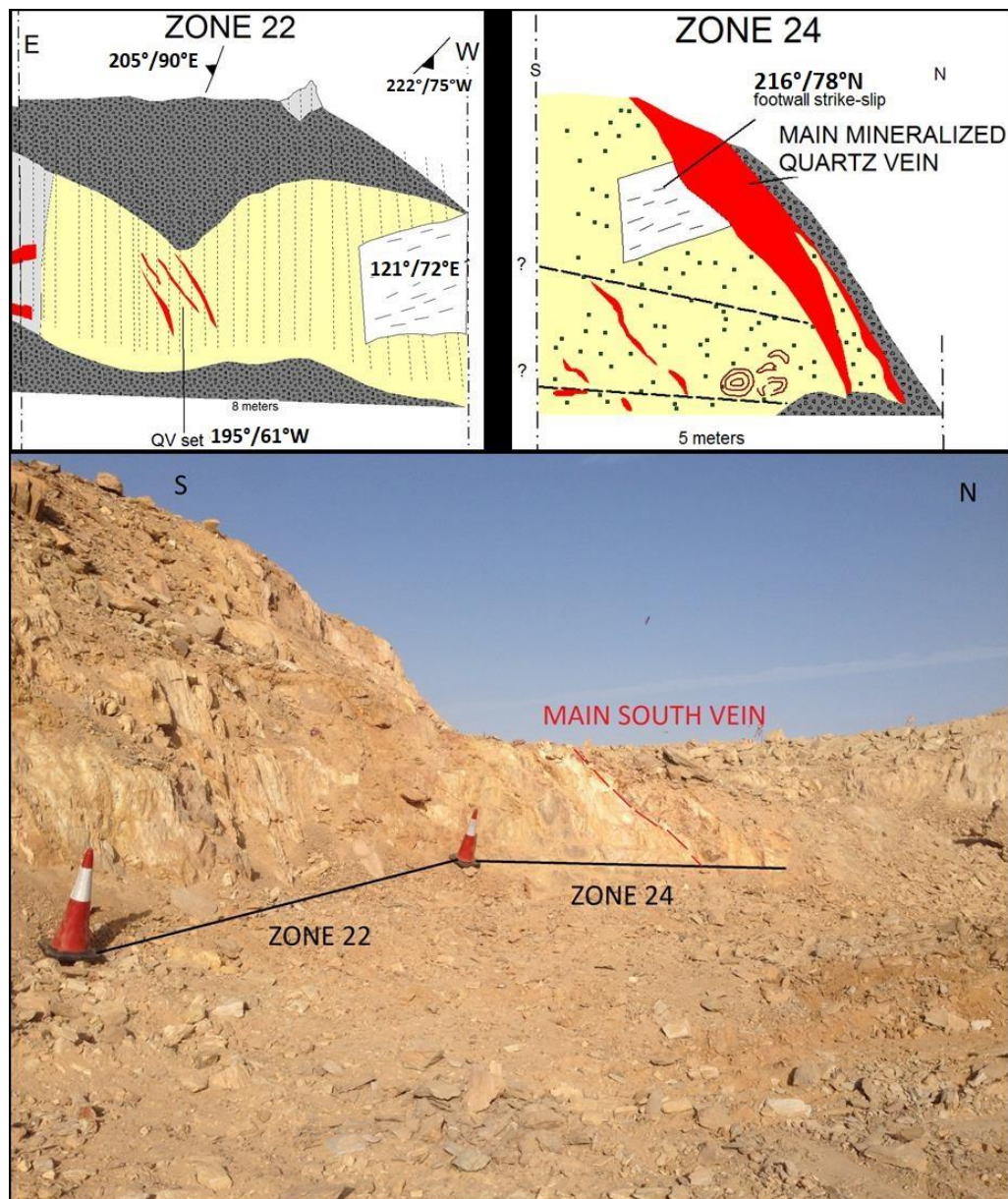
Figure 3.14. Wall map of Zone 22 and Zone 24. The lower photo illustrates field appearance of the zones. (Please refer to Figure 3.4 for map legend).

3.2.2. Southern Vein: West Pit Mapping

In order to understand the mechanism of the quartz vein system and different types of mineralized or unmineralized quartz veins, wall mapping studies done in this region by choosing 20 meters long walls. 6 different parts of the main open pit wall mapped for this purpose.

The eastern pit comprises 16 zones while the western pit, 7 zones (Figure 3.1).

As the blasting operations are focused on the northern wall of the Abu South West Pit, only south wall of this area is available for wall mapping.

Generally, for the Southern Vein system, gold mineralization can be described as sinistral strike-slip controlled quartz veins faulted with minor and major strike-slip and reverse faults. There are sheeted veins (1cm to 1m) parallel to the main quartz vein. Main quartz vein is East-West trending and quartz vein is dipping 70-80º to the North. Thickness of the quartz vein is changing between 1 to 4 meters in general, however reaching up to 13 meters in the middle because of combining of all sheeted veins at this part.

Dextral, almost N-S secondary strike-slip faults are also measured at the west zone.

First mapped part of the Southern Vein west pit is Zone 02 and Zone 04 (Figure 3.15). These two zones are the best places to see the main mineralized quartz vein on the wall. For mining purposes, the vein is completely facing almost 15 meters long with changing thickness between 2-5 meters.

As the upper part of the vein is already mined out, it is also possible to clearly see the wall rock alteration with tension cracks.

At some parts, there are some vertical tunnels that have been opened by artisanal miners to produce gold.

Figure 3.15. Zone 02 and Zone 04 wall map. (a) First 10 meters of Zone 02. (b) Second 10 meters of Zone 02. (c) First 10 meters of Zone 04. (d) Second 10 meters of Zone 04. (Please refer to Figure 3.4 for map legend).

It is easy to see the mined-out quartz vein shape from the photo of the Zone 06 (Figure 3.16). In the middle of the Zone 06 a dextral strike-slip fault (95/76°N R=0) in the middle of high oxidation zone is an example of secondary dextral strike-slip faults perpendicular to the main quartz vein and the sinistral strike-slip faults that controls main mineralized quartz vein.
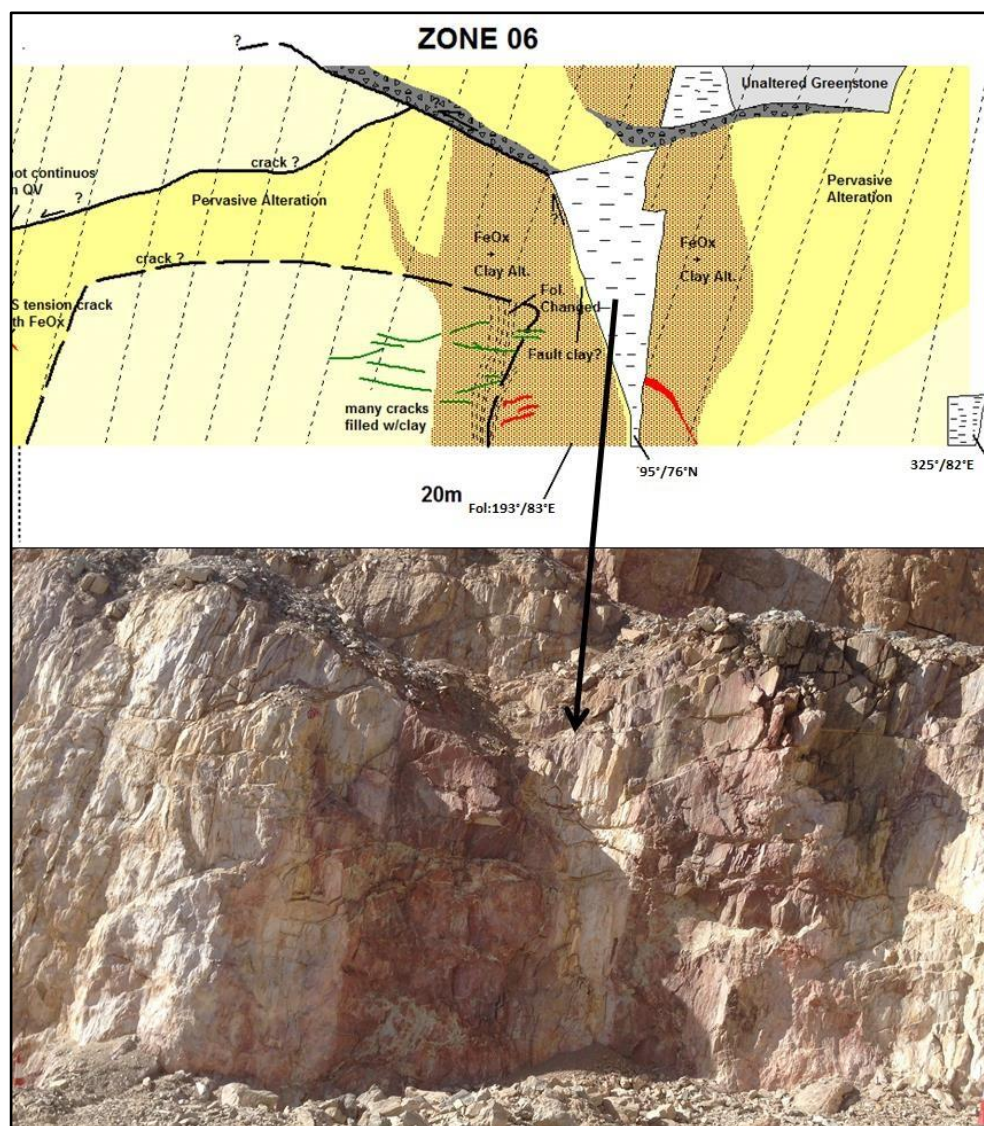
Figure 3.16. Zone 06 wall map with photo of the exact part. (Please refer to Figure 3.4 for map legend).

There is numerous strike-slip faulting in the Southern Vein west pit area. It is hard to decide which of these faults are the mineralization-controlling faults. Zone 08 is the

place where mineralized quartz veins with strike-slip fault contact which are all parallel to each other. These vein sets are also parallel to the main mineralized quartz vein of the South Pit (Figure 3.17).
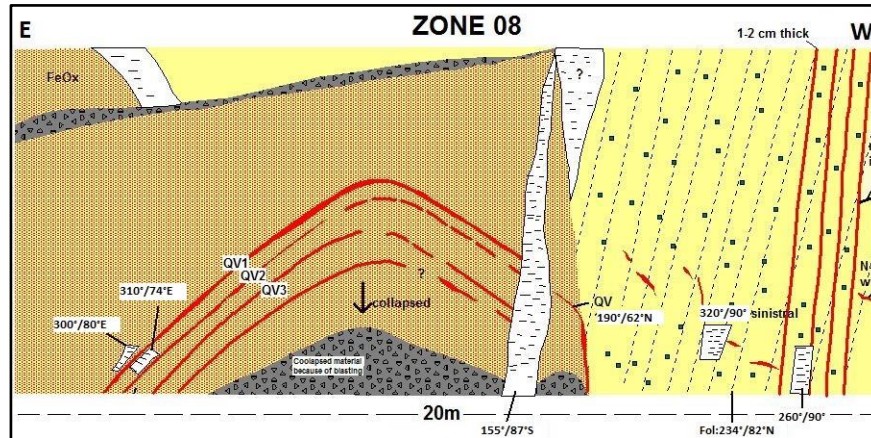
Figure 3.17. Sketch map showing Zone 08 and parallel mineralized veinlet system. (Please refer to Figure 3.4 for map legend).

QV1 is the closest veinlet to the main quartz vein and has the highest gold value. As far as the veinlets are getting far away from the main vein, gold grades are decreasing. These veinlets are 40-50 cm to each other and 2-5 cm thick (Figure 3.18). All of the veinlet boundaries are strike-slip faults, almost parallel to the main mineralization, suggesting that also the main quartz vein is controlled by strike-slip faulting.

Figure 3.18. Parallel mineralized veinlet system.

Last zones in Southern Vein west pit are Zone 10 and Zone 12. Zone 10 is an area dense faulting and intense foliation. On the other hand, because of a landslide as a result of blasting studies in the pit, only a polished surface with a joint system left on the wall of Zone 12 (Figure 3.19).
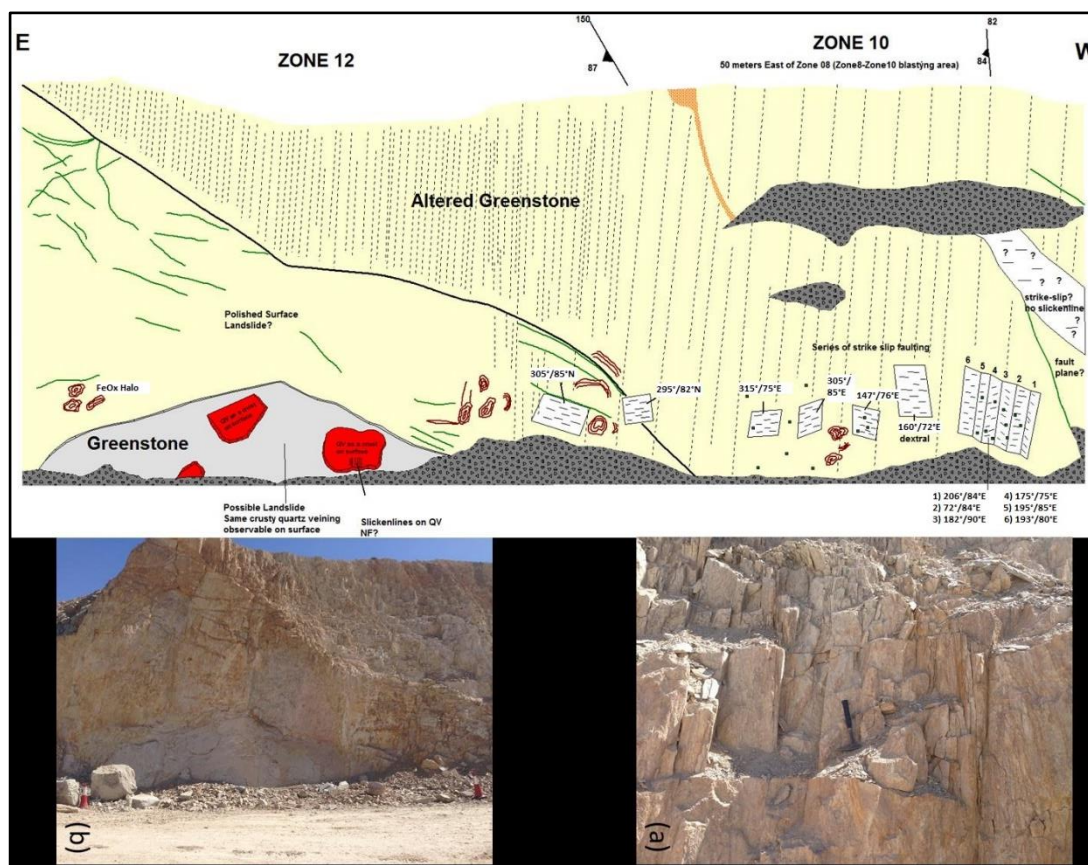
Figure 3.19. 20 m wall map of Zone 10 and Zone 12. (a): Sets of fractures with strike-slip faults. (b): Slide surface with joint sets on top. (Please refer to Figure 3.4 for map legend).

3.3. Northern Vein Mapping

Northern Vein is a large-scale NE–SW-trending quartz vein and provides evidence for typical mineralization, strike-slip faulting and shearing. Northern Vein pit is located at the northern part of the Abu Sari mine area. This type of mineralization which is characterized by mm- to cm- scale quartz veining in shear zone occurs only in the Northern Vein pit with rare massive quartz veining. Abu North-east pit consists

of more than one trenches. There is only about 40 meters of pit wall available for mapping (Figure 3.20).

Figure 3.20. Map showing defined zones of Northern vein. See Figure 1.1 for location.

A total of 6 zones are mapped along this pit (Figure 3.21). The detailed description of these zones will be given in the following paragraphs.

Zone 01 (see Figure 3.20 for location) represents the most northern part of the Northern Vein along its western wall. The wall limits the north-eastern extension of Northern Vein (Figure 3.22). The wall is characterized by intense alteration of greenstones and pyrite occurrences. Tension cracks are common; they are filled with quartz but there is no gold grade. Major structures are N−S-trending (blind) thrust. There appears no alteration in its hanging wall but the footwall is extensively altered. This may suggest a genetic link between thrust faulting and alteration. NW−SE-trending and south-dipping faults also form major structural elements (Figure 3.2).

Figure 3.21. A view from the eastern wall of the Northern Vein pit illustrating mapped zones (looking from Zone 01; ENE to WSW)
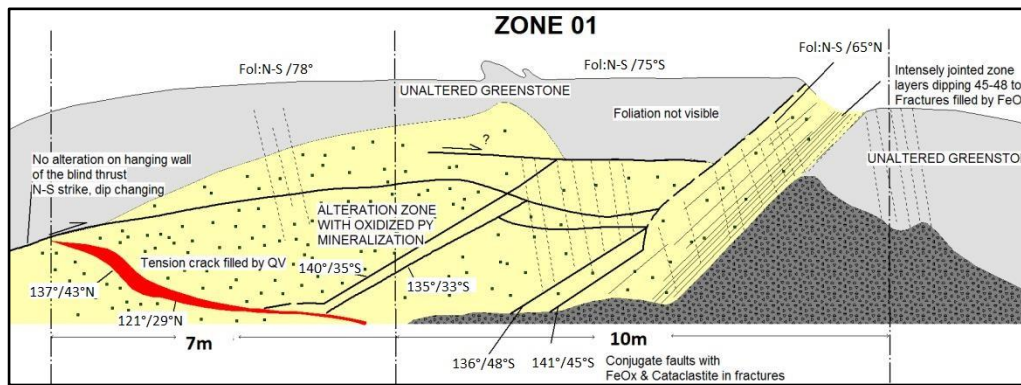
Figure 3.22. Wall map of Zone 01. F– foliation; QV– quartz vein. (Please refer to Figure 3.4 for map legend).

Zone 02 and Zone 03 of the Northern Vein represent almost opposite side of Zone 01. These zones show many structural features, such as lazy-Z shaped en échelon tension gashes, thrust faults, normal faults, strike-slip faults, joints, and tension cracks (Figure

3.23). None of these quartz veinlets and alteration zones contains gold mineralization of any economic interest.

Zone 04 and Zone 05 are the most significant areas of Northern Vein to understand the general trend and type of gold mineralization. Northern Vein ore starts from the middle of the Zone 04 with a strike-slip fault, and the ore ends at the end of Zone 05, again with another strike-slip fault (Figure 3.24).

Northern Vein main ore can be described as an intense argillic alteration zone with sericite and pyrites; quartz veining in the form of tension gashes and stockwork is extensive. Gold mineralization occurs in both altered greenstone and quartz veins. Gold grade increases with an increase in the density of the quartz veins. The thickness of the quartz veins is about 0.5 meters. They may reach up to 2 m (personal communication with mining geologists) but they are all mined out.

Strike-slip faults labelled as A, B, C, and D on Zone 04 and Zone 05 map are very important as they appear to control and/or limit the alteration zone. Main ore and alteration stars with the strike-slip C and ends with the strike-slip D. Attitude of these two faults are 360°/85°E (fault C) 337°/87°E (fault D); slickenlines are horizontal (rake angle R= 00°) on both fault planes. Field observations confirm that the ore at this part of the Northern Vein trends in North–South direction.
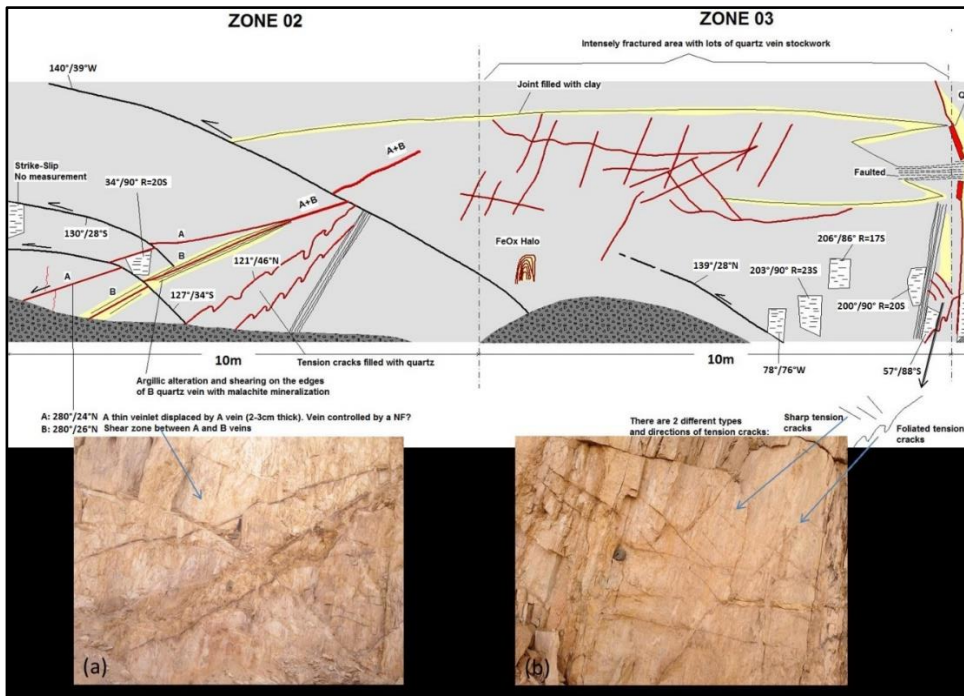
Figure 3.23. 20 m wall map of Zone 2 and Zone 03. Field vies from (a) sets of quartz veinlets displaced by thrust faults and (b) two different directions and types of tension cracks that may suggest two different stages of deformation. (Please refer to Figure 3.4 for map legend).
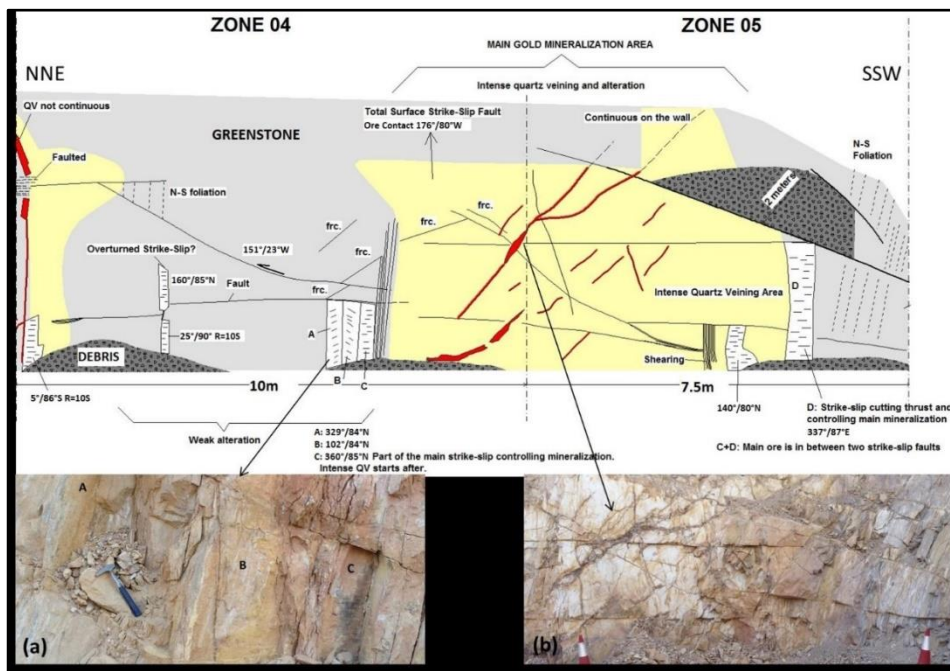
Figure 3.24. Wall map of Zone 04 and Zone 05. Field vies from (a) series of strike-slip faults (A, B, and C) and (b) main ore. (Please refer to Figure 3.4 for map legend).

66

Zone 06 is located where the Northern Vein has a sharp bend to the east (Figure 1.1); there the thickest quartz vein occurs. The area where Zone 05 and Zone 06 intersect forms the place of very high gold mineralization. This mineralized shear zone and alteration end with an N–S strike-slip fault. Thereafter a zone of strike-slip faulting starts (Figure 3.25).
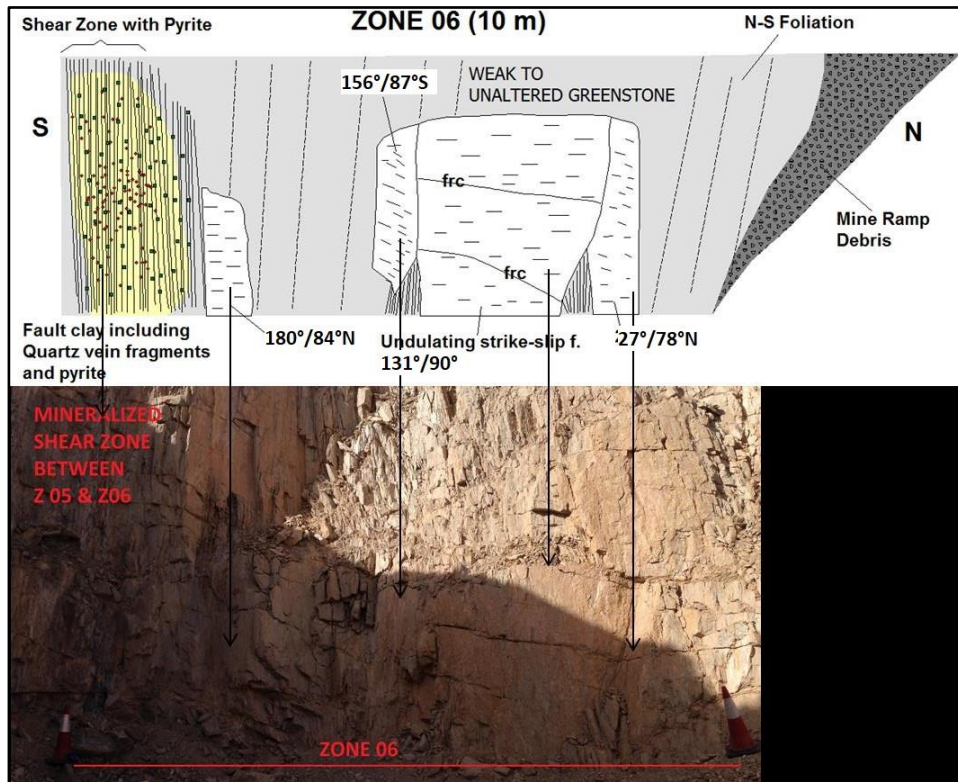
Figure 3.25. Wall map of Zone 06. Note evidence for intense deformation but no gold mineralization and alteration are observed. Field view illustrates the mineralized shear zone between Zone 05 and Zone 6 where the approximately N–S vein has a sharp bend and acquires a NE trend. (Please refer to Figure 3.4 for map legend).

3.4. Eastern Vein Mapping

Eastern Vein is also named as Arya vein system. It shows a very complicated mineralization pattern as marked by many mineralized quartz veins with different strikes. Arya main vein is controlled by strike-slip faulting and there are almost vertical boudinaged veins that are cut and displaced by the main vein. As only the main vein is visible on the surface, boudinaged vein systems are not mapped before

excavation. The boudinaged veins are visible after 20–25 meters of excavation (Figure 3.26).
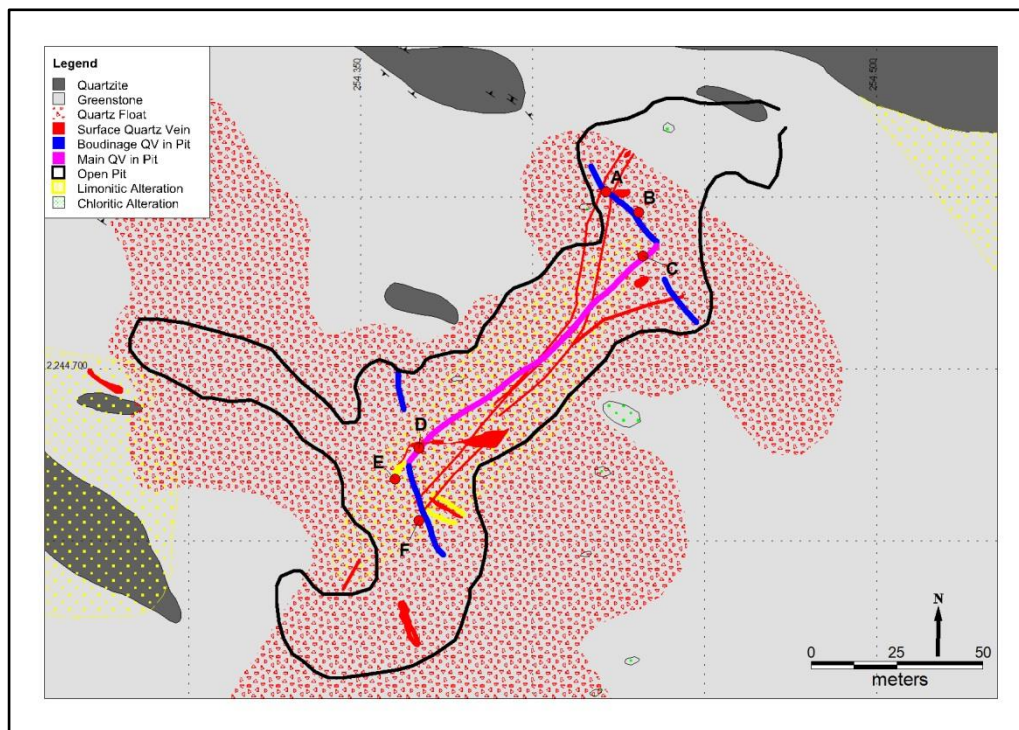
Figure 3.26. A compilation map of the Eastern Vein. Red dots show key locations where evidence for mineralization is available. The dots C and D are on the main mineralized quartz vein and representing the field observation locations of displaced older boudinaged quartz veins. The dots A, B, E, and F are on the boudinaged quartz veins and the related pictures and more information is given below paragraphs.

The Eastern Vein area is covered with quartz floats hiding most of the geology and general structure. The intensity of the quartz floats suggests a possible buried quartz vein system beneath, or fracturing and weathering of an existing quartz vein outcrop.

Site observations confirm the presence of two different quartz veining system in the area. First group is represented by boudinaged quartz veins; they occur parallel to the foliation in the greenstones and are mostly 1–2 meters thick (Figure 3.27). Pinch-and-swell structure forms common features of the boundinaged veins. These quartz veins are cut by a blind thrust (114°/30°N) (Figure 3.28). At the footwall of the blind thrust, the second phase quartz vein occurs; they cut both foliation and the first phase

68

boudinaged quartz veins. Gold grade of the younger quartz vein is higher than the boudinaged veins. Lack of wall rock alteration on the selvedge's of boudinaged veins may suggest metamorphic fluid circulation during gold deposition.
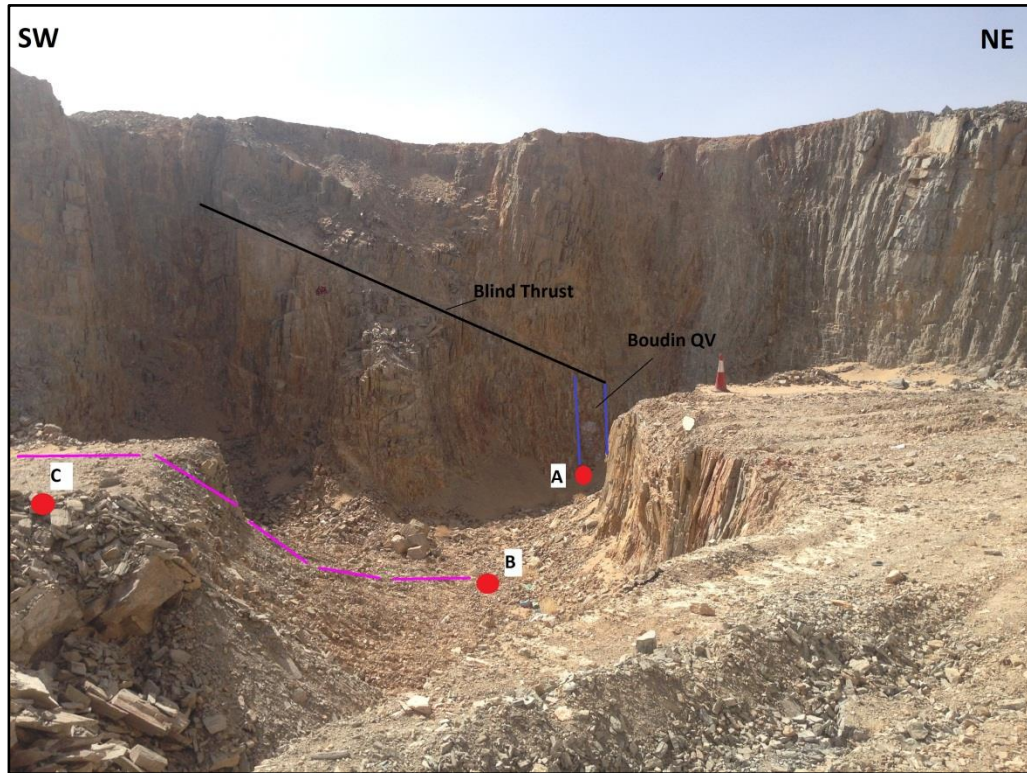
Figure 3.27. Field view showing the trend of the main quartz vein (purple line) and the boudinaged quartz vein (blue line). See Figure 3.26 for the locations of red dots labeled A, B and C.

On the other hand, 2–4 meters wide younger quartz vein has a properly developed alteration zonation. Up to 5 meters of alteration and intense pyrite mineralization suggest that not only metamorphic fluids bring gold to the system but also hydrothermal activities have also taken place.

Undulating trend of the main West Vein shows a general strike of NE–SW direction. Steeply dipping vein cuts and displaces boudinaged veins in two different locations. Relative positions of the displaced parts of the boudinaged veins indicate a right-lateral movement (Figure 3.29).

69

Figure 3.28. Field views illustrating boundinaged quartz vein cut by a thrust fault. Note well-developed with pinch-and-swell structure in the close-up view.
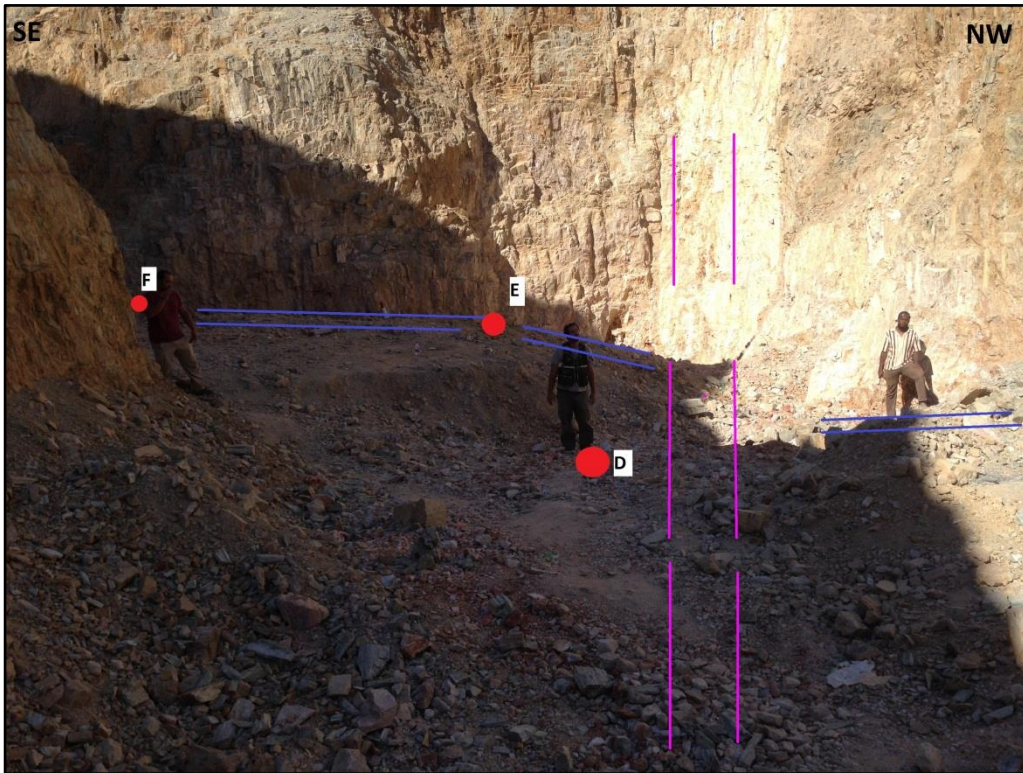
Figure 3.29. Field view from the Eastern Vein pit showing the trend of the main quartz vein (purple line) and the boudinaged quartz vein (blue line). See Figure 3.26 for the locations of red dots labeled D, E and F.

CHAPTER 4

STRUCTURAL INTERPRETATION

4.1. Introduction

In this chapter, detailed information about geological structures, both in macro-scale and micro-scale, will be discussed. During these discussions, geochemical data will also be incorporated in order to understand the relationship between gold mineralization and the structures; it is now commonly accepted that high grade shoots commonly occur where structures bend, intersect and/or interact. That is why it is important to know if there is a change in gold grade, where it occurs and what is its relation to the vein orientation, bending or intersection with other veins(s) or fault(s). Kinematic indicators in relation to these structures will also be discussed.

The most common structures in the Abu Sari area are foliation, lineation, strike-slip faults (both sinistral and dextral), reverse faults, quartz veins, normal faults, en échelon tension gashes, and pinch-and-swell structures. These structures will be described briefly in the following sections.

According to site observations, 5 distinct structures occur in the study area. Attitude of fault planes is measured, where available the orientation of the slickenlines (rake) are noted and the relative sense of motion along the fault plane is interpreted. Collected structural data are filtered and a total of 273 measurements are analysed by using Win-Tensor and Dips software; the raw data is presented in Appendix A.

The common structures in all of the studied pits include: (i) penetrative foliation in the metamorphic rocks; there are relatively thin (1 mm – 50 cm) boudinaged veinlets and veins that are broadly parallel to the local foliation; (ii) auriferous quartz veins, they occur in two distinct orientations as ~E –W and ~ (N)NE–(S)SW; (iii) NE–SW- and

NW–SE-trending thrust and reverse faults; (iv) NE–SW- and NW–SE-trending normal faults and (v) NNE–SSW- and NW–SE-trending strike-slip faults (Table 4.1).

Table 4.1. *General trend of the measured structures for each site.*

Structure	Approximate Orientation	Inferred Principal Stress Orientation	Deformation Phase
Foliation & Folds	~ENE–WSW	$\sigma_{1=}$ ~N–S	D_1
	(N)NE–(S)SW	$\sigma_{1=}$ ~(W)NW–(E)SE	D_2
Reverse Faults	~E–W	$\sigma_{1=}$ ~N–S	D_1
	NW–SE	$\sigma_{1=}$ NE–SW	D_2
Strike-slip Faults	NW–SE & N(NE)–(S)SW	$\sigma_{1=}$ NNW–SSE	D_3
	W(SW)–(E)NE	$\sigma_{1=}$ NE–SW	D_5 (?)
Veins	~E–W	$\sigma_{1=}$ ~N–S	D_1
	NE–SW	$\sigma_{1=}$ NNW–SSE	D_3
Normal Faults	NW–SE	$\sigma_{3=}$ NE–SW	D_4 (or D_3)

WSW–ENE sinistral strike-slip faults and auriferous quartz veins form other structural elements of the study area. They are interpreted as coeval with nearby syn- to post-orogenic granitic intrusion(s) (ca. 600–554 Ma; 554 Ma Kongnyuy et al. 2010, 2012). They also form the active structures of the first stage gold mineralization.

The relatively youngest structures are represented by NNE–SSW-trending sinistral strike-slip faults/shear zone; they have displaced and/or bended the first stage WSW–ENE-trending quartz veins. They have also opened new pathways for auriferous

hydrothermal solution flow and circulation; thus, new fault parallel quartz veins have formed. It is also noted that this phase has resulted in enrichment of gold mineralization as indicated by high-grade shoots at the intersection of the WSW–ENE- and NNE–SSW-trending veins; this phase is interpreted as the second phase of quartz veining and gold mineralization (Table 4.1).

The characteristic features of these structures will be summarized in the following subsections.

4.2. Foliation

'Foliation' term is used as a general term to define planar structures in the metamorphic host rocks (greenstones and quartzites) of the vein system. These penetrative planar structures have formed during metamorphism and intense deformation associated with the Pan African Orogeny. In the Abu Sari area, greenstone facies rocks are mostly characterized by a well-developed, NNE–SSW trending, west-dipping foliation disturbed by later tectonic events. The foliation is penetrative (Figure 4.1) and mineral lineation is relatively crude but in places it is visible. The foliation is microscopically defined by preferred parallel alignment of mica minerals (sericite and chlorite) and elongated quartz grains (with their long axes) (Figure 4.2).

Attitude of the foliation changes from one location to another due to large-scale open folding of the metasedimentary host rocks (Figure 4.3); the stereoplot of the foliation data reflects two main orientations as ca. N–S and E–W (Figure 4.4) whereas NW–SE and NE–SW occurs as secondary orientations. Nevertheless, the ca. N–S structures occur in two distinct orientations as NNE–SSW (015–020□) and ~N–S (000–010□) (Figures 4.4 and 4.5). The former is generally parallel to the NNE–SSW-trending sinistral strike-slip faults and associated shear zone while the latter is oriented parallel to the dominant vein direction in the region (see Figure 2.1).

73

Figure 4.1. Field view from North–South foliation planes dipping to the west and are cut by a dextral strike-slip fault ($263^0/84^0$S R= 00^0).
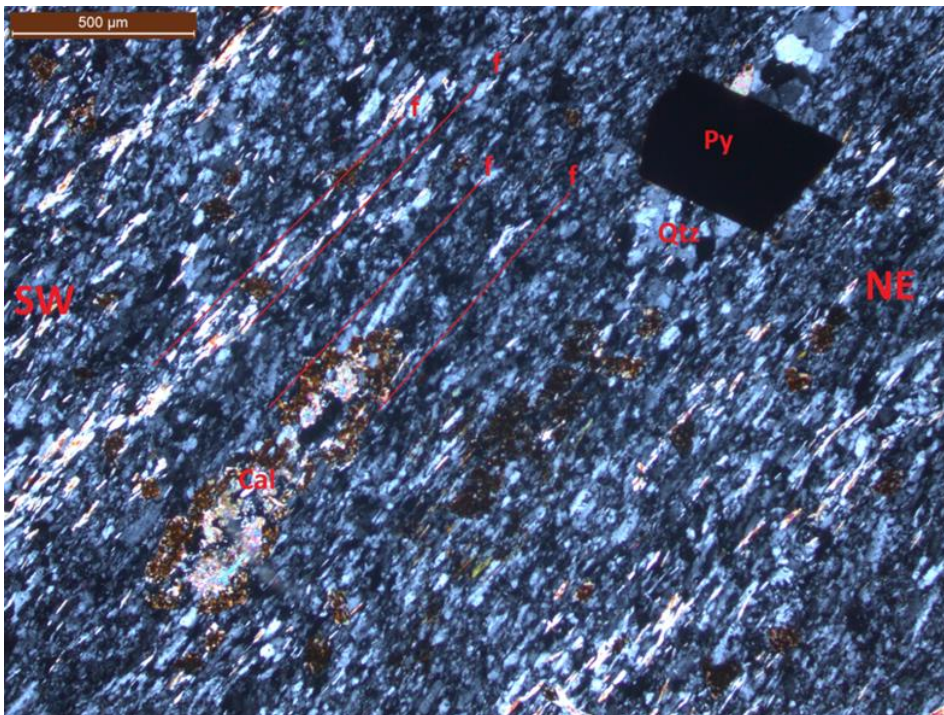
Figure 4.2. Calcite minerals with iron oxide halo and quartz crystals are lined parallel to the foliation. Large pyrite crystal appears overgrowing over the N–S foliation and suggests post-foliation or late stage pyrite mineralization.
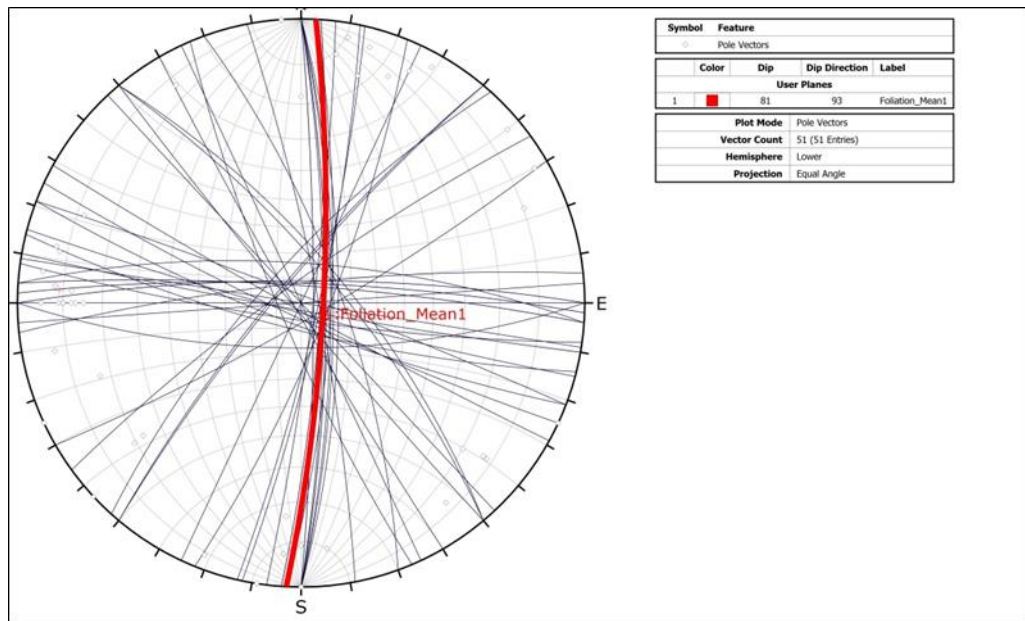
Figure 4.3. Stereonet of the foliation planes from the Abu Sari gold prospect area, plotted as poles to planes and great circles on an equal area. There appear four distinct directions as approximately N–S, E–W, NE–SW and NW–SE.
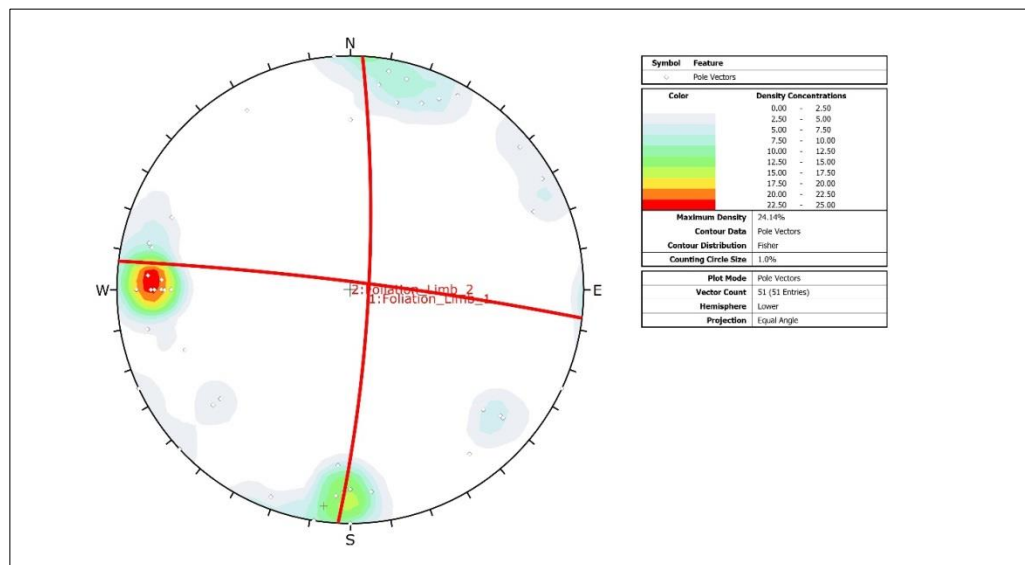
Figure 4.4. Contour graph of the associated poles to the foliation planes, showing the best fit great circles. The diagram illustrates two dominant foliation orientations in the study area.

Preliminary field observation around Abu Sari region suggests that the folds axes trend general in two distinct directions: WNW–ESE and to (N)NE–(S)SW directions. The former fold axes orientation is almost parallel to the variably sized quartz veins in the

region (Figure 1.1). The regional WNW–ESE penetrative foliation appears to be deformed along (N)NE–(S)SW-trending open folds, thus suggesting an approximately (N)NW–(E)SE-trending shortening during their formation. The undulated geometry of the large-scale veins is interpreted as open folds and attributed to this phase of folding (Figure 1.1).

Plot Mode	Rosette
Plot Data	Apparent Strike
Face Normal Trend	0.0
Face Normal Plunge	90.0
Bin Size	10°
Outer Circle	15 planes per arc
Planes Plotted	51
Minimum Angle To Plot	45.0°
Maximum Angle To Plot	90.0°
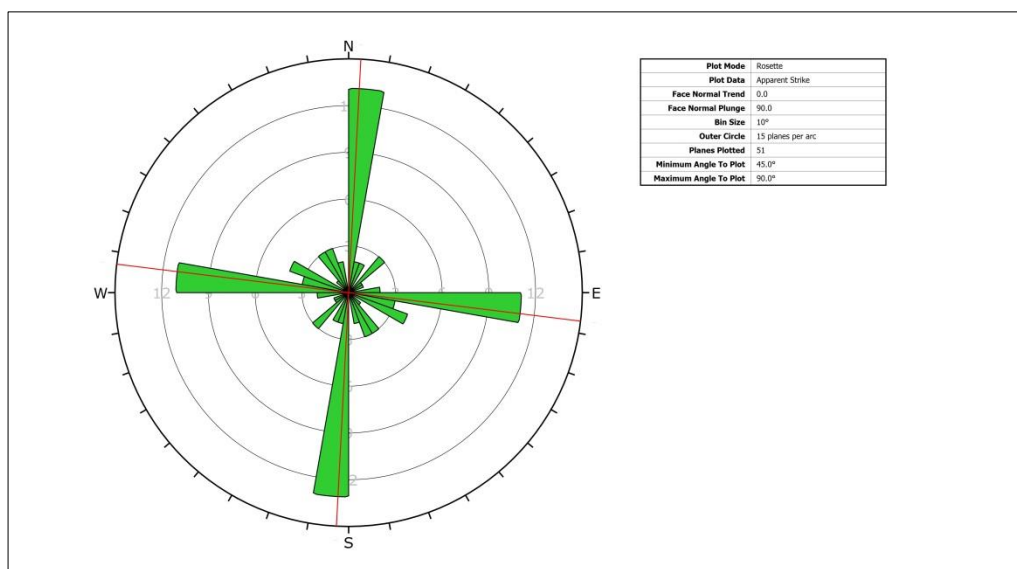
Figure 4.5. Rose diagrams of foliation trends of the greenstones (110 measurements). The two directions ca. N–S and E–W form the dominant sets.

Pinch and swell structures occur commonly where foliation-parallel quartz veins reach to a critical thickness (Figures 4.6 and 4.7). The term is used here as a shape of boudins, which is an oscillation in the thickness of a vein. Boudinage of the stiff quartz vein results in pinch-and-swell structures with ductile necking of the host rock greenschists where neck folds are well developed; whereas intense fracturing of quartz veins in the neck area is pronounced (Figure 4.6). Some of the parts of the boudinaged vein become unconnected to the main body, is completely separated and occur as isolated asymmetric small bodies within the greenschist matrix. In some places, the necks appear broken and/or displaced and filled with a secondary mineral like calcite or quartz (Figure 4.6).

76

These structures are attributed to difference in stiffness between the boudinaged quartz vein and the host rocks (cf. Davis and Reynolds 1996). These veins are interpreted to form during first phase of mineralization and they tend to parallel the local foliation.
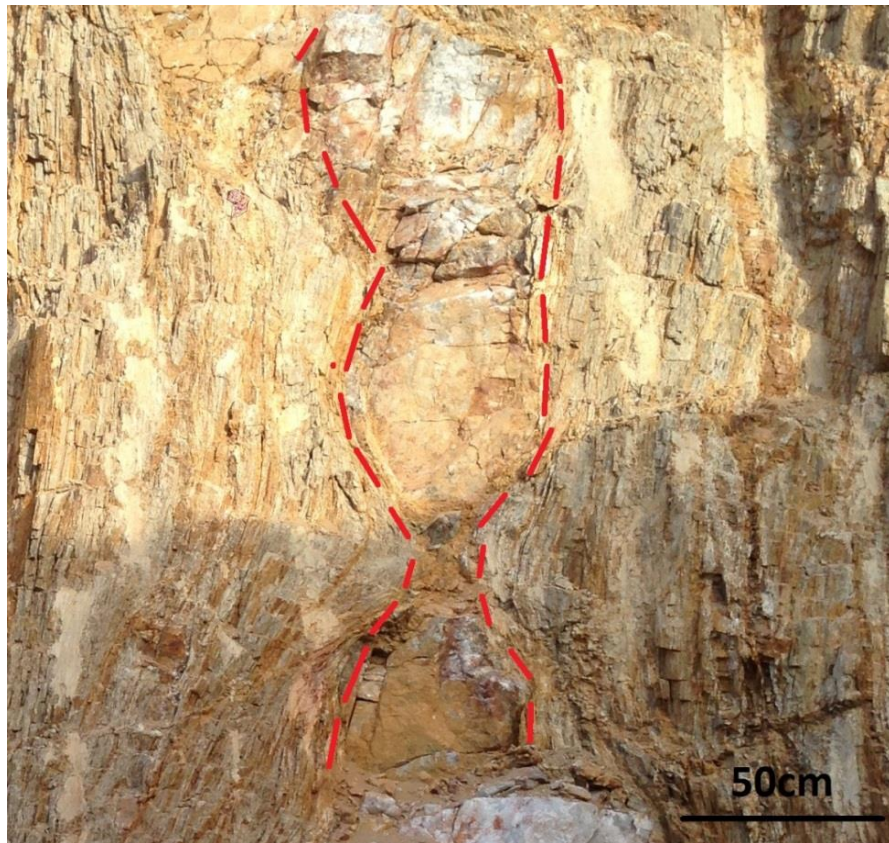
Figure 4.6. Stiff, light colored quartz vein is stretched to the point that it necked and results in the formation of isolated asymmetric boudins and/or pinch-and-swell structures.

4.3. Reverse Faults

Reverse faults form other common structures in all of the vein pits. Unfortunately, no slip data is observed along these structures but their reverse character is inferred from the offset markers. These low- to moderately- dipping (10°–42°) structures are oriented in NW–SE (107°–140°N) direction whereas the dip direction varies and is either to the NE or SW (Figures 4.8–4.11). These structures may be oblique-slip faults with reverse component but no clue is available in the field. The attitude of these faults is almost the same in southern (Figure 4.8), northern (Figure 4.9) and eastern (Figure

4.10) veins with almost no exception (please refer to Figure 1.1 for vein locations); the common orientation in all pits suggests a genetic link and that they must be associated with the same deformation event. If one considers the strike orientation of these structures, an approximately NE–SW-directed compressional stress may be envisaged (Figure 4.11). Although observed very rarely, the reverse faults may also occur in ~E–W and NW–SE direction as well.

Figure 4.7. Boudinaged calcite veins parallel to the foliation cutting actinolite minerals.
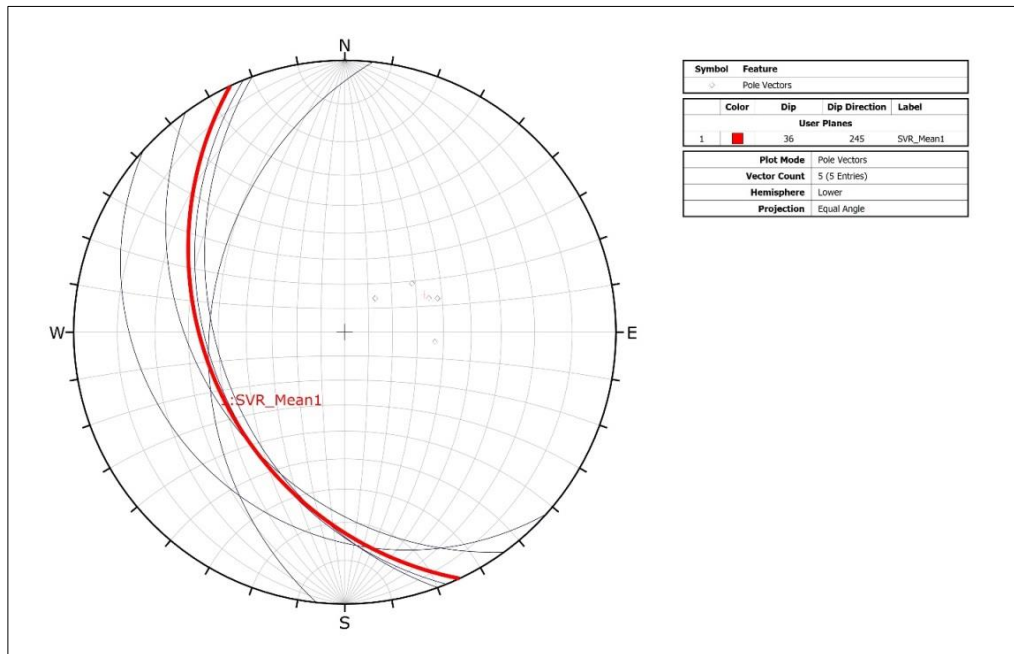
Figure 4.8. Stereonet of the reverse fault planes from the Southern vein pit, plotted as poles to planes and great circles on an equal area. Mean attitude of the faults is 155°N, 36°SW.
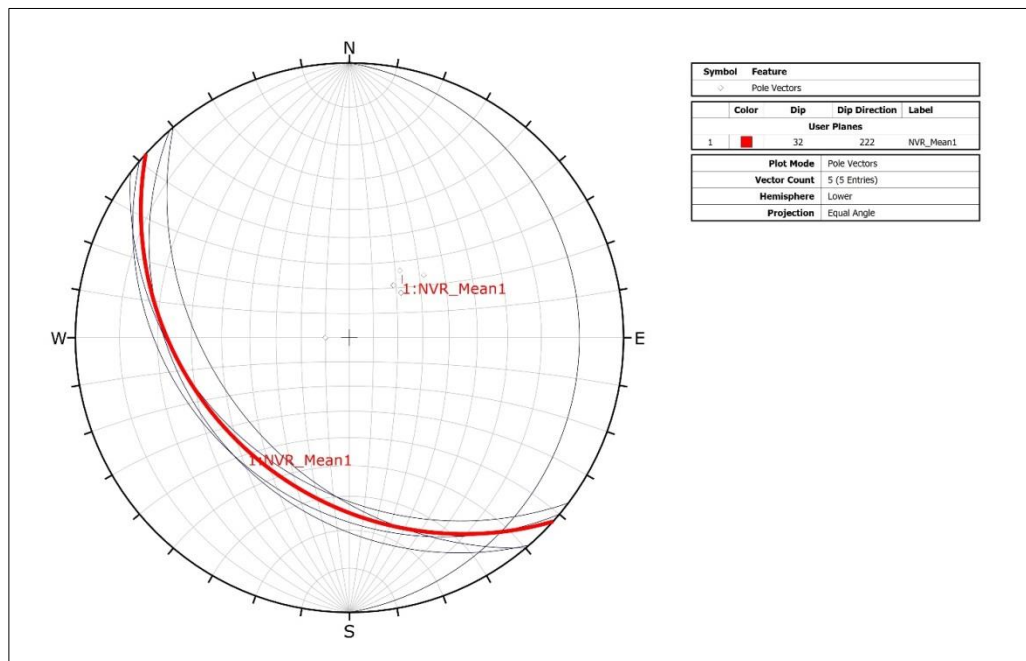
Figure 4.9. Stereonet of the reverse fault planes from the Northern vein pit, plotted as poles to planes and great circles on an equal area. Mean attitude of the faults is 132°N, 32°SW.
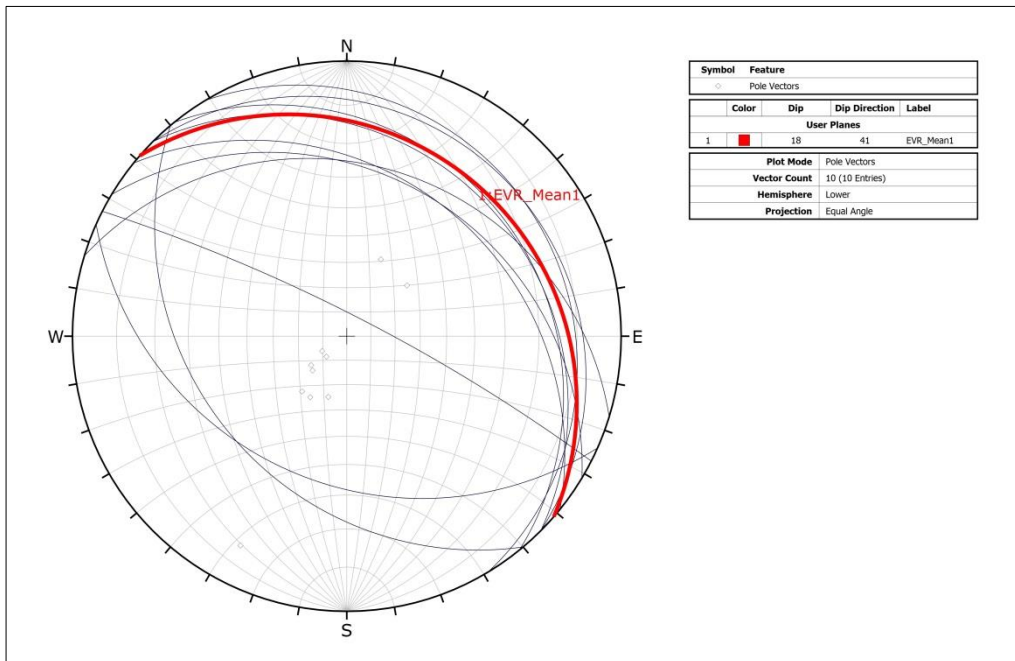
Figure 4.10. Stereonet of the reverse fault planes from the Eastern vein pit, plotted as poles to planes and great circles on an equal area. In this pit, the reverse faults develop as conjugate structures. Mean attitude of the faults is 131°N, 18°NE or SW.
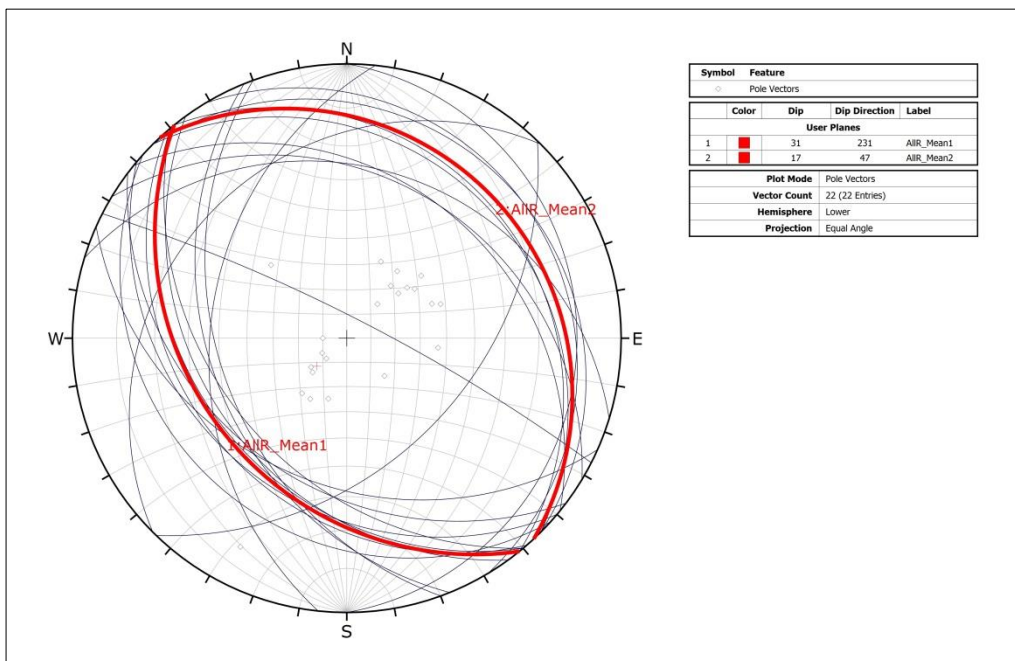
Figure 4.11. Stereonet of all reverse fault planes from the study area, plotted as poles to planes and great circles on an equal area. Mean attitude of the fault planes are 131°N, 31°SW and 137°N, 17°SW. Considering the strike of faults, a NE–SW directed compression may be suggested.

4.4. Normal Faults

Normal faults are also common structural elements in all of the vein pits. The normal character is inferred from the offset markers but almost all show no preserved striations on the fault planes. They occur as low- to moderately- dipping (14°–50°) corrugated structures and are oriented in NW–SE (100°–145°N) direction whereas the dip direction is variable to NE or SW (Figures 4.12–4.15).

These structures may be oblique faults with normal component but no clue is available in the field. The attitude of these faults is almost the same in southern (Figure 4.12), northern (Figure 4.13) and eastern (Figure 4.14) veins; the common orientation in all pits suggests a genetic link and that they must be associated with the same deformation event. If one considers the strike orientation, these faults might have been related to NE–SW-directed tensional stress (Figure 4.15).
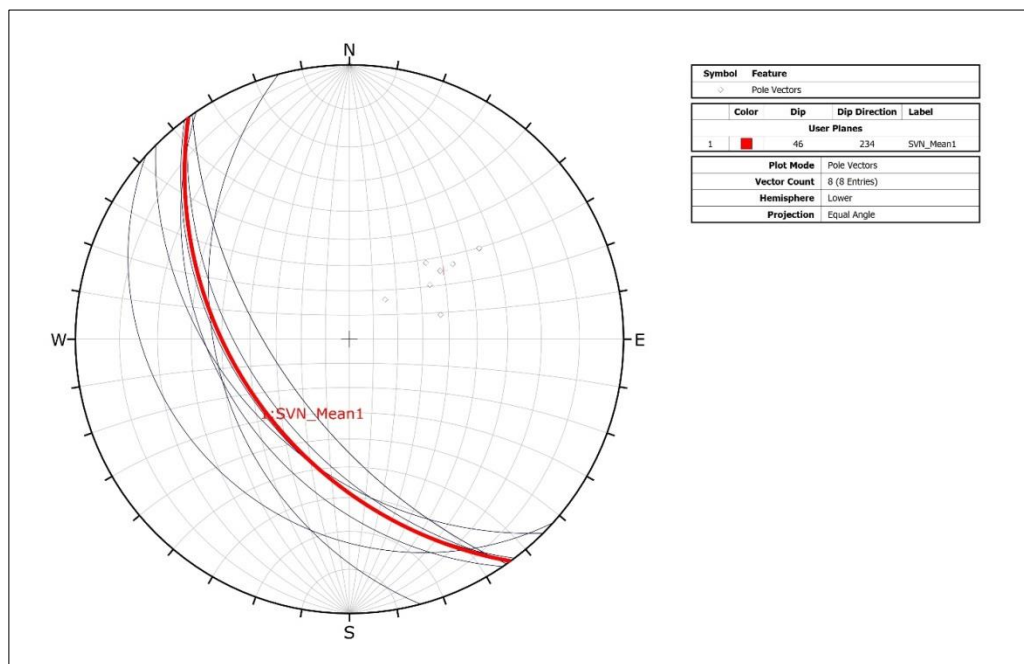
Figure 4.12. Stereonet of the normal fault planes from the Southern vein pit, plotted as poles to planes and great circles on an equal area. Mean attitude of the faults is 154°N,46°SW.

	Color	Dip	Dip Direction	Label
		User Planes		
1		40	228	NVN_Mean1

Plot Mode	Pole Vectors
Vector Count	4 (4 Entries)
Hemisphere	Lower
Projection	Equal Angle
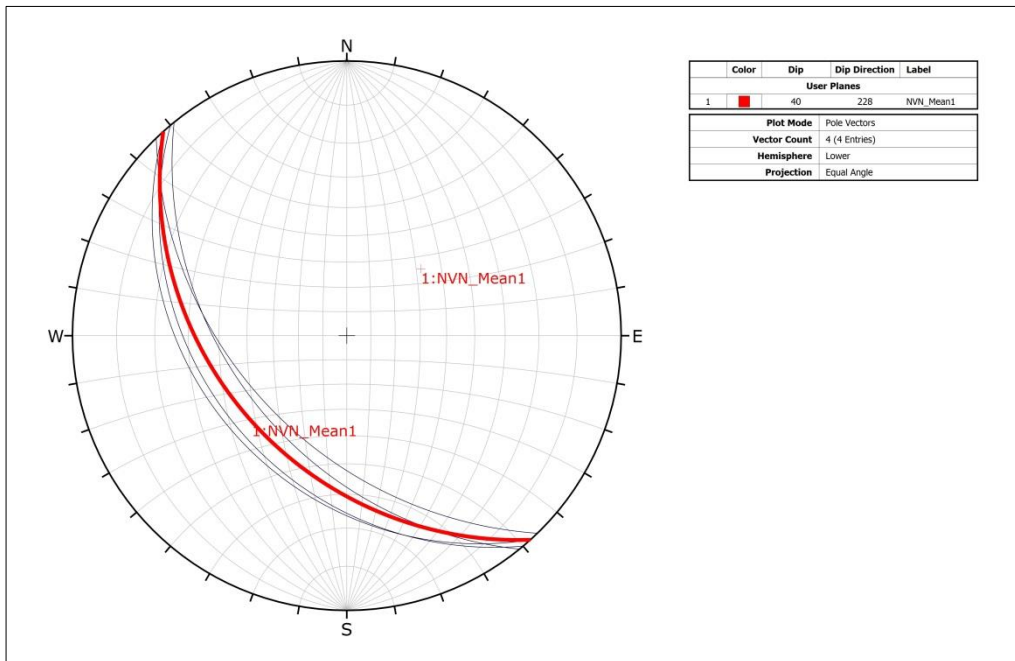
Figure 4.13. Stereonet of the normal fault planes from the Northern vein pit, plotted as poles to planes and great circles on an equal area. Mean attitude of the faults is 138°N, 40°SW.

Symbol	Feature			
◇	Pole Vectors			

	Color	Dip	Dip Direction	Label
		User Planes		
1		32	194	EVN_Mean1
2		44	25	EVN_Mean2

Plot Mode	Pole Vectors
Vector Count	7 (7 Entries)
Hemisphere	Lower
Projection	Equal Angle
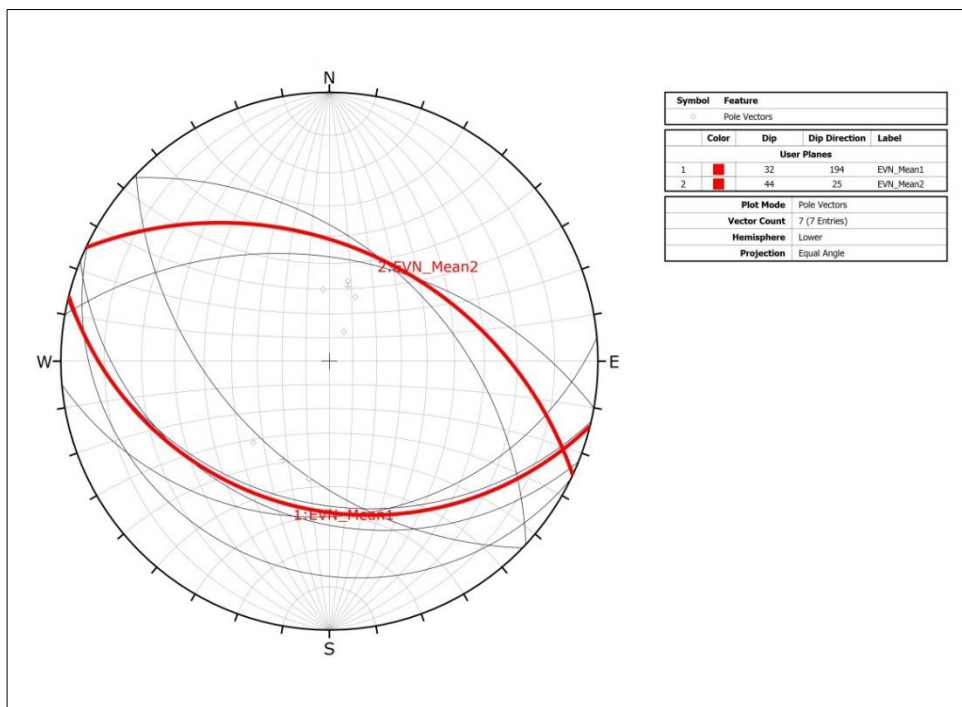
Figure 4.14. Stereonet of the normal fault planes from the Eastern vein pit, plotted as poles to planes and great circles on an equal area. In this pit, the normal faults develop as conjugate structures. Mean attitudes of the faults are 134°N, 32°SW and 115°N, 44°NE.

82
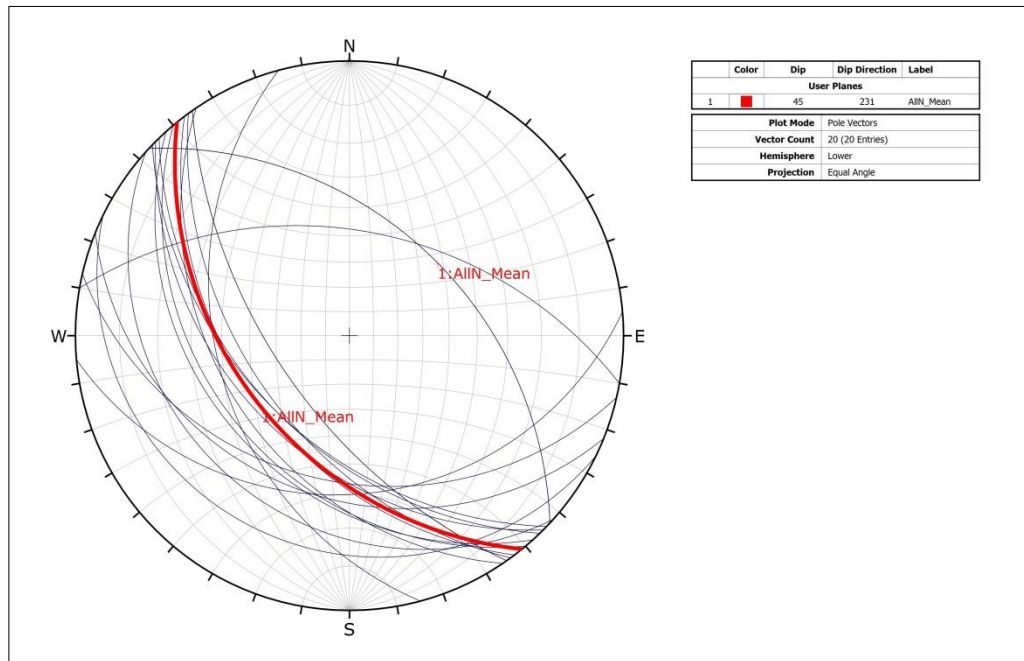
Figure 4.15. Stereonet of all normal fault planes from the study area, plotted as poles to planes and great circles on an equal area. Mean attitude of the fault plane is 141°N, 45°SW. Considering the strike of faults, a NE–SW-directed tensional stress may be suggested.

4.5. Strike-Slip Faults

Strike-slip faults form the most conspicuous structures in the study area. They occur as high-angle to vertical structures where dip amount ranges between 74° and 90°. They are common in all of the pits and define a fault zone / shear zone that contains several parallel to subparallel corrugated segments. In many cases, the fault planes are well-developed; where preserved, the planes are ornamented by slickenlines, ridges and grooves, and gutters. These structures are all developed parallel to each other and in many occasions suggest almost horizontal motion along the fault planes. The stereonet of strike-slip faults suggest that they commonly occur in three distinct directions as NNE–SSW, NW–SE, and (W)SW–(E)NE (Figures 4.16–4.19).

The computed results of the inverse analysis of fault-slip measurements define horizontal σ1 axes (01°) and gently plunging σ3 axes (14°); their trend is 171° and 081°, respectively. The attitude of σ2 axis is 76°/265° (Figure 4.20). The results are

83

consistent with strike-slip faulting (with minor dip-slip component) and an approximately NNW−SSE compression.
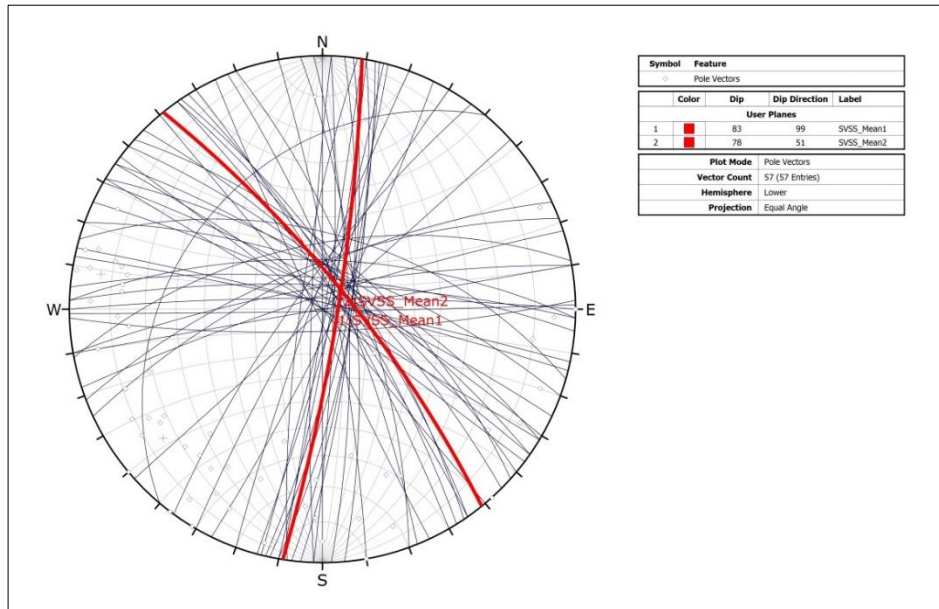
Figure 4.16. Stereonet of the strike-slip fault planes from the Southern vein pit, plotted as poles to planes and great circles on an equal area. Mean attitudes of the faults are 009°N,83°E and 321°N, 75°NE.
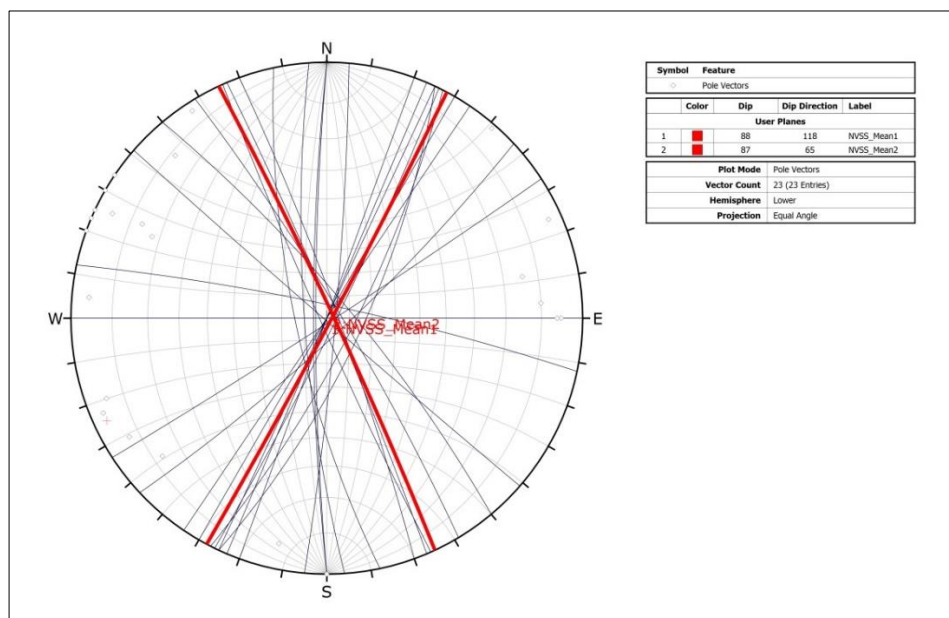
Figure 4.17. Stereonet of the strike-slip planes from the Northern vein pit, plotted as poles to planes and great circles on an equal area. Mean attitudes of the faults are 028°N, 88°SE and 335°N, 87°NE.

84

Symbol	Feature
◇	Pole Vectors

	Color	Dip	Dip Direction	Label
User Planes				
1	🟥	83	330	EVSS_Mean1
2	🟥	88	351	EVSS_Mean2
3	🟥	86	63	EVSS_Mean3

Plot Mode	Pole Vectors
Vector Count	39 (39 Entries)
Hemisphere	Lower
Projection	Equal Angle
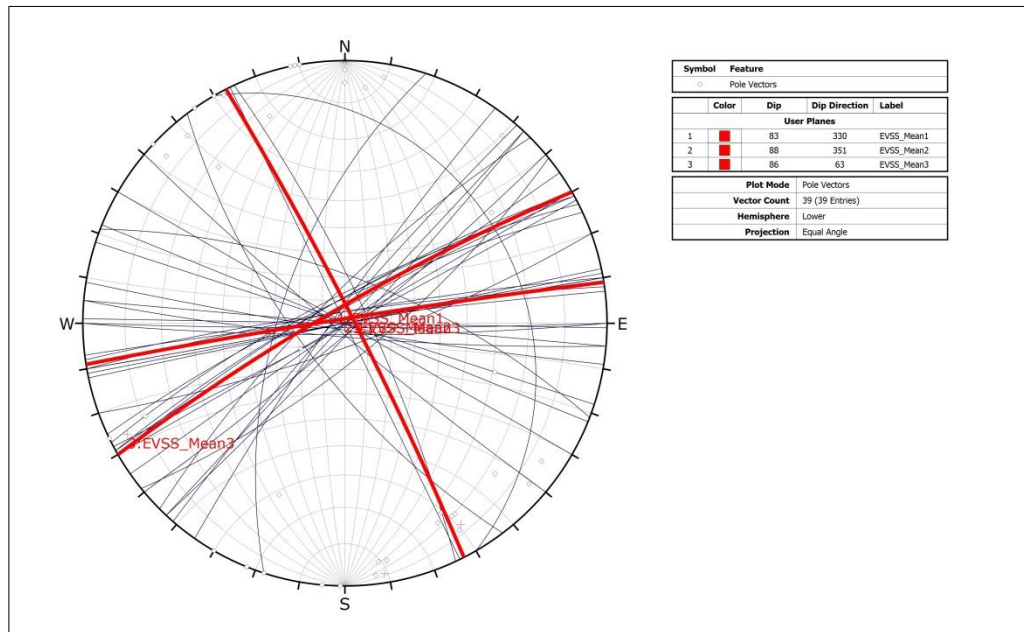
Figure 4.18. Stereonet of the strike-slip planes from the Eastern vein pit, plotted as poles to planes and great circles on an equal area. In this pit, the normal faults develop as conjugate structures. Mean attitudes of the faults are 060°N, 83°NW; 081°N, 88°NW and 333°N, 86°NE.

Symbol	Feature
◇	Pole Vectors

	Color	Dip	Dip Direction	Label
User Planes				
2	🟥	86	111	AllSS_Mean1
3	🟥	86	350	AllSS_Mean2
4	🟥	85	63	AllSS_Mean3
5	🟥	88	331	AllSS_Mean4

Plot Mode	Pole Vectors
Vector Count	119 (119 Entries)
Hemisphere	Lower
Projection	Equal Angle
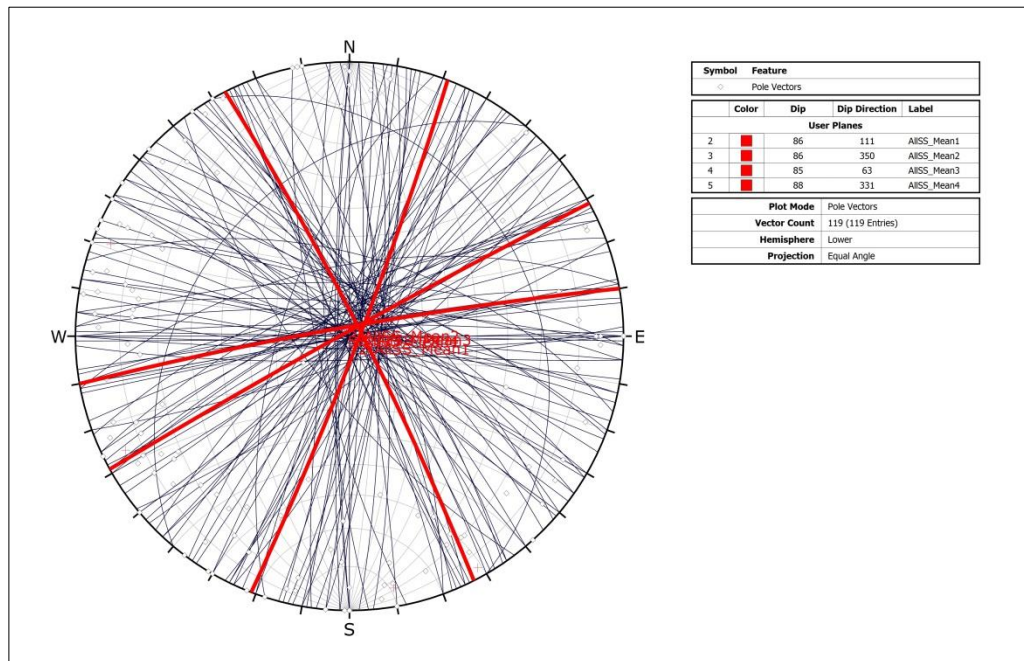
Figure 4.19. Stereonet of all strike-slip planes from the study area, plotted as poles to planes and great circles on an equal area. Mean attitudes of the fault planes are 021°N, 86°SW; 080°N, 86°N; 333°N, 85°NE and 061°N, 88°BW.

85
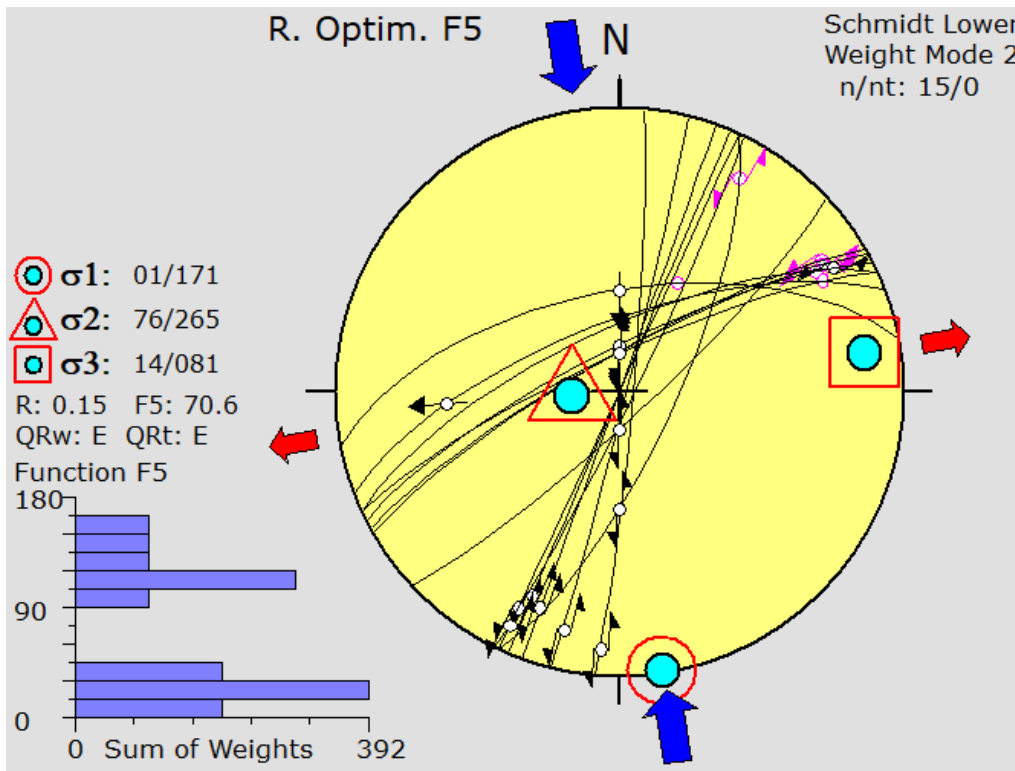
Figure 4.20. Schmidth lower hemisphere equal-area projections show stress inversion of fault-slip data from all of the strike-slip faults in the study area.

4.6. Veins

Quartz veins form the most spectacular structures of the study area when the main scope of the present thesis is concerned. The veins cut into the greenschists and granitoids; they occur as curvilinear to undulated structures and display varying orientations and possibly generations. Vein widths vary from a few centimeters to 5 m, even more in places. The along-strike lengths may extend up to ≥1.5 km. Within the greenschists, numerous foliation-parallel small-scale veins/veinlets are common. In many locations, the veins appear to be deformed and folded with the host metasediments. Relatively large-scale veins occur broadly in two distinct prominent directions as WNW–ESE and NNE–SSW; they form both in the metasediments and granitoids.

Unlike smaller veins/veinlets within greenschists, the large-scale veins are mostly associated with relatively narrow (<1 m wide) alteration halos; alteration is more

pronounced and most clearly developed around veins cutting the granitoids. The replacement of feldspars in granitoids by kaolinite (?) suggest either sericitic or illitic supergene weathering. The alteration is more pronounced in granitoids but is either absent or relatively weak around quartz veins within the schists.

The veins either display crystalline texture with quartz crystals or occur as quartz-cemented vein breccias. The mostly massive white-grey crystalline quartz veins have disseminated pyrite in minor amounts; pyrite is also present in minor amounts in the host rock within the alteration halo. Muscovite and tourmaline occur in minor amounts whereas malachite (a green copper carbonate hydroxide, $Cu_2(CO_3)(OH)_2$) is local and rare. In places, especially within the granitoids, veins display brecciated texture and stockworks within their immediate surroundings.

Because of the active mining operations, main quartz vein of the Southern Vein is almost mined out and therefore the vein itself and related structures are not observable in most parts of the open pit. Where preserved, the corrugated nature of the vein walls is very well observed. The limited number of measurements from the Southern and Eastern veins gives WNW–ESE and NE–SW orientation (Figures 4.21 and 4.22). The general orientation of the veins in the Southern pit is parallel to the regional vein structure (see Figure 2.1 for details).
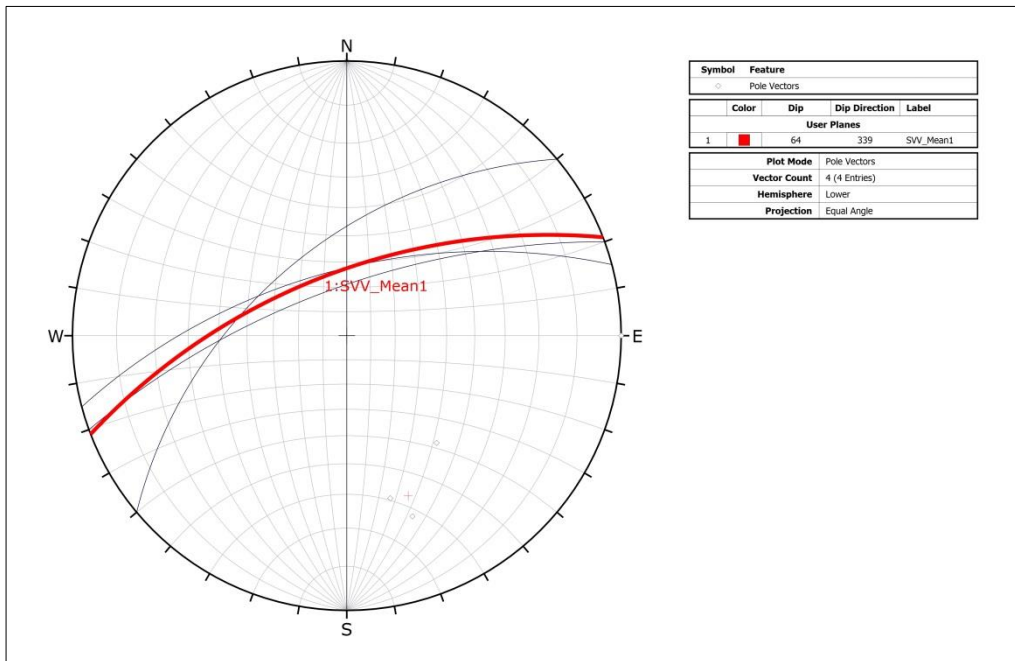
Figure 4.21. Stereonet of veins from the Southern vein pit, plotted as poles to planes and great circles on an equal area. Mean attitude of the veins is 069°N, 64°NW.
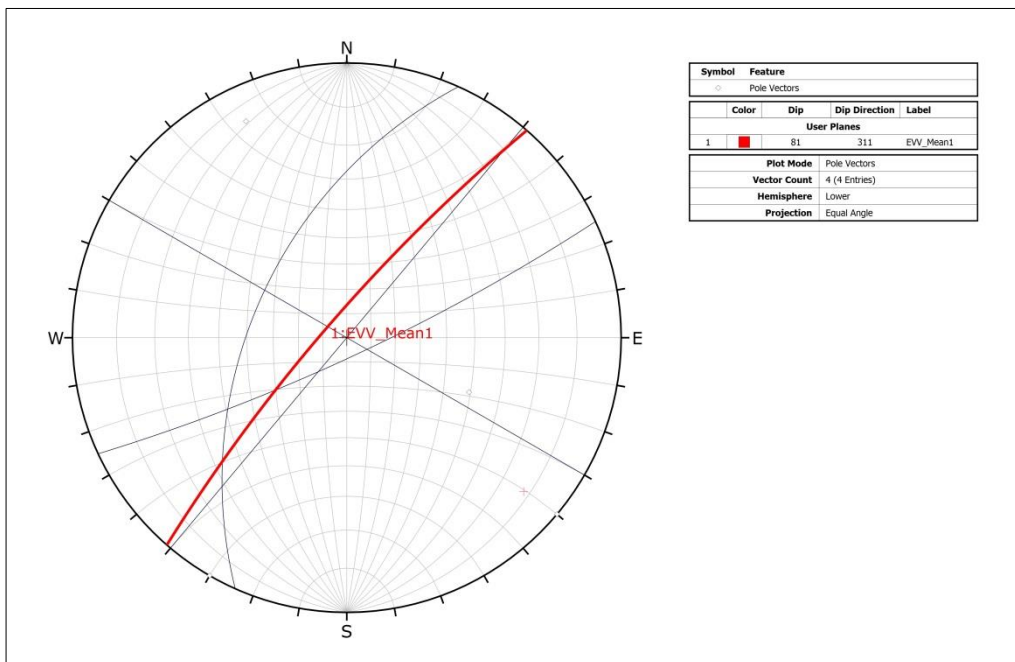
Figure 4.22. Stereonet of veins from the Eastern vein pit, plotted as poles to planes and great circles on an equal area. Mean attitude of the veins is 041°N, 81°NW.

En échelon tension gashes also occur at several locations within open pits of three vein systems. They indicate the presence of semi brittle shear zones with sinistral motion; thus, they comply with dominant strike-slip faulting in the region (Figures 4.23 and 4.24). Many shows sigmoidal forms with typical Z-shaped geometry.

The interpretation of these structures and correlation with the regional constrains will be discussed in the next chapter.

Figure 4.23. Field view from Lazy-Z shaped en échelon gash veins; their geometry is consistent with a top-to-the-left motion.

Figure 4.24. Field view from interconnecting gash veins.

CHAPTER 5

TOWARDS A WORKING MODEL OF GOLD MINERALIZATION

The Neoproterozoic–early Cambrian mobile belt, known as Pan-African Orogen (e.g., Stern 1994; Abdelsalam et al. 2002, 2003a, b) or East African orogen (EAO) (Fritz et al. 2013), forms the boundary between the Arabian-Nubian Shield (ANS) in the east and the Mozambique Belt (MB) in the west (Figure 5.1). The orogen is attributed to the closure of Mozambique Ocean, subsequent continent-continent collision of East and West Gondwana and accompanying mountain building and destruction processes that lasted between ~850 Ma and ~500 Ma. The ANS represents a juvenile Neoproterozoic crust while the MB consists mainly of pre-Neoproterozoic crust. These rock units have been deformed and overprinted during Neoproterozoic–early Cambrian polyphase tectono-thermal event(s) (intense metamorphism, deformation and granitoid magmatism).

The studied veins are located within the TCSZ. Thus, the age and evolution of this zone can be used as a reference to discuss the tectonic meaning and significance of structures studied in the study area. There is not much done on the geology of this region in Sudan. In fact, there is no a proper geological map of the region. There appears only one paper specific to this region, in particular to the TCSZ, by Abdelsalam et al. (2003a). The authors have briefly described the main geological structures in around the shear zone and proposed an evolutionary scheme. It is therefore decided to take this paper as reference in further discussion of geological structures observed and studied during thesis research.
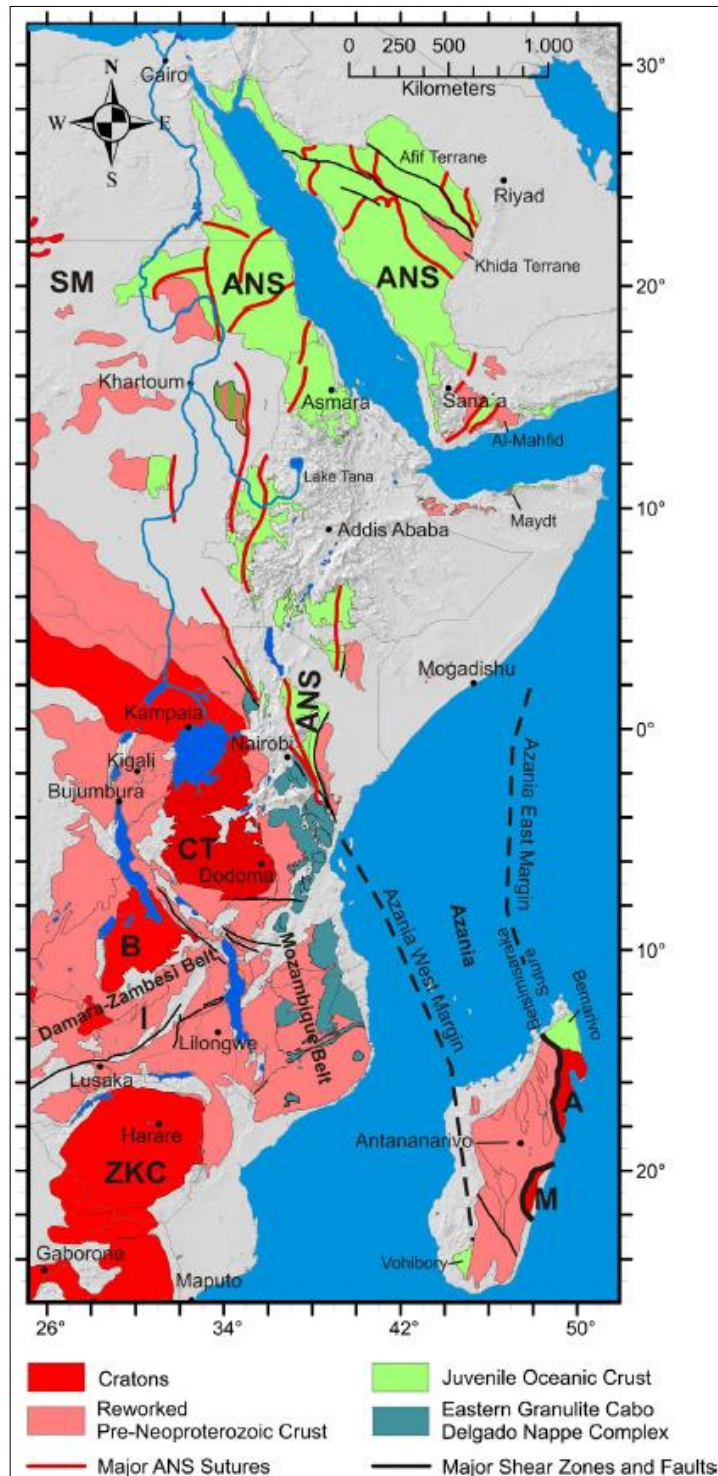
Figure 5.1. Distribution of crustal domains in the East African Orogen. SM, Sahara Metacraton; CTB, Congo–Tanzania–Bangweulu Cratons; ZKC, Zimbabwe–Kalahari Cratons; I, Irumide Belt; A, Antogil Craton; M, Masora Craton; ANS, Arabian Nubian Shield. Capital names indicated here are not labelled on subsequent maps.

Site observations, structural measurements, geochemical results, and drilling data shows that there is more than one deformation stage in the area and that the gold mineralization is controlled by geological structures. The existing questions relate to (i) number, mechanism and relative age of the deformation phases and (ii) which structures control gold mineralization; the following sections will try to address these questions.

5.1. Geological Structures: Summary

The geological structures in the study area and nearby surroundings include five major structures. These structures are regional penetrative foliation and similarly trending folds, reverse faults, normal faults, strike-slip faults and veins. All of them are curvilinear structures and characterized by undulations; that is why along-strike variations are common. The faults have corrugations. Most are defined by polished slickensides and few show preserved slickenlines to indicate the sense of motion. Almost all of the normal and reverse faults are observed to offset marker horizons but no well-preserved slickenside surfaces. The normal and reverse faults are most likely oblique-slip structures with considerable dip-slip component; but for simplicity they are assumed as dip-slip structures. The strike orientations of the structures represent the best fit great circles (see Chapter 4) and are summarized in Table 5.1. As many of these structures possess no fault planes with slickenlines, the direction of maximum principal stress axes is inferred from their common orientations; stress axes appear as NNW–SSE to NNE–SSW, except for (N)NE–(S)SW and NW–SE thrust faults.

Table 5.1. *Summary of geological structures observed and mapped during this research. The orientation of principal stress axes is inferred assuming that the normal and reverse faults are pure dip-slip structures whereas the σ1 orientation for strike-slip faults comes from the paleostress analyses. The orientation of the structures represents the best fit great circles.*

Structure	Approximate Orientation	Inferred Principal Stress Orientation	Deformation Phase
Foliation & Folds	~ENE–WSW	$\sigma_{1=}$ ~N–S	D_1
	(N)NE–(S)SW	$\sigma_{1=}$ ~(W)NW–(E)SE	D_2
Reverse Faults	~E–W	$\sigma_{1=}$ ~N–S	D_1
	NW–SE	$\sigma_{1=}$ NE–SW	D_2
Strike-slip Faults	NW–SE & N(NE)–(S)SW	$\sigma_{1=}$ NNW–SSE	D_3
	W(SW)–(E)NE	$\sigma_{1=}$ NE–SW	D_5 (?)
Veins	~E–W	$\sigma_{1=}$ ~N–S	D_1
	NE–SW	$\sigma_{1=}$ NNW–SSE	D_3
Normal Faults	NW–SE	$\sigma_{3=}$ NE–SW	D_4 (or D_3)

5.2. Interpretation of Faults logical Structures: Summary

Because the study area lies within the NNW- to NNE-trending sinistral strike-slip TCSZ, the geological structures will be interpreted with reference to shear zone. The inverse analysis of strike-slip faults as part of the TCSZ define a horizontal σ1 axes trending in 171°N direction. This σ1 axis is taken as the reference and the structures are interpreted using terminology of Riedel shears within an idealized sinistral strike-slip fault pattern (Figure 5.2). It appears that veins, normal and strike-slip faults fit well with the fault pattern whereas WSW–ENE-trending strike-slip faults, NW–SE reverse faults and (N)NE–(S)SW folds are not compatible with this pattern and they suggest a more ENE –WSW shortening during their deformation.
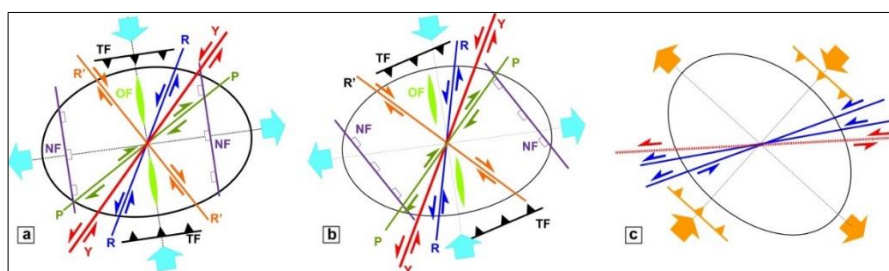
Figure 5.2. The interpretation of the geological structures in the study area. (a) Idealized sinistral strike-slip fault pattern according to the 171°N-directed σ1 axis; (b) the orientation of different structures that fits well with the sinistral faulting; (c) the structures not compatible with this σ1 axis.

The NNE–SSW-trending (ca. 021°N, 86°SW) sinistral strike-slip faults are taken as the Y-shear of the fault system. The NW–SW trending dextral faults, N–S sinistral faults and NE –SW-trending sinistral faults are interpreted as R'-shear, R-shear and P-shear of this fault system (see Figure 4.19 for detail information). The ca. W–E-trending thrust faults and associated auriferous quartz veins might also have formed in this NNW–SSE shortening tectonic setting.

The NW–SE-trending (141°N, 45°SW; Figure 4.15) moderately-dipping normal faults may fit into this pattern; if this works, then they must be oblique-slip fault component. The best fit great circle is about 30° to ideal orientation in this system. It is therefore speculated that, owing to their generally low-angle geometry, the normal faults may belong to a different phase of deformation and that they might have been associated with post-orogenic (collapse) extensional deformation (see next section).

The (N)NE–(S)SW-trending folds that deforms the regional penetrative foliation form common structural elements of this region (Abdelsalam et al. 2003a) and they suggest an ~(W)NW–(E)SE shortening during their formation. Similarly, NW–SE-trending (141°N, 31°SW and 137°N, 17°NW; Figure 4.11) low- to moderately-dipping thrust faults are not compatible with this sinistral fault pattern and suggest a NE–SW shortening. It is here speculated that ca. N–S folds and these thrust faults may be genetically related. It is important to note that the general orientation of the thrust faults fits well with the Abu Haned fold-and-thrust belt (Figure 1.11).

The WSW–ENE-trending (260°N,86°N and 241°N,88°NW; Figure 4.19) strike-slip faults are also not compatible. Their general orientation and comparison with NW–SE thrust/reverse faults may suggest genetic relationships (Figure 5.1c). In this case, these faults have formed and reactivated similarly-trending large-scale vein margins as sinistral strike-slip faults. Additionally, the Google Earth image of the study area illustrates the presence of similarly-trending faults in the region (Figure 5.3). These faults appear to offset the Nile river course sinistrally, otherwise N–S running river; in these locations the river flows in WSE–ENE direction. The strike-slip faults appear

to cut and displace the TCSZ and are therefore interpreted as the youngest structures in the region. If this inference is correct, then WSW–ENE faults are reactivated sinistral structures.

5.3. Interpretation of Veins

The veins occur in three distinct forms: (i) relatively thin veins and veinlets parallel to the penetrative foliation; (ii) WSW–ESE-trending large-scale auriferous quartz veins and (iii) NNE-SSW-trending auriferous veins. The first group of veins have no alteration halos around them. These structures are interpreted as syn-metamorphic veining. The absence of alteration may be explained by the fact that the mineralizing hydrothermal fluids might have comparable temperatures and/or chemistry with respect to the metamorphic conditions of the greenschist rocks or ore-bearing hydrothermal fluids were not acidic enough to cause alteration in the host rocks. If the first inference is the working hypothesis, it may be used to suggest that quartz veining was synchronous with regional low-grade metamorphism. The presence of biotite, sericite and chlorite in metasediments and, chlorite, actinolite, and epidote in metavolcanics suggest that the metamorphism have reached to greenschist facies conditions in this part of the Pan-African Orogen.
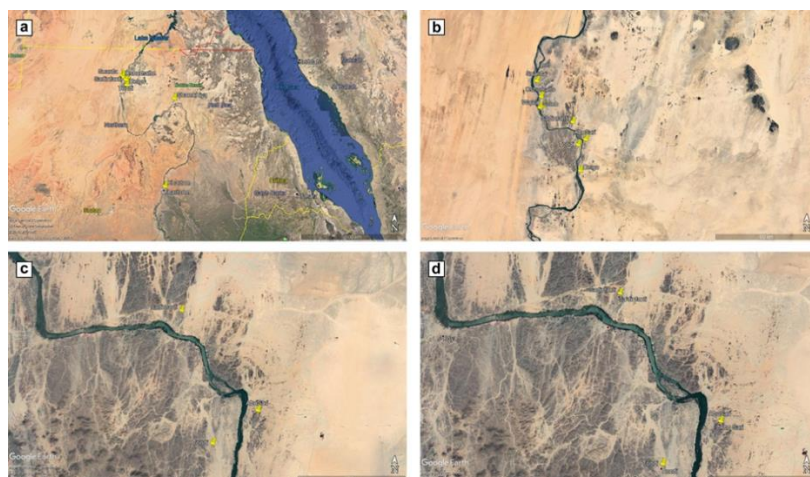
Figure 5.3. Google Earth images from Northern Sudan. Note the sharp bends in the general course of the River Nile in (a). (b) Close-up view of the ~N–S flowing river course and sharp ca. W–E bends. (c, d) the W–E river course appears almost parallel to the sharp lineaments; it is speculated that these bends correspond sinistral offset along similarly trending strike-slip faults.

96

The WSW–ESE-trending large-scale veins have both crystalline and brecciated textures. The breccia texture is attributed to both mechanical fragmentation and, fluid-assisted veining and brecciation processes. The textures are therefore consistent with multiple stages of veining or progressive veining. The general parallelism of vein trends, reverse faults and folds in the greenschists may indicate possible genetic or kinematic association of veining with reverse faults. It is therefore suggested that these veins form syn-kinematically with possibly oblique-slip reverse/thrust faults and that they are syn- and post-deformational with respect to the main low-grade tectono-metamorphic event that caused metamorphism, folding and thrusting of host rock greenschists. The map pattern of these WSW–ESE-trending veins illustrated open undulations; this is attributed to folding event following their formation (Figure 5.4).
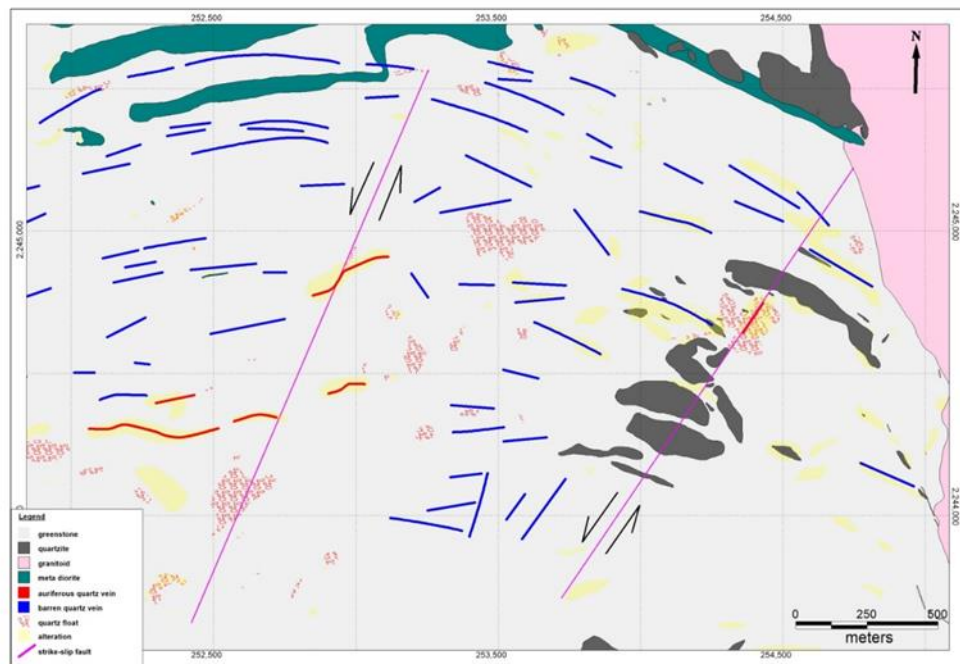
Figure 5.4. Simplified map showing distribution of large-scale WSW–ESE-trending quartz veins and their relation to NNE–SSW-sinistral shear zones in the study area. Note the open undulations along the Southern Vein strike. The mapping of these structures is not done in detail and therefore miss many pronounced undulations along strike of the veins. These undulations are attributed to folding of the veins and associated greenschists that have fold axes trending in ca. N–S direction.

97

The NNE- to NNW-trending veins mostly show brecciated textures and are interpreted to be associated with sinistral TCSZ. Breccias indicate active faulting during their genesis. This phase of vein formation has resulted in enrichments at the intersection areas of WSW–ESE- and NNE- to NNW-trending quartz veins. Thus, strike-slip faults are active structures of the vein formation. There appears that the wall of WSW–ESE-trending veins were later reactivated as sinistral strike-slip faults (Figure 5.5). The grade distribution along these veins illustrate that highest gold grade occurs at the center and tips of the vein(s) and while low-grades occur along the margins (Figure 5.5). This illustrate the fact that the high-grade mineralization occurs along-fault and around-tip damage zones (Figure 5.6; cf. Choi et al. 2016), and at fault intersections.
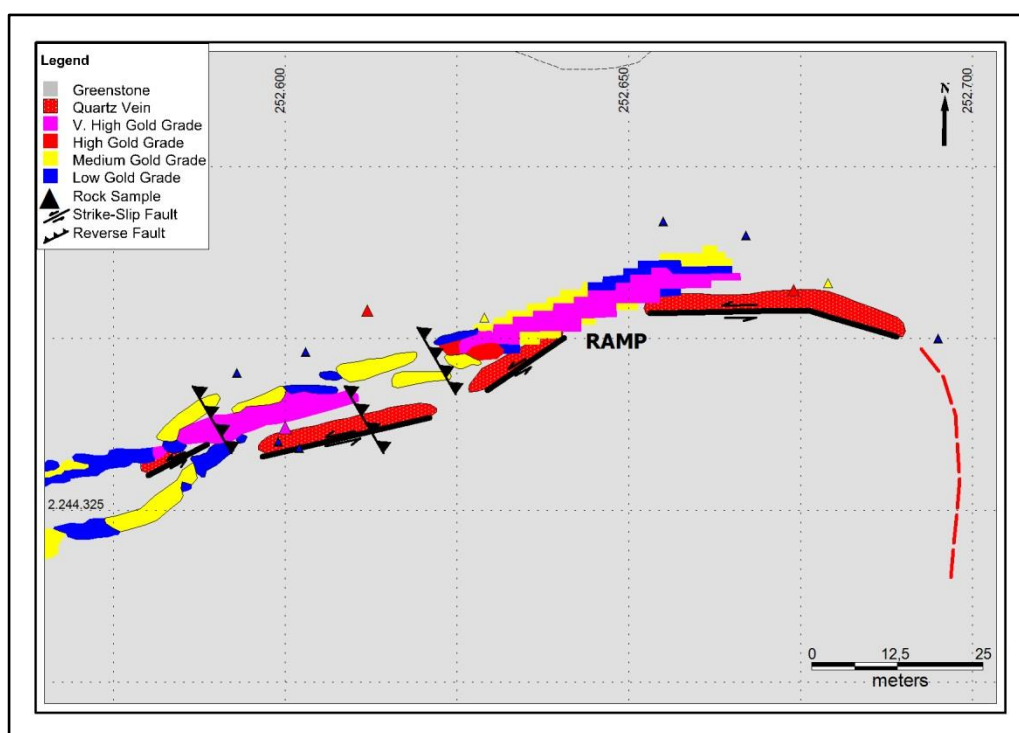
Figure 5.5. Micromine software model of the most eastern part of the Southern Vein with major structural features and gold mineralization. The model is generated according to drilling assay results. As can be seen in the figure the highest grade of gold is in the centre of the vein system and at the eastern tip of the vein where fractures are dominant. Also, the eastern part occurs at the intersection zone with the sinistral shear zone structures. Note also that the NW–SE-trending thrust/reverse faults cut and displace the vein, suggesting that they are relatively younger than WSW–ESE-veining.

98

The correlation of vein structure and geochemical data illustrates the fact that: (i) gold grade is not homogenously distributed within the vein system; (ii) gold mineralization occurs mostly in the quartz veins and the alteration halos around them quartz; (iii) gold grades reach highest values where there are more fractures, and where shear zone fabrics are available; (iv) there is considerable enrichment in gold grade where faults/shear zones bend and/or intersect and (v) in most cases, milky and massive quartz veins have relatively the lowest gold grades or they are barren. In the places where one or more structures intersect, intense fracturing and shearing induces secondary porosity and permeability, and provides pathways for fluid flow and finally form suitable sites/traps for precipitation of ore minerals from solution (Figures 5.6, 5.7, and 5.8). Similarly, both drilling and surface sampling results confirm that the overlapping zones between quartz veins also form suitable locations for gold accumulation.
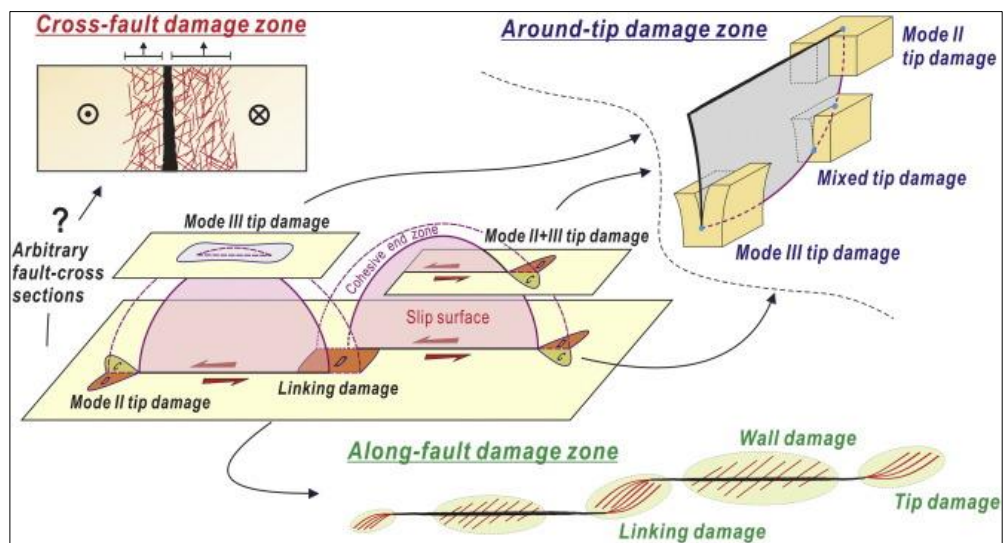
Figure 5.6. Simple 3D schematic illustration of the fault damage zones around a segmented left-lateral fault (from Choi et al. 2016).
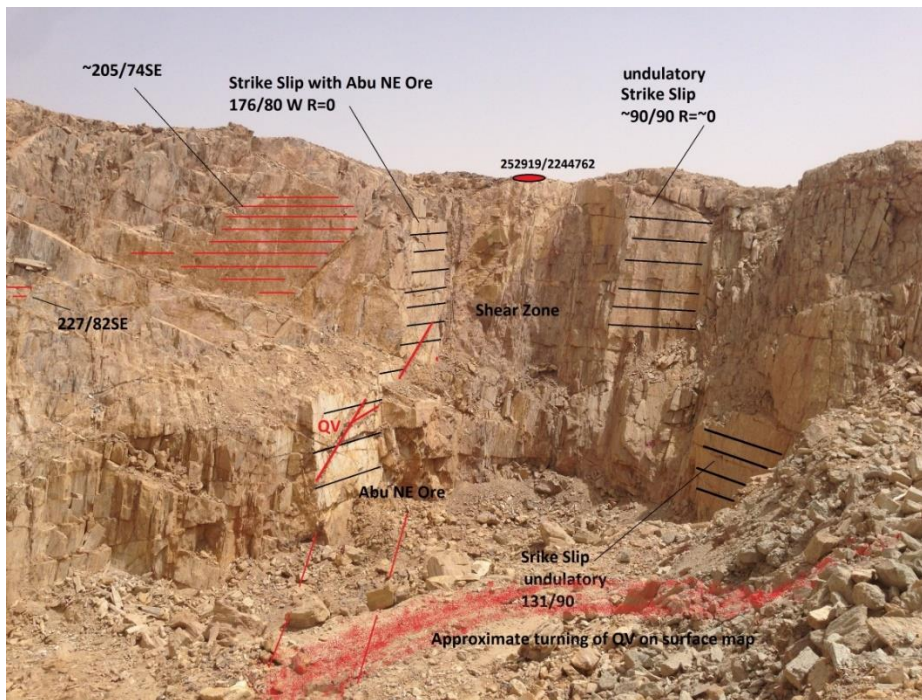
Figure 5.7. Looking from north to south, open pit of the North Vein showing the intersections and relationship of different strike-slip faults. Approximate route of the quartz vein is given as a red shadow.
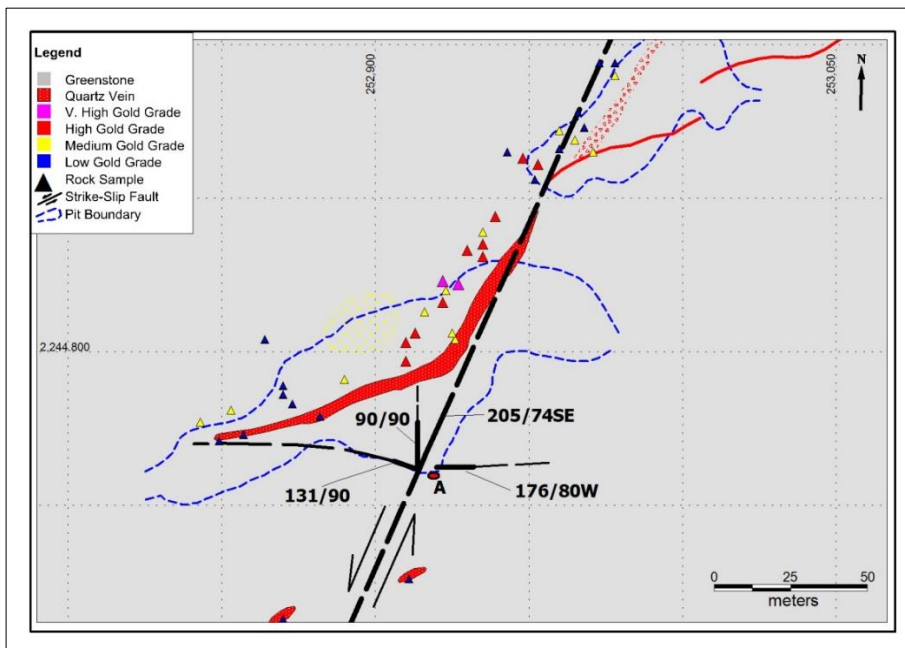
Figure 5.8. Map showing the fault relationships and the surface gold mineralization. Point A on the intersection of the faults is the point where located as 252919/2244762 UTM WGS 84 in Figure 5.7.

100

These inferences confirm that the auriferous veins represent typical mesothermal orogenic gold precipitation in association with the later stages of Pan-African orogeny. There is close association of deformation plus metamorphism and veining. The lack of alteration along the margins of mostly boundinaged foliation-parallel quartz veins may support syn-metamorphic veining in equilibrium with greenschist-facies conditions and therefore a metamorphic fluid origin. The large-scale veins are associated with reverse/thrust faults and indicate both syn- to post-metamorphic processes. NNE- to NNW-trending veins form relatively latter in the geologic history as part of the sinistral TCSZ deformation. The source of hydrothermal fluids is problematic here. It is known that the metamorphic rocks are intruded by syn- to post-deformational A-type granitoids, some of which are also deformed within the sinistral shear zone. The ore-bearing fluids might have been released from these plutons but lack of reported base metals preclude this origin. The rare occurrence of copper mineral malachite occurrence may support volatile contribution from the intruding plutons. It is here suggesting that the origin of the gold-bearing hydrothermal fluids is mostly metamorphic origin, derived from the country rocks at depth during prograde metamorphism, with possible weak contribution from the A-type granitoids. This brings a question of whether the auriferous quartz veins are truly orogenic gold deposits or intrusion-related/influence orogenic gold deposits. This requires further detailed petrographic, geochemical and fluid inclusion composition analyses, which lies outside scope of the present thesis.

5.4. Deformation Phases

The low-grade metamorphics are interpreted to represent arc assemblages. These metamorphics occurs within a ca. N–S-trending belt that also comprises dismembered ophiolites; all of these rocks are intruded by syn- to post-orogenic granitoid bodies of varying composition.

The relationships between geological structures in the study area suggest that the region has suffered from five distinct phases of deformation (D1 to D5; Table 5.1);

they all form part of a progressive deformation during collision and post-orgenic regional extension. The following information about the different phases of deformation and their possible relationship to different stages of Pan-African orogeny is adopted from Abdelsalam et al. (2003a); the authors have suggested three deformation phases but here two more phases are incorporated into the tectono-metamorphic-magmatic evolution of the region.

The first phase (D1) is attributed to the emplacement of ophiolites onto the passive margin sediments towards S- to SE; the major structures occur within a ca. E–W-trending fold-and-thrust belt; the reverse faults are interpreted to host the WSW–ENE quartz-veining. D1 forms the main deformation in the area is directly related to the East (Pan) African Orogeny between 850 and 500 Ma. Almost NE–SW collision of the West Gondwana and East Gondwana caused intense deformation and metamorphism of the arc-related volcano-sedimentary sequence and resulted in the formation of foliated greenstone facies rocks. According to the site observations, after this deformation process, almost N–S foliation and 1 mm to 50 cm boudinaged vein sets parallel to foliation have formed as first stage. The metamorphic fluids derived from the deeper parts of the orogen are responsible for gold mineralization in veins parallel to the foliation or those localized along reverse faults.

The second phase (D2) is represented by N- to NNE-trending open folds and is consistent with ca. E–W shortening. The folding has also affected the quartz veins as indicated by open undulations along strike of the veins. This event is associated with NW–SE oblique collision along Keraf Suture at the boundary between the Saharan Metacraton in the west and the Arabian-Nubian Shield in the east at ~650–590 Ma. The NW–SE-trending thrust/reverse faults have also formed during this phase. The WSW–ENE-trending sinistral strike-slip faulting might have taken place during this phase and reactivated similarly-trending large-scale vein walls. The N- to NNE-trending TCSZ was formed during later stages of this phase when compressional regime has shifted to sinistral transpressional regime; thus, the collision zone was reactivated as a sinistral shear zone.

The third phase (D3) is associated with continuing strike-slip deformation along the TCSZ. The TCSZ is a typical sinistral strike-slip shear zone that comprises several parallel to subparallel NNW- to NNE-trending sinistral and dextral fault segments. The collision-related crustal thickening resulted in the formation of A-type granitoids that intrude the host rock greenschists. This event has lasted by about ∼590–550 Ma. The formation of strike-slip-parallel auriferous gold veining has possibly occurred during this phase. There is weak evidence that the volatiles release from the intruding pluton(s) have contributed to the gold mineralization. This stage has resulted in the formation of shear zone-parallel fractures, intense brittle deformation and thus extensive vein formation and associated second phase of economic gold mineralization.

Thickening of the Saharan Metacraton lithosphere triggered orogenic collapse induced regional extension (D4) with NW-trending low- to moderate-angle normal-slip faults developed after 550 Ma.

The last phase of deformation in the region is represented by WSW–ENE-trending strike-slip faulting. D5 deformation strike-slip faults appear to be the youngest structures. Their traces are readily be recognizable in Google Earth images (Figure 5.3). These faults appear to cut and displace the Nile River course as well. It is here speculated that the WSW–ENE faults formed during D2 deformation are reactivated during D5 deformation.

In this model, the early phase of gold mineralization was associated with regional deformation and prograde metamorphism and has occurred along thrust/reverse faults (Figure 5.9) The second stage was induced by crustal-scale shear zone deformation (Figure 5.10). The TCSZ represents trans-crustal fault zone that has formed the pathways for hydrothermal fluids to move upward. The shear zone deformation represents the late orogenic shift from compressional to transpressional regimes. These veins therefore form very typical examples of shear-hosted mesothermal auriferous quartz veins.
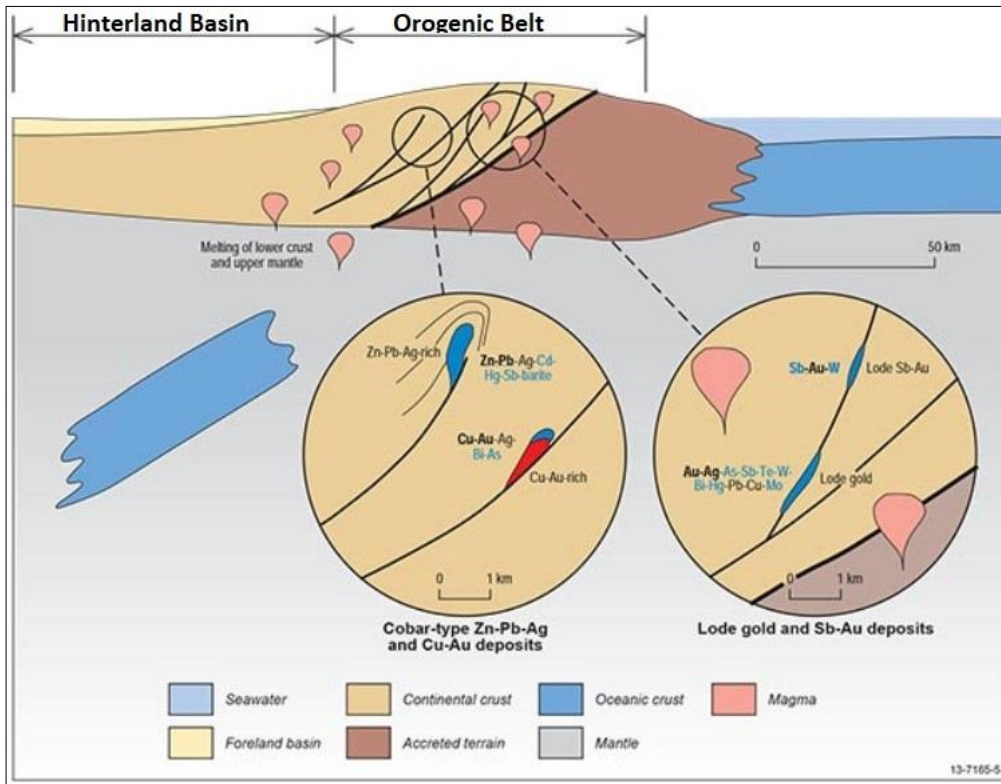
Figure 5.9. Diagrammatic sketch of the orogenic mineral system illustrating the relative location of deposits types within the overall setting deposit types, associated with continental margin accretionary (oceanic-continental) and collisional (continent-continent) orogens (modified from Geoscience Australia website).
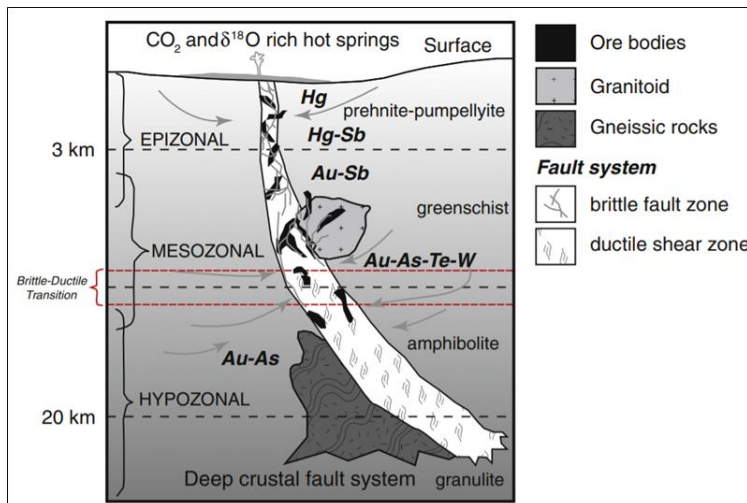
Figure 5.10. Hypothetical cross section showing orogenic gold deposit formation at different structural levels within the crust. These deposits form over a variety of depths, from as shallow as 3 km to as deep as 20 km, typically during late orogenic shifts from compressional to transpressional or transtensional regimes (from Goldfarb and Groves, 2015).

104

The contribution of A-type granitoid intrusion(s) to the shear zone mineralization is unknown as there is no base metals reported in the Abu Sari deposit or no geochemical and fluid inclusion studies in the area. But, rare occurrence of copper mineral malachite may be used as circumstantial evidence that there is some input from the intrusion. Thus, it is yet not clear if one can name Abu Sari mesothermal gold deposit as an example of classical orogenic gold or intrusion-related gold deposits. The answer to this question needs further geochemical work in the deposit

REFERENCES

Abdelfadil, K.M., Obeid, M.A., Azer, M.K., Asimov, P.D., 2018. Late Neoproterozoic adakitic lavas in the Arabian-Nubian shield, Sinai Peninsula, Egypt. Journal of Asian Earth Sciences 158, 301–323.

Abdel-Rahman, E.M., Matheis, G., Schandelmeier, H., Karfis, M.A., Gadir, I., El Khedir, M., 1993. Evolution of the Keraf back-arc basin: Constraints on the Nubian Shield margin. In: Thorweihe, U., Schandelmeier, H. (Eds.), Geoscientific Research in NE Africa. Balkema, Amsterdam, pp. 93–98.

Abdelsalam, M.G., Dawoud, A.S., 1991. The Kabus ophiolitic melange, Sudan, and its bearing on the W boundary of the Nubian Shield. Journal Geological Society, London 148, 83–92.

Abdelsalam, M.G., Stern, R., 1993. Structure of the late Proterozoic Nakasib suture, Sudan. Journal of the Geological Society, London, Vol. 150, 1993, pp. 1065-1074, 13 figs.

Abdelsalam, M.G., Stern, R., 1993. Tectonic evolution of the Nakasib suture, Red Sea Hills, Sudan: evidence for a late Precambrian Wilson Cycle. Journal of the Geological Society, London, Vol. 1150, 1993, pp. 393-404, 15 figs, 2 tables.

Abdelsalam, M.G., Stern, R., Schandelmeier, J., Sultan, H.M., 1995. Deformational history of the Keraf zone in northeast Sudan, revealed by Shuttle Imaging Radar. J. Geol. 103, 475–491.

Abdelsalam, M.G. & Stern, R.J. 1996. Mapping Precambrian structures in the Sahara Desert with SIR-C/X-SAR Radar: the Neoproterozoic Keraf Suture, NE Sudan. Journal of Geophysical Research 101, 23063–23076.

Abdelsalam, M.G., Stern, R.J., Copeland, P., Elfaki, E.M., Elhur, B., Ibrahim, F.M., 1998. The Neoproterozoic Keraf suture in NE Sudan: Sinistral transpression along the eastern margin of West Gondwana. Journal Geology 106, 133–148.

Abdelsalam, M.G., Liegeois, J.-P., Stern, R.J., 2002. The Saharan Metacraton. J. Afr. Earth Sci. 34, 119–136.

Abdelsalam, M.G., Abdeen, M.M., Dowaidar, H.M., Stern, R.J., Abdelghaffar, A.A., 2003. Structural evolution of the Neoproterozoic Western Allaqi–Heiani suture, southeastern Egypt. Precambrian Research, 124, 87-104.

Ahmed, A.A.M., 1998. Sudan industrial minerals & rocks. Khartoum, Sudan: Centre for Strategic Studies

Azer, M. K., 2014. Petrological studies of Neoproterozoic serpentinized ultramafics of the Nubian Shield: spinel compositions as evidence of the tectonic evolution of Egyptian ophiolites. Acta Geologica Polonica, Vol. 64, No. 1, pp. 113-127.

Babiker, Insaf & Elsayed Zeinelabdein, Khalid & Elnadi, Abdel., 2015. Geological Mapping and Gold Prospecting of Wadi Umm Beckol-Wadi Akasha Area, Northern Sudan Based on Remote Sensing. American Journal of Earth Sciences. 2. 172-179.

Barbour, K. M., 1961, The Republic of the Sudan: A Regional Geography. London: UCL Press.

Bierlein, F. P., Reynolds N., Arne D., Bargmann C., McKeag S., Bullen, W., Al-Athbah, H., McKnigh, S., Maas, R., 2016. Petrogenesis of a Neoproterozoic magmatic arc hosting porphyry Cu-Au mineralization at Jebel Ohier in the Gebeit Terrane, NE Sudan. Ore Geology Reviews, 79, 133–154.

Blasband, B., White, S., Brooijmans, P., De Boorder, H., Visser, W., 2000. Late Proterozoic extensional collapse in the Arabian-Nubian Shield: Journal of the Geological Society, London, Vol. 157, 2000, pp. 615-628.

Choi, J., Edwards, P., Ko, K., Kim, Y., 2016. Definition and classification of fault damage zones: A review and a new methodological approach: Earth Science Reviews, Volume 152, p. 70-87.

Cox, G.M., Foden, J., Collins, A.S., 2018. Late Neoproterozoic adakitic magmatism of the eastern Arabian Nubian Shield. Geoscience Fronteers, 1-12.

Denkler, T., Franz, G., Schandelmeier, H., 1994. Tectonometamorphic evolution of the Neoproterozoic Delgo suture zone, northern Sudan. Geologische Rundschau 83, 578–590.

El-Bialy, M.Z., Shata, A.E., 2018. Geochemistry, petrogenesis and radioactive mineralization of two coeval Neoproterozoic post-collisional calc-alkaline and alkaline granitoid suites from Sinai, Arabian Nubian Shield. Chemie der Erde https://doi.org/10.1016/j.chemer.2017.12.001.

Elsamani, Y., Almuslem, A. A., El Tokhi, M., 2001. Geology and Geotectonic Classification of Pan-African Gold Mineralizations in the Red Sea Hills, Sudan. International Geology Review, Vol. 43, 2001, p. 1117-1128.

Franz, G., Harms, U., Denkler, T., Pasteels, P., 1993. Late Cretaceous igneous activity in the Delgo uplift (Northern Province, Sudan). Geoscientific Research in Northeast Africa, Thorweihe & Schandelmeier (eds), 227-230.

Fritz, H., Abdelsalam, M., Ali, K.A., Bingen, B., Collins, A.S., Fowler, A.R., Ghebreab, W., Hauzenberger, C.A., Johnson, P.R., Kusky, T.M., Macey, P., Muhongo, S., Stern, R.J., Viola, G., 2013. Orogen styles in the East African Orogen: a review of the Neoproterozoic to Cambrian tectonic evolution. J. Afr. Earth. Sci. 86, 65–106.

Gass.T, G. 1981. Pan-African (Upper Proterozoic) plate tectonics of the Arabian-Nubian Shield. In: Precambrian Plate Tectonics (edited by Kroner, A.), Elsevier, Amsterdam, 387-405.

Goldfarb, R. J., Groves, D. I., Gardoll, S., 2001. Orogenic gold and geologic time: a global synthesis. Ore Geology Reviews, 18, 1–75.

Goldfarb, Richard & Groves, D., 2015. Orogenic gold: Common or evolving fluid and metal sources through time. Lithos. 233. 2-26.

Harms, U., Darbyshire, D.P.F., Denkler, T., Hengst, M., Schandelmeier, H., 1994. Evolution of the Neoproterozoic Delgo suturs zone and crustal growth in northern Sudan: geochemical and radiogenic isotope constrains. Geologische Rundschau 83, 591– 603.

Hondorf, A., Meinhold, K. D., Vail, J. R., 1994. Geochronology of anorogenic igneous complexes in the Sudan: isotopic investigations in North Kordofan, the Nubian Desert and the Red Sea Hills. Journal of African Earth Sciences, Vol. 19, No. 1/2, pp. 3-15.

Ibrahim, W. S., Watanabe, K., Yonezu, K., 2016. Structural and litho-tectonic controls on Neoproterozoic base metal sulfide and gold mineralization in North Hamisana shear zone, South Eastern Desert, Egypt: The integrated field, structural, Landsat 7 ETM+ and ASTER data approach. Ore Geology Reviews, 79, 62–77.

Klemm, Dietrich & Klemm, Rosemarie & Murr, Andreas., 2001. Gold of the Pharaohs – 6000 years of gold mining in Egypt and Nubia. Journal of African Earth Sciences. 33. 643-659.

Kröner, A. & Stern, R.J. 2004. Pan-African orogeny. Encyclopedia of Geology 1, 1–12.

Kongnyuy, S. C., Giulio, M., Satir, M., 2012. Archaean Zircon U-Pb Age Paradox in Juvenile Neoproterozoic Granitoids, Central North Sudan, Saharan Metacraton. Turkish Journal of Earth Sciences (Turkish J. Earth Sci.), Vol. 21, 2012, pp. 97–125.

Küster, D., Liégeois, J.-P., Matukov, D., Sergeev, S., Lucassen, F., 2008. Zircon geochronology and Sr, Nd, Pb isotope geochemistry of granitoids from Bayuda Desert and Sabloka (Sudan): evidence for a Bayudian event (920–900 Ma) preceding the Pan-African orogenic cycle (860–590 Ma) at the eastern boundary of the Saharan Metacraton. Precambrian Research 164, 16–39.

Neuendorf, K. K. E., Mehl Jr., J.P. & Jackson, J. A., 2011: Glossary of Geology, 5th ed., revised.Alexandria, VA, American Geological Institute, 800 pp.

Richards, J., 2010. Report on Block 17 Site Visit, Sudan. 9-11 July 2010 for Tahe International Metal Mining Inc. Internal independent report on behalf of Tahe International Metals Mining Inc.

Satir, M., Morteani, G., Fuganti, A., von Drach, V., 1991. K–Ar ages, Sr-isotope composition and chemistry of late Cretaceous–Tertiary basalts from the Nubian Desert (northern Sudan). European Journal of Mineralogy 3, 943–955.

Schandelmeier, H., Richter, A., Harms, U., 1987. Proterozoic deformation of the East Sahara Craton in southeast Libya, south Egypt and north Sudan. Tectonophysics 140, 233–246.

Schandelmeier, H., Wipfler, E. Küster, D., Sultan, M., Becker, R., Stern, R.J., Abdelsalam, M.G., 1994a. Atmur-Delgo suture: a Neoproterozoic oceanic basin extending into the interior of northeast Africa. Geology 22, 563–566.

Schandelmeier, H., Abdel Rahman, E.M., Wipfler, E., Küster, D., Utke, A., Matheis, G., 1994b. Late Proterozoic magmatism in the Nakasib suture, Red Sea Hills, Sudan. J. Geol. Soc. Lond. 151, 485–497.

Shang, C.K., Satir, M., Morteani, G. & Taubald, H. 2010a. Zircon and titanite age evidence for coeval granitization and migmatization of the early Middle and early Late Proterozoic Saharan Metacraton; example from the central North Sudan basement. Journal of African Earth Sciences 57, 492–524.

Shang, C.K., Morteani, G., Satir, M. & Taubald, H. 2010b. Neoproterozoic continental growth prior to Gondwana assembly: constraints from zircon-titanite geochronology, geochemistry and petrography of ring complex granitoids, Sudan. Lithos 118, 61–81.

Stern, R.J. and Dawoud, A. S., 1991, Late Precambrian (740 Ma) charnockite, enderbite, and granite from Jebel Moya, Sudan: a link between the Mozambique Belt and the Arabian-Nubian Shield: Jour. Geology, v. 99, p. 648-659.

Stern, R.J. and Kröner, A., 1993, Geochronologic and isotopic constraints on the late Precambrian crustal evolution in NE Sudan: Jour. Geology, v. 101, p. 555-574.

Stern, R.J., Kröner, A., Reischmann, T., Bender, R. and Dawoud, A. S., 1994, Precambrian basement around Wadi Halfa: a new perspective of the evolution of the East Saharan Craton: Geol. Rundschau, v. 83, p. 564-577.

Stern, R.J., 1994. Neoproterozoic (900–550 Ma) arc assembly and continental collision in the East African Orogen: implications for the consolidation of Gondwanaland. Annu. Rev. Earth Planet. Sci. 22, 319–351.

Stern, R. J., and Johnson, P., 2010. Continental lithosphere of the Arabian Plate: a geologic, petrologic, and geophysical synthesis. Earth-Science Reviews, 101, 29-67.

Stoeser, D. B., and Camp, V. E., 1985, Pan-African microplate accretion of the Arabian Shield: Bulletin of the Geological Society of America, v. 96, p. 817-826.

Vail, J.R., 1971. Geological reconnaissance in part of Berber District, Northern

Province. Geological Survey Department of the Sudan, Bulletin 18, Khartoum,

76 pp.

Vail, J.R., 1976. Outline of the geochronology and tectonic units of the basement complex of Northeast Africa. Proc. Royal Soc. London, Ser. A 350, 127–141.

Vail, J.R., 1983. Pan-African crustal accretion in north-east Africa. J. Afr. Earth Sci. 1 (3–4), 285–294.

APPENDICES

A. Paleostress Measurement Table

ANS: Abu Sari Northern Vein Strike Slip Component Fault						
ANR: Abu Sari Northern Vein Reverse Component Fault						
ANN: Abu Sari Northern Vein Normal Component Fault						
ANV: Abu Sari Northern Vein Quartz Vein						
ANVlt: Abu Sari Northern Vein QuartzVeinlet						
(Similarly AE: Abu Sari Eastern Vein, AS: Abu Sari Southern Vein)						
ID	**Easting**	**Northing**	**Rake**	**Strike**	**Dip**	**Dip Dir**
ANS-03	252930	2244785	0	78	76	258
ANS-04	252930	2244785	23	203	90	113
ANS-05	252930	2244784	17	206	86	116
ANS-06	252929	2244783	20	200	90	110
ANS-08	252929	2244782	10	5	86	95
ANS-09	252927	2244779	10	25	90	115
ANS-19	252912	2244767	0	131	89	221
ANS-21	252919	2244762	0	205	74	115
ANS-22	252919	2244762	0	227	82	137
ANS-23	252919	2244762	0	90	90	0
AES-08	254362	2244659	0	60	80	330
AES-09	254362	2244658	0	61	80	331
AES-10	254362	2244658	0	63	78	333
AES-11	254363	2244657	0	65	80	335
AES-30	254399	2244697	75	18	62	288
AES-34	254411	2244709	36	61	84	331
ASS-01	252191	2244326	0	98	79	2
ASS-02	252199	2244326	0	259	61	349
ASS-03	252200	2244326	0	330	82	60
ASS-04	252204	2244326	0	286	57	16
ASS-05	252211	2244326	0	325	82	55
ASS-06	252218	2244324	0	95	76	5
ASS-07	252232	2244321	0	260	90	350
ASS-08	252234	2244320	0	320	90	50
ANS-03	252930	2244785	0	78	76	258
ANS-04	252930	2244785	23	203	90	113
ANS-05	252930	2244784	17	206	86	116

ANS: Abu Sari Northern Vein Strike Slip Component Fault	
ANR: Abu Sari Northern Vein Reverse Component Fault	
ANN: Abu Sari Northern Vein Normal Component Fault	
ANV: Abu Sari Northern Vein Quartz Vein	
ANVlt: Abu Sari Northern Vein QuartzVeinlet	
(Similarly AE: Abu Sari Eastern Vein, AS: Abu Sari Southern Vein)	

ID	Easting	Northing	Rake	Strike	Dip	Dip Dir
ANS-06	252929	2244783	20	200	90	110
ANS-08	252929	2244782	10	5	86	95
ANS-09	252927	2244779	10	25	90	115
ANS-19	252912	2244767	0	131	89	221
ANS-21	252919	2244762	0	205	74	115
ANS-22	252919	2244762	0	227	82	137
ANS-23	252919	2244762	0	90	90	0
AES-01	254356	2244668	NA	231	75	141
AES-02	254356	2244668	NA	240	80	160
AES-03	254357	2244666	NA	120	90	30
AES-04	254358	2244665	NA	108	90	18
AES-05	254359	2244664	NA	82	85	352
AES-06	254360	2244663	NA	109	87	189
AES-07	254361	2244661	NA	112	90	22
AES-12	254364	2244656	NA	225	78	315
AES-13	254364	2244654	NA	334	90	64
AES-14	254365	2244652	NA	310	86	220
AES-15	254366	2244650	NA	270	85	180
AES-28	254373	2244675	NA	95	90	5
AES-29	254376	2244679	NA	60	90	150
AES-31	254404	2244702	NA	111	70	21
AES-32	254404	2244702	NA	35	85	305
AES-33	254408	2244706	NA	155	80	65
AES-35	254431	2244723	NA	150	22	60
AES-36	254431	2244723	NA	43	90	133
AES-37	254437	2244731	NA	80	85	350
AES-38	254437	2244731	NA	79	90	169
AES-39	254437	2244731	NA	55	90	145
AES-16	254357	2244674	NA	78	90	168
AES-17	254358	2244674	NA	80	90	170
AES-18	254363	2244679	NA	143	70	233
AES-19	254381	2244691	NA	50	86	140
AES-20	254382	2244691	NA	43	86	133

ANS: Abu Sari Northern Vein Strike Slip Component Fault						
ANR: Abu Sari Northern Vein Reverse Component Fault						
ANN: Abu Sari Northern Vein Normal Component Fault						
ANV: Abu Sari Northern Vein Quartz Vein						
ANVlt: Abu Sari Northern Vein QuartzVeinlet						
(Similarly AE: Abu Sari Eastern Vein, AS: Abu Sari Southern Vein)						
ID	Easting	Northing	Rake	Strike	Dip	Dip Dir
AES-21	254386	2244693	NA	90	88	180
AES-22	254389	2244695	NA	91	90	1
AES-23	254389	2244695	NA	41	86	311
AES-24	254389	2244695	NA	95	84	185
AES-25	254392	2244697	NA	83	88	353
AES-26	254409	2244711	NA	80	90	170
AES-27	254409	2244712	NA	62	89	152
AES-01	254356	2244668	NA	51	75	141
AES-02	254356	2244668	NA	60	80	150
AES-03	254357	2244666	NA	120	90	30
AES-04	254358	2244665	NA	108	90	18
AES-05	254359	2244664	NA	82	85	352
AES-06	254360	2244663	NA	109	87	199
AES-07	254361	2244661	NA	112	90	22
AES-12	254364	2244656	NA	45	78	315
AES-13	254364	2244654	NA	154	90	64
AES-14	254365	2244652	NA	130	86	220
AES-15	254366	2244650	NA	90	85	180
ANS-01	252935	2244798	NA	30	90	120
ANS-02	252937	2244797	NA	34	90	124
ANS-10	252927	2244779	NA	160	85	70
ANS-11	252926	2244777	NA	329	84	59
ANS-12	252926	2244776	NA	102	84	12
ANS-13	252925	2244774	NA	360	85	270
ANS-14	252924	2244773	NA	176	80	266
ANS-15	252922	2244770	NA	140	80	50
ANS-16	252921	2244768	NA	337	87	67
ANS-17	252916	2244765	NA	180	84	270
ANS-18	252914	2244766	NA	156	87	246
ANS-20	252912	2244767	NA	27	78	117
ASS-09	252238	2244319	3	155	87	245
ASS-10	252247	2244315	2	300	80	30
ASS-11	252247	2244316	2	310	74	40

	ANS: Abu Sari Northern Vein Strike Slip Component Fault					
	ANR: Abu Sari Northern Vein Reverse Component Fault					
	ANN: Abu Sari Northern Vein Normal Component Fault					
	ANV: Abu Sari Northern Vein Quartz Vein					
	ANVlt: Abu Sari Northern Vein QuartzVeinlet					
	(Similarly AE: Abu Sari Eastern Vein, AS: Abu Sari Southern Vein)					
ID	Easting	Northing	Rake	Strike	Dip	Dip Dir
ASS-12	252307	2244300	3	206	84	116
ASS-13	252307	2244300	2	72	84	342
ASS-14	252308	2244300	3	182	90	270
ASS-15	252308	2244300	3	175	75	85
ASS-16	252309	2244299	3	195	85	105
ASS-17	252309	2244299	3	193	80	103
ASS-18	252311	2244299	3	160	72	70
ASS-19	252312	2244299	2	145	76	55
ASS-20	252314	2244299	2	305	85	35
ASS-21	252315	2244298	2	315	75	45
ASS-22	252319	2244298	3	295	82	25
ASS-23	252322	2244297	2	305	75	35
ASS-24	252643	2244349	3	178	78	88
ASS-25	252642	2244348	2	80	80	350
ASS-26	252637	2244347	2	132	67	42
ASS-27	252635	2244346	3	148	78	58
ASS-28	252634	2244346	3	158	80	68
ASS-29	252604	2244337	2	20	85	290
ASS-30	252601	2244336	2	69	70	339
ASS-31	252589	2244332	2	65	72	335
ASS-32	252547	2244311		40	30	310
ASS-33	252540	2244308	2	2	85	272
ASS-34	252526	2244304	2	90	85	0
ASS-35	252499	2244299	2	5	77	95
ASS-36	252497	2244298	3	170	84	80
ASS-37	252497	2244298	3	30	84	300
ASS-38	252496	2244297	2	10	86	100
ASS-39	252495	2244297	3	9	80	99
ASS-40	252493	2244296	3	146	74	56
ASS-41	252491	2244296	2	110	71	20
ASS-42	252468	2244291	2	121	72	31
ASS-43	252468	2244293	3	36	78	306
ASS-44	252660	2244381	2	88	80	178

	ANS: Abu Sari Northern Vein Strike Slip Component Fault					
	ANR: Abu Sari Northern Vein Reverse Component Fault					
	ANN: Abu Sari Northern Vein Normal Component Fault					
	ANV: Abu Sari Northern Vein Quartz Vein					
	ANVlt: Abu Sari Northern Vein QuartzVeinlet					
	(Similarly AE: Abu Sari Eastern Vein, AS: Abu Sari Southern Vein)					
ID	Easting	Northing	Rake	Strike	Dip	Dip Dir
ASS-45	252660	2244381	2	89	89	179
ASS-46	252656	2244380	3	14	88	104
ASS-47	252635	2244368	3	48	90	318
ASS-48	252624	2244366	2	12	78	102
ASS-49	252621	2244365	2	123	90	31
ASS-50	252620	2244365	2	10	76	100
ASS-51	252599	2244361	3	8	80	278
ASS-52	252598	2244361	2	104	87	14
ASS-53	252599	2244361	2	102	87	12
ASS-54	252596	2244360	2	92	68	2
ASS-55	252587	2244359	2	127	90	37
AER-08	254406	2244704	NA	140	32	230
AER-09	254429	2244721	NA	117	81	27
AER-10	254406	2244748	NA	114	34	204
AER-01	254358	2244675	NA	141	19	51
AER-02	254386	2244694	NA	149	12	59
AER-03	254394	2244698	NA	135	12	45
AER-04	254410	2244713	NA	121	29	31
AER-05	254410	2244713	NA	107	26	17
AER-06	254415	2244720	NA	135	20	45
AER-07	254419	2244727	NA	129	29	39
ANR-01	252925	2244809	NA	0	10	90
ANR-02	252938	2244799	NA	127	34	217
ANR-03	252938	2244799	NA	130	28	220
ANR-04	252933	2244791	NA	140	39	230
ANR-05	252931	2244787	NA	139	28	229
ASR-01	252650	2244351	NA	45	22	315
ASR-02	252651	2244351	NA	132	19	222
ASR-03	252620	2244342	NA	44	42	134
ASR-04	252610	2244338	NA	144	34	234
ASR-05	252593	2244333	NA	6	37	276
ASR-06	252568	2244321	NA	160	40	250
ASR-07	252562	2244318	NA	158	37	248

ANS: Abu Sari Northern Vein Strike Slip Component Fault ANR: Abu Sari Northern Vein Reverse Component Fault ANN: Abu Sari Northern Vein Normal Component Fault ANV: Abu Sari Northern Vein Quartz Vein ANVlt: Abu Sari Northern Vein QuartzVeinlet (Similarly AE: Abu Sari Eastern Vein, AS: Abu Sari Southern Vein)						
ID	**Easting**	**Northing**	**Rake**	**Strike**	**Dip**	**Dip Dir**
AEN-01	254364	2244655	NA	133	45	43
AEN-06	254404	2244702	NA	134	48	224
AEN-07	254431	2244723	NA	100	48	10
AEN-02	254409	2244712	NA	103	34	193
AEN-03	254410	2244713	NA	112	29	202
AEN-04	254410	2244713	NA	116	14	206
AEN-05	254418	2244725	NA	85	30	175
AEN-01	254364	2244655	NA	133	45	43
ANN-01	252935	2244816	NA	141	45	231
ANN-02	252935	2244816	NA	136	48	226
ANN-03	252932	2244814	NA	138	33	228
ANN-04	252932	2244814	NA	140	35	230
ASN-01	252636	2244369	NA	132	22	222
ASN-02	252632	2244368	NA	146	39	236
ASN-03	252629	2244367	NA	145	60	235
ASN-04	252628	2244367	NA	145	60	235
ASN-05	252623	2244366	NA	135	43	225
ASN-06	252601	2244361	NA	165	38	255
ASN-07	252590	2244360	NA	143	45	233
ASN-08	252586	2244359	NA	144	50	234
ASF-01	252157	2244316	NA	184	82	94
ASF-02	252173	2244323	NA	184	82	94
ASF-03	252195	2244326	NA	183	78	93
ASF-04	252207	2244326	NA	0	80	90
ASF-05	252217	2244324	NA	193	83	103
ASF-06	252234	2244320	NA	234	82	324
ASF-07	252307	2244299	NA	84	82	354
ASF-08	252320	2244297	NA	150	87	240
ASF-09	252330	2244292	NA	90	72	180
ASF-10	252646	2244349	NA	40	80	310
ASF-11	252631	2244345	NA	42	81	310
ASF-12	252596	2244334	NA	169	83	79
ASF-13	252589	2244332	NA	0	81	90

118

ANS: Abu Sari Northern Vein Strike Slip Component Fault **ANR:** Abu Sari Northern Vein Reverse Component Fault **ANN:** Abu Sari Northern Vein Normal Component Fault **ANV:** Abu Sari Northern Vein Quartz Vein **ANVlt:** Abu Sari Northern Vein QuartzVeinlet (Similarly AE: Abu Sari Eastern Vein, AS: Abu Sari Southern Vein)						
ID	**Easting**	**Northing**	**Rake**	**Strike**	**Dip**	**Dip Dir**
ASF-14	252564	2244319	NA	0	80	90
ASF-15	252532	2244305	NA	60	83	150
ASF-16	252506	2244300	NA	140	72	50
ASF-17	252473	2244292	NA	25	90	295
ASF-18	252470	2244291	NA	42	75	312
ASF-19	252660	2244381	NA	0	78	90
ASF-20	252627	2244367	NA	22	79	112
ASF-21	252610	2244363	NA	12	82	102
ASF-22	252599	2244361	NA	7	85	97
ASF-23	252593	2244360	NA	160	74	70
ASF-24	252583	2244359	NA	140	75	50
ANF-01	252938	2244818	NA	0	75	90
ANF-02	252930	2244813	NA	0	77	90
ANF-03	252927	2244779	NA	0	85	90
ANF-04	252919	2244765	NA	0	80	90
ANF-05	252915	2244765	NA	0	85	90
AEF-01	254357	2244667	NA	274	83	4
AEF-02	254362	2244658	NA	272	82	2
AEF-03	254365	2244652	NA	270	81	0
AEF-12	254378	2244681	NA	137	90	47
AEF-13	254374	2244676	NA	140	87	230
AEF-14	254400	2244698	NA	98	83	188
AEF-15	254404	2244702	NA	86	90	176
AEF-16	254408	2244705	NA	119	87	209
AEF-17	254428	2244720	NA	105	86	195
AEF-18	254433	2244724	NA	111	87	21
AEF-19	254406	2244748	NA	90	90	0
AEF-04	254359	2244675	NA	157	81	247
AEF-05	254378	2244689	NA	115	84	205
AEF-06	254384	2244692	NA	155	90	65
AEF-07	254391	2244696	NA	111	81	201
AEF-08	254410	2244713	NA	99	90	9
AEF-09	254413	2244717	NA	100	87	190

ANS: Abu Sari Northern Vein Strike Slip Component Fault **ANR:** Abu Sari Northern Vein Reverse Component Fault **ANN:** Abu Sari Northern Vein Normal Component Fault **ANV:** Abu Sari Northern Vein Quartz Vein **ANVlt:** Abu Sari Northern Vein QuartzVeinlet (Similarly AE: Abu Sari Eastern Vein, AS: Abu Sari Southern Vein)						
ID	**Easting**	**Northing**	**Rake**	**Strike**	**Dip**	**Dip Dir**
AEF-10	254414	2244719	NA	94	74	4
AEF-11	254417	2244724	NA	104	79	194
AEF-01	254357	2244667	NA	94	83	4
AEF-02	254362	2244658	NA	92	82	2
AEF-03	254365	2244652	NA	90	81	0
ASV-01	252157	2244317	NA	230	54	320
ASV-02	252162	2244319	NA	180	90	270
ASV-03	252166	2244321	NA	250	70	340
ASV-04	252175	2244324	NA	230	54	320
ASV-05	252181	2244325	NA	180	90	270
ASV-06	252187	2244326	NA	250	70	340
ASV-07	252204	2244326	NA	255	63	345
ASVt-01	252237	2244319	NA	190	62	280
ASVt-02	252645	2244349	NA	141	42	231
ASVt-03	252645	2244349	NA	13	23	103
ASVt-04	252606	2244337	NA	134	16	44
ASVt-05	252601	2244336	NA	135	30	45
ASVt-06	252575	2244325	NA	0	55	90
ASVt-07	252603	2244336	NA	50	59	320
ASVt-08	252603	2244336	NA	52	62	322
ASVt-09	252603	2244336	NA	50	60	320
ASVt-10	252603	2244336	NA	32	55	122
ASVt-11	252603	2244336	NA	32	58	122
ASVt-12	252557	2244315	NA	151	23	241
ASVt-13	252551	2244313	NA	0	20	90
ASVt-14	252550	2244312	NA	0	45	90
ASVt-17	252536	2244307	NA	0	40	90
ASVt-18	252536	2244307	NA	0	45	90
ASVt-19	252528	2244305	NA	156	22	66
ASVt-20	252528	2244305	NA	156	20	66
ASVt-21	252517	2244302	NA	0	24	90
ASVt-25	252501	2244299	NA	143	25	53
ASVt-26	252501	2244299	NA	140	38	50

ANS: Abu Sari Northern Vein Strike Slip Component Fault **ANR:** Abu Sari Northern Vein Reverse Component Fault **ANN:** Abu Sari Northern Vein Normal Component Fault **ANV:** Abu Sari Northern Vein Quartz Vein **ANVlt:** Abu Sari Northern Vein QuartzVeinlet (Similarly AE: Abu Sari Eastern Vein, AS: Abu Sari Southern Vein)						
ID	**Easting**	**Northing**	**Rake**	**Strike**	**Dip**	**Dip Dir**
ASVt-27	252501	2244299	NA	143	43	53
ANVt-01	252928	2244811	NA	121	29	31
ANVt-02	252938	2244799	NA	280	24	10
ANVt-03	252937	2244798	NA	280	26	10
ANVt-04	252936	2244796	NA	121	46	31
AEV-01	254356	2244669	NA	245	82	155
AEV-02	254355	2244669	NA	120	90	310
AEV-04	254406	2244748	NA	120	90	30
AEV-03	254365	2244681	NA	24	52	294
AEVt-01	254386	2244693	NA	105	64	15
AEVt-02	254414	2244719	NA	95	63	5
AEVt-03	254411	2244714	NA	111	71	21
AEVt-04	254420	2244730	NA	100	90	10
AEV-01	254356	2244669	NA	65	82	155
AEV-02	254355	2244669	NA	120	90	30